# Development of Dielectric Spectroscopic monitoring methods for the prediction of viable cell density and volume in mammalian cell culture

By

Timothy O' Regan, BSc

This thesis is submitted to Dublin City University for the degree of MSc in Biotechnology

January 2012

Director: Professor Ian W. Marison
Laboratory of Integrated Bioprocessing, School of Biotechnology, Dublin City University, Dublin 9.

*I hereby certify that this material, which I now submit for assessment on the programme of study leading to the award of Master of Science in Biotechnology is entirely my own work, that I have exercised reasonable care to ensure that the work is original, and does not to the best of my knowledge breach any law of copyright, and has not been taken from the work of others save and to the extent that such work has been cited and acknowledged within the text of my work.*

Signed: _____ (Candidate) ID No.: 55635250

Date: _____

# Table of Contents

# Abstract

The objective of this study is to examine the potential of off-line biomass monitoring methods for the real-time prediction of viable cell density and viable cell volume in Chinese hamster ovary cell cultures.

This work focuses on the use of Biomass Monitor for the monitoring of biomass. Two dual frequency settings and 2 temperatures were examined. The effects of interferences when the Biomass Monitor probe is present in a bioreactor are also investigated. The feasibility of constructing a prediction model for viable cell density and viable cell volume for in-line use is examined as there is an increased focus on monitoring techniques that adhere to the guidance in the United States Food and Drug Administration's Process Analytical Technology framework.

It was found that interferences to the Biomass Monitor include proximity of the biomass probe to vessel walls, $pO_2$ probe and sparger with the bubbles from aeration having a significant effect on the signal.

The three prediction models were a high cell density suspension serially diluted to a low cell density, real time culture suspension data and combination of the high cell density and real time data.

From the prediction models, capacitance versus viable cell density at the dual frequency of 0.2 and 10 MHz at 30 °C showed best predictions with error of all three models between 0.26 - 0.36 $\times 10^6$ cells/ml.

All models for viable cell volume were accurate at the lower ranges, with error increasing as the viable cell volume increased. Combination of high cell density suspension and real time data allowed the best cell volume predictions at 37 °C with errors of 1.1 – 1.2 x $10^9$ $\mu m^3$ $ml^{-1}$.

Optical density and an automated cell counter were also investigated for the estimation of viable cell density and were found to be not as accurate as the capacitance prediction of viable cell density.

# Acknowledgements

I wish to thank Professor Ian W. Marison for supervising my work, for many interesting discussions, patient corrections, and for both challenging and encouraging me and also Professor Nigel Jenkins in NIBRT for the provision of the CHO 320 cell line. Thanks also go to all of my colleagues at the Laboratory of Integrated Bioprocessing, for providing a nice atmosphere in which to work and re-assurance in times of difficulty especially Dr. Siobhán Hennessy and Brian Freeland.

A special word of thanks to Science Foundation Ireland for funding the research undertaken in this document.

Finally, I would like to thank my family and friends for putting up with me.

# List of Figures

# List of Tables

# List of Equations

# List of Abbreviations

| | |
|---|---|
| AC | Alternating current |
| B | Batch |
| BHK | Baby hamster kidney |
| BM | Biomass Monitor |
| C | Capacitance |
| CER | Carbon dioxide evolution rate |
| CHO | Chinese hamster ovary |
| $CO_2$ | Carbon dioxide |
| DC | Direct Current |
| $DHFR^-$ | Dihydrofolate reductase negative |
| DNA | Deoxyribonucleic acid |
| EPO | Erythropoietin |
| FB | Fed Batch |
| FDA | Food and Drug Administration |
| FSH | Follicle stimulating hormone |
| HCD | High cell density |
| HCD + RT | High cell density and real time |
| HEK | Human Embryonic Kidney |
| IFN-γ | Interferon - Gamma |
| IMS | Industrial methylated spirits |
| ln | Natural log |
| MHz | Megahertz |
| mM | Millimolar |
| MTX | Methotrexate |
| MUC 1 | Mucin 1 |
| NaOH | Sodium Hydroxide |
| NMR | Nuclear Magnetic Resonance |
| NSO | Mouse myeloma cell line |
| $OD_{600}$ | Optical density at 600 nm |
| $O_2$ | Oxygen |
| PAT | Process Analytical Technology |
| pF/cm | Pico farads per cm |

| | |
|---|---|
| RMSEP | Root Mean Squared Error of Prediction |
| RPM | Revolutions per minute |
| RT | Real time |
| V | Viability |

# 1. Introduction

## 1.1 Background

In the early 1970s, fermentation processes, (for example, the production of penicillin) were thought to be as much an art as a science. Making antibiotics was not much more sophisticated than making wine; ingredients were put into a tank, closed, manually sterilised and inoculated with cells, followed by agitation and aeration for a number of days. Data collection consisted of operators periodically recording values from gauges and other apparatus onto a clipboard and transferring the data to a manufacturing docket (Alford 2006).

Over the past 20 years, recombinant proteins, particularly those from mammalian cell lines have gained an increasingly important status for therapeutic applications. Combined with this, the number of proteins both approved and sent into clinical trials has been continually increasing (Matasci et al. 2008). Biopharmaceuticals represent one quarter of new pharmaceuticals being brought onto the market, generating €30 billion in sales annually. The majority of these biopharmaceuticals are produced as recombinant animal proteins and as an outcome, a huge focus of the pharmaceutical industry lies on this particular area of biotechnological application (Burgemeister et al. 2010).

Mammalian cells are powerful tools in the production of recombinant therapeutic proteins (Irani, Beccaria and Wagner 2002; Sugiura and Kakuzaki 1998; Gawlitzek et al. 1995) as such proteins require post translational modifications. The most important post translational modification is glycosylation (Zhang et al. 2010; Andersen and Krummen 2002) with insect cells gaining relevance in the production of recombinant proteins due to their ability to perform such post translational modifications (Gouveia et al. 2010; Douris et al. 2006; Yamaji et al. 2006).

Chinese hamster ovary (CHO) cells are easy to cultivate in suspension and are able to produce high levels of recombinant protein with a high degree of complex glycosylation, which is very important for protein activity as well as solubility, secretion, stability and folding (Burteau et al. 2003). For these reasons CHO cell lines are frequently used by the biopharmaceutical industry in the production of recombinant proteins, (Sunley and Butler 2010; Yoon et al. 2006; Sun and Zhang 2004). Cell lines such as those originating from baby hamster kidney (BHK) (Kallel

et al. 2002), human embryo kidney (HEK-293) (Huang et al. 2005) and mouse myeloma (NSO) (Schlaeger and Schumpp 1992) are also common choices in the production of recombinant proteins.

Some examples of therapeutic proteins produced by CHO cell lines include and interferon - gamma (IFN-γ) (Farges et al. 2008), erythropoietin (EPO), a drug used for treatment of individuals with anaemia or during the course of cancer treatment, follicle stimulating hormone (FSH), a drug that regulates the development, growth, pubescent maturation, and reproductive progression of the body (Yoon et al. 2006) the fusion protein Mucin 1 (MUC 1), a candidate for use in specific immunotherapy against breast cancer (Link et al. 2004).

In this study, a CHO 320 cell line expressing IFN-γ, a cytokine that is crucial in both innate and adaptive immunity against viral and intracellular bacterial infections and for tumour control has been used. IFN-γ is also used in the treatment of osteoporosis (Park et al. 2007).

### 1.2 Bioprocess Monitoring and Process Analytical Technology

Once a biopharmaceutical production procedure has been approved based on a given process, any significant deviation from the production procedure may require new clinical trials to examine the safety of the resulting product ("process defines the product"). Since clinical trials are costly, process improvements are made under very rigorous constraints, therefore processes are normally run far below maximum performance (Sommerfeld and Strube 2005).

As a consequence of this, pharmaceutical companies are beginning to re-evaluate their bioprocess analysis techniques with some beginning to embrace Process Analytical Technology (PAT) (Teixeira et al. 2009). Process Analytical technologies are "systems for analysis and control of manufacturing processes based on timely measurements of critical quality parameters (U.S. Department of Health and Human Services: Food and Drug Administration 2004) and performance attributes of raw materials and in-process products, to assure acceptable end – product quality at the completion of the process", i.e. quality by design, (Lopes et al. 2004). Figure 1 shows some critical quality parameters which may be monitored over the course of a bioprocess.

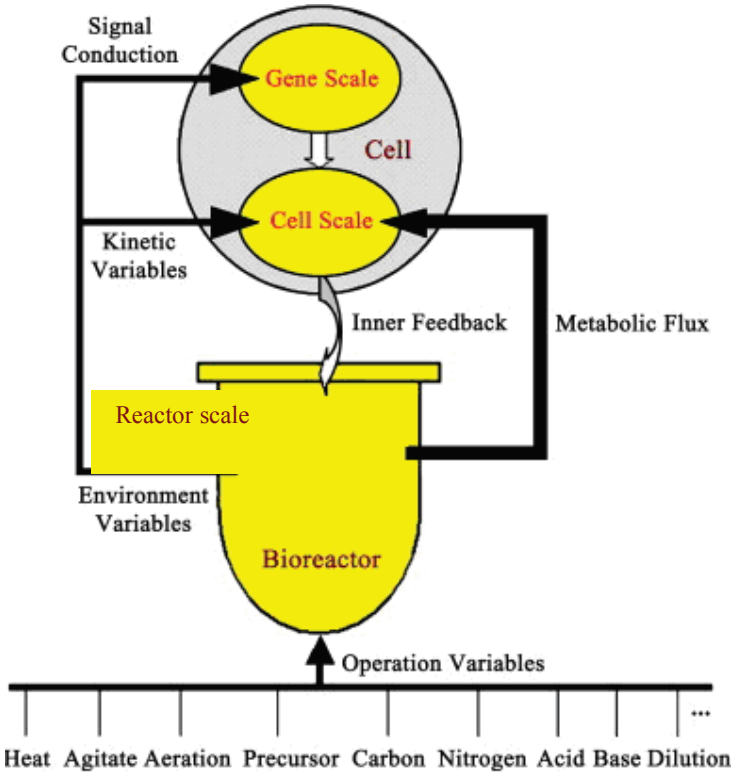


**Figure 1:** Summary of the parameters to be controlled and monitored in a bioreactor (Wang et al. 2009, p.990, Fig 1.).

The PAT initiative, launched by the FDA in 2004, encourages companies producing biopharmaceuticals to approve the use of modern tools for bioprocess monitoring based on on-line analysis of key parameters mentioned above (see Figure 1) which will allow early fault detection. The aim of PAT is to maximise the probability of attaining excellent product quality at the end of the process or cutting the process short if major variations are apparent. PAT requires easy-to-use process analysers, mathematical integration tools for data analysis and feedback control methods to perform any necessary process adjustments (Teixeira et al. 2009), (U.S. Department of Health and Human Services: Food and Drug Administration 2004).

PAT involves the application of process analytical chemistry (i.e., in process monitoring techniques), chemometrics (e.g., data-based modelling techniques) and

process control techniques (intelligent use of process data and prediction or diagnosis strategies of a culture condition) (Lopes et al. 2004).

### 1.3 Techniques

Traditionally physical parameters such as temperature, headspace pressure and agitation along with chemical parameters, pH and dissolved oxygen concentration have customarily been monitored during the course of a bioprocess. In order to gain a better understanding of the process and to implement reliable control techniques, knowledge of biological parameters such as cell density (viable and maximum), viability and specific growth rate are imperative (Wang et al. 2009; Maskow et al. 2008; Xiong et al. 2008)

The definition of biomass itself must first be considered. Cells may be classified in relation to their concentration as number, dry mass or volume or to their physiological condition and metabolic activity. The definition of a viable cell is also related to the techniques that are used to determine it. A viable cell can be defined as a cell that has the ability to catalyze a biochemical reaction (trypan blue staining), a volume enclosed by a membrane (dielectric spectroscopy) or a cell with a volume above a set lower limit (Ducommun et al. 2001). Numerous techniques have been developed as a consequence of this need and they can be classed into direct and indirect measurement methods.

Indirect measurement methods rely on parameters that can be related to biomass concentration, an example being the rates of compounds that are produced or consumed during a culture such as glucose consumption throughout a culture.

Direct methods for the determination of biomass concentration are based on biological quantification (viable cell counting or plate counts), or in the exploration of physical properties of cells such as their optical, acoustic, magnetic or electrical properties (Dabros et al. 2009). Optical density is the most commonly used direct method, but is subject to inaccuracies especially in in-situ environments due to its sensitivity to air bubbles, cell aggregation and non cellular scattering of particles present in the medium. It also fails to distinguish between viable and non-viable cells (Marose et al. 1999). A summary of indirect and direct methods for the determination of biomass is given in Table 1 and Table 2 respectively.

In line with PAT, it is generally accepted that knowing the growth rate is important at early stages of a culture. Traditionally cell counts are taken off-line

using a haemocytometer, with the disadvantage of this technique being variable operator accuracy and long analysis time. A less accurate but faster measurement such as optical density can suffer from dilution errors, sampling errors and does not distinguish viable and non-viable cells (Vojinović, Cabral and Fonseca 2006). The disadvantage of off-line methods is that they are often time consuming, inaccurate, can be influenced by operator judgement (microscopic cell count) and provide a limited number of measurements during shift hours. Also off-line methods are not capable of exhibiting the critical changes in viable cell mass during fermentation in real time (Xiong et al. 2008)

**Table 1:** Indirect Methods for monitoring mammalian cell densities during a culture.

| **Method** | **Measured variable** | **Advantage** | **Disadvantage** | **Reference** |
|---|---|---|---|---|
| Oxygen uptake rate (OUR) | $O_2$ uptake rate | Non invasive | Specific rates may fluctuate during a process leading to errors | (Xiong et al. 2008) |
| Carbon dioxide evolution rate (CER) | $CO_2$ evolution rate | Non invasive | Specific rates may fluctuate during a process leading to errors | (Xiong et al. 2008) |
| Fluorescence spectroscopy | NADH Fluorescence | Representative of intracellular state of cells | Expensive to implement | (Siano and Mutharasan 1991) |

**Table 2:** Direct Methods for monitoring mammalian cell densities during a culture.

| Method | Measured variable | Advantage | Disadvantage | Reference |
|---|---|---|---|---|
| NMR spectroscopy | Nuclear magnetic resonance | Non invasive | Time and lack of sensitivity | (Vojinović, Cabral and Fonseca 2006) |
| Conductivity | Conductivity of suspension | Only viable cell density information | Low sensitivity reported | (Soley et al. 2005) |
| Capacitance | Polarisation of plasma membrane | Only viable cell density information | Low sensitivity reported | (Cannizzaro et al. 2003) |
| Optical Density | Optical density | Rapid | Does not distinguish viable and non-viable cells | (Marose et al. 1999) |
| Trypan blue exclusion | Cells ability to catalyse biochemical reaction | Ease to perform | Variation of samples and users | (Ducommun et al. 2001) |

Ideally measurements are taken on-line. On-line instruments currently available are based on optical density (example generic Photometer with dip probe or bypass), fluorescence spectroscopy (Bioview, Delta Light and Optics, Lyngby, Denmark), turbidity (Aqua ant Messtechnik AG, Bubendorf, Switzerland) and capacitance or conductivity measurements (Biomass Monitor, Aber instruments Ltd, Aberystwyth, UK). The results of these on-line measurement techniques are also validated by means of off-line techniques, for example counting cells using a haemocytometer and

a microscope as was done in this work. The off-line validation is necessary due to the fact that on-line measurements may be affected by more parameters than just cell density, for example sensors can drift over time or there can be changes in physical or chemical environment (addition of acid, bases, antifoam to a process) (Joeris et al. 2002)

### 1.4 Importance of Biomass

Knowledge of biomass concentration (cell density) is required by definition, for the purpose of determining of any specific yield, metabolic rate, and mass balance equation and is commonly used as criteria to assess a variety of culture processes including specific growth rate, productivity and maximum or final cell concentration (Ducommun et al. 2001). On-line and real time measurement of biomass is still an active area of research, with new sensors being developed and established technologies being improved.

Numerous criteria must be fulfilled if a new biomass detection system is to be implemented. The technique must fit easily into an established fermentor system, be able to withstand the harsh in-situ sterilisation cycles of a reactor and the probe materials must be inert. An ideal measuring system should be capable of measuring numerous cell types, in both suspension and immobilised structures, with the ability to measure a varying range of biomass concentrations (Davey and Kell 1998).

Of the more recent applications for determination of biomass, the Biomass Monitor (dielectric spectroscopy) offers considerable advantages when compared to other measurement techniques, for example it detects only viable cells with an intact plasma membrane, does not become affected by solid particles or lysed cells and can be used in both suspension systems and with immobilised cells, such as a fluidised bed bioreactor in which other methods would not suffice ( Zeiser et al. 1999; Noll and Biselli 1998).

In the last number of years many studies have been carried out based on the estimation of cell density of different suspended and immobilised organisms such as *Saccharomyces cerevisiae* (Xiong et al. 2008), bacterial culture and biofilms (Jass, O'Neill and Walker 2001), mycelial cell cultures *Streptomyces clavuligerus* (Neves et al. 2000) *Pichia pastoris* and *Streptomyces virginiae* (Fehrenbach, Comberbach and Pêtre 1992) and plant cell culture (Markx et al. 1991). Dielectric spectroscopy can

also be applied by the medical industry, for example in the analysis of malignant and normal human lymphocytes (white blood cells) (Polevaya et al. 1999).

The Biomass Monitor has recently been used by a number of researchers to monitor cell density in mammalian cultures being operated under a variety of characteristic frequencies with all capacitance data from on-line determinations being compared to off-line data either from the coulter counter, microscope and haemocytometer, optical density or a combination of the methods (Justice et al. 2011; Ansorge, Esteban and Schmid 2007; Cannizzaro et al. 2003; Ducommun et al. 2002; Guan, Evans and Kemp 1998;Fehrenbach, Comberbach and Pêtre 1992)

### 1.5 Principle of dielectric spectroscopy

The theory of dielectric spectroscopy in a bioprocessing context has been described by various authors (Soley et al. 2005; Markx and Davey 1999; Kell and Todd 1998; Kell et al. 1990). The term "dielectric" was originally introduced by William Whewell after Michael Faraday observed the need to describe a material in which an electric field passes through (Greek - "dia" = through).

Maxwell gave a firm theoretical foundation to the field of dielectrics which included the derivation of an analytical solution for the conductivity of a suspension (dilute) of spherical particles. Maxwell's equation was adapted so it could be used to describe the dielectric properties of cell suspensions, in which a cell was modelled as a conducting spheroid surrounded by a non-conducting membrane (Maxwell 1873).

There was rapid progression after World War II, in particular by Schwan (1957) who performed measurements of cell suspensions and tissues over a much broader frequency range than was previously possible. Pohl pioneered the study of the movement of particles through alternating current (AC) electric fields, and introduced the term dielectrophoresis in the early 1950s to describe the movement of particles induced by non-uniform electric fields (Pohl 1978).

Further progress followed with the development of electro-orientation, electrorotation and travelling wave dielectrophoresis techniques (all based on movement of particles in an alternating current (AC) electric field). The application of AC to the study of cells continues to be developed and has been particularly successful due to the ways cells are constructed (Markx and Davey 1999). Among the systems for biomass measurements, the dielectric analysis of cell suspensions is a useful system in the estimation of cell concentration because it is capable of both a

real time and automated monitoring and is applicable to complex media (Soley et al. 2005).

As the frequency of an electrical field rises, the capacitance (permittivity) of a material tends to fall in a series of step like changes. Such step changes can be referred to as dispersions, which are due to losses in the polarisation processes as the frequency is increased. The α-dispersion is due to the tangential flow of ions across the surface of a cell, the γ-dispersion is due to the dipolar rotation of small molecules, in particular water. In terms of biomass monitoring, the β-dispersion results in the charge build-up at cell membranes due to the Maxwell-Wagner effect (Ansorge, Esteban and Schmid 2007; Markx and Davey 1999).

For modelling purposes, a cellular suspension can be regarded as three separate parts, the cytoplasm, the outer plasma membrane and the suspension medium (Carvell and Dowd 2006).

The cell cytoplasm is exceedingly complicated, containing large amounts of salts, proteins, nucleic acids and smaller molecules. In cells such as eukaryotes, various membrane structures including the nucleus and vacuoles can also affect the dielectric properties (Markx and Davey 1999). The plasma membrane surrounding a cell is a lipid bilayer (4 - 10 nm in thickness) which contains a lot of proteins. The influence of proteins and water on the membrane's dielectric properties is unclear. It is known that the application of large direct current (DC) or low frequency AC electric fields to a cell induces a large potential drop across the plasma membrane which can cause dielectric breakdown. Applications of this technique include killing cells, electrofusion to create new hybrids and electroporation which is a process used in the introduction of new genetic material into cells. The effect of the membrane potential on the β-dispersion is most likely restricted, but on the α-dispersion is potentially great.

A suspension medium for cell culture is in general aqueous and ionic (Carvell and Dowd 2006). When an electric field is applied to a suspension of cells in an ionic aqueous solution, the ions in the solution are forced to move, resulting in the positively charged ions being pushed in the direction of the electric field while the negatively charged ions will be pushed in the opposite direction, see Figure 2. The presence of cells however, means that the ions both inside and outside can only move so far before they encounter the plasma membrane, which acts as a non-conducting barrier, preventing extra movement (Carvell and Dowd 2006; Noll and Biselli 1998).

The result of this is a development of a charge separation or polarisation across the plasma membrane (Figure 2).

The magnitude of the charge separation is measured by its capacitance which is measured in pico-Farads (pF). Measurement of capacitance at one or more appropriate frequencies allows the biomass to be approximated (Kell et al. 1990). As the volume fraction of the cells increases, the area of polarized membranes increases and thus gives a higher reading for capacitance. An advantage of dielectric spectroscopy is that, non-biomass solids or other particles present in the media, including lysed cells do not contain intact plasma membranes and will not contribute to capacitance readings (Kiviharju et al. 2007).

At moderately low frequencies (< 0.1 MHz), there is enough time to allow the cells to become completely polarized, and the capacitance as a result will be high. As the excitation frequency is increased, capacitance decreases due to the incomplete polarisation at the plasma membrane. The resulting loss in the polarisation of the cells normally occurs between 0.1 and 10 MHz and is referred to as the β-dispersion (Davey and Kell 1998). As non biomass particles that lack an intact plasma membrane, including dead cells, may be present in the medium there is no resulting significant change in capacitance and thus disturbance from these non-cellular sources can be minimised by setting a reference frequency (≥ 10 MHz), with the measured capacitance at this frequency being subtracted from the measured capacitance at the lower frequency (Kiviharju et al. 2007)**.** This frequency is sometimes referred to as the characteristic frequency. With the exception of viruses, all living matter consists of cells which are similar in structure consisting of cytoplasm that is surrounded by a membrane. In many cases (plant and most micro-organisms), the cell is further enveloped with a cell wall (Davey and Kell 1998).

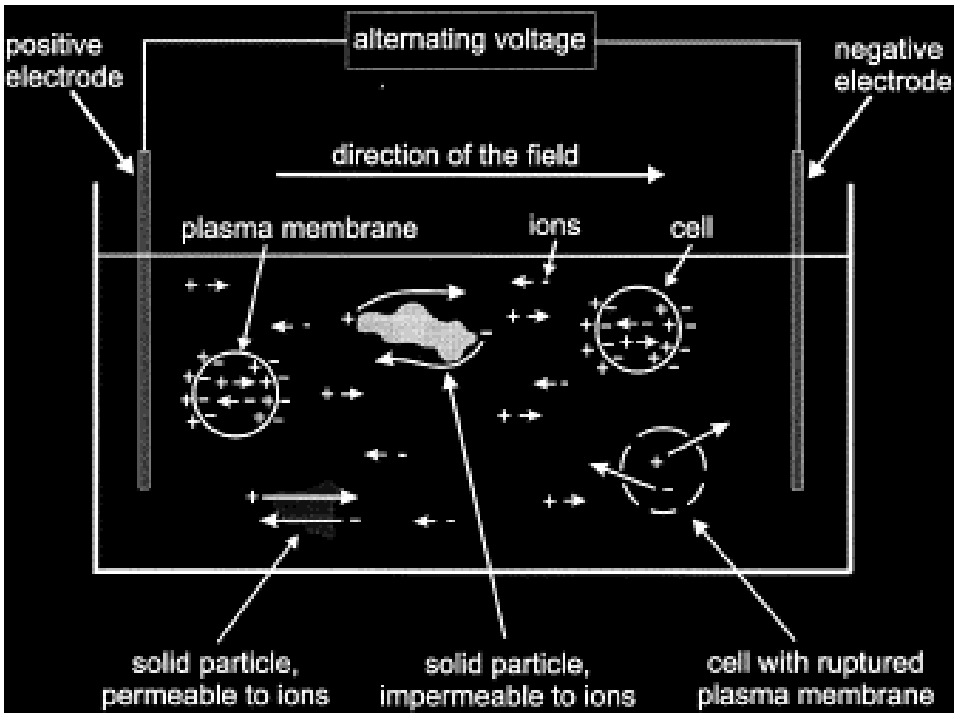


**Figure 2**: Schematic diagram showing the principle of dielectric measurement in a suspension of biological cells (Noll and Biselli 1998, p.189, Fig 1).

Capacitance readings from the Biomass Monitor can be subject to interference from vessel walls, stirrer speed, aeration and the metal structures of the reactor including the baffles and $pO_2$ probe (Dabros et al. 2009; Davey and Kell 1998). A low sensitivity has also been reported to be a disadvantage when monitoring mammalian cell lines with mammalian cell culture minimal detection is in the range of 0.2 - 0.5 x $10^6$ cells/ml; (Dabros et al. 2009; Aber Instruments 2008).

### 1.6 Aims

- Characterisation of CHO 320 Batch and Fed Batch culture growth kinetics including specific growth rate ($\mu$) and maximum cell density in order to assess growth characteristics of the cell line
- To investigate the effect of the surrounding environment on the capacitance signal
- Construction of prediction models of capacitance versus viable cell density and viable cell volume data and application to real time data
- Investigation of the effect of a changing dual frequency and also changing temperature on the calibration models and comparison of the data

The aims stated above were necessary in order to achieve the overall objective of establishing the optimal calibration model for measuring cell density for mammalian cell cultures in real time.

# 2. Materials and Methods

### 2.1 Cell line and medium

The experiments were performed using suspension-adapted CHO 320 cells bearing the recombinant interferon gamma (IFN-γ) gene, which was sourced from the National Institute of Bioprocessing Research and Training (NIBRT) Ireland. The cells were cultivated in EX-CELL CHO DHFR$^-$ animal component free medium (Sigma Aldrich, C8862), supplemented when required for culturing with L-glutamine and methotrexate (MTX) (Sigma Aldrich M9929). The L-glutamine was used at a concentration of 4 mM which was a 1/50 dilution of the 200 mM stock. The concentration of MTX used was 1 μM which was obtained by preparing a 1/2200 dilution from a stock of 2.2 mM.

#### 2.1.2 CHO 320 Cultivation Conditions

Banked CHO 320 cells were thawed from an ampoule (Appendix A.1) stored in liquid nitrogen (-196 °C), re-suspended in media supplemented to 4 mM L-glutamine and 1 μM methotrexate (MTX) at 37 ºC with no $CO_2$ and an agitation of 100 RPM (Excella E24 Incubator Shaker series). After 6 days the cells were sub-cultured into 250 ml Erlenmeyer flasks for real time experiments or 500 ml Erlenmeyer flasks for higher cell density experiments.

### 2.2 Biomass measurement techniques

Four methods were employed for estimation of biomass in this work, including microscope and haemocytometer counts which were used as the reference method throughout the work. The Countess automated cell counter (Invitrogen, C10281) was also used and both the reference method and the Countess cell counter method are based on the trypan blue exclusion method (Appendix A.2) Optical density ($OD_{600}$) with a spectrophotometer (Spectrophotometer, Helios Epsilon, ThermoSpectronic) and capacitance measurements using the Biomass Monitor 210 (BM 210) with a 25 mm probe (NBLP 470) were also investigated. All methods were compared to the reference method in terms of accuracy and interferences and limitations of the Biomass Monitor were also investigated. A brief description of the procedures for

each method can be noted in the sections below and a more detailed step-by-step procedure is outlined in Appendices B.1 – B.4.

### 2.2.1 Cell counts with microscope and haemocytometer

Cell counts were conducted by the trypan blue exclusion method and counted with a microscope and haemocytometer. The Erlenmeyer flask was gently swirled so the cell suspension was uniform and a 20 µl sample of cell suspension was removed with a pipette. This was diluted at a 1:1 ratio with 0.4 % solution of trypan blue (T8174) in a 1.5 ml micro-centrifuge tube (molecular bio-products), before being incubated for 3 minutes at room temperature. Two 10 µl aliquots of the cell suspension/trypan blue mixture were pipetted onto a haemocytometer (Improved Neubauer, Hawskley BS.748, Depth 0.1 mm, 1/400 $mm^2$) and counted in duplicate with a microscope (Leica). Viable cells remained colourless while non-viable cells were stained blue. Both viable and non-viable cells were counted.

### 2.2.2 Countess automated cell counter

Sample preparation for cell counting was as described in section 2.2.1, except that 10 µl of the cell suspension/trypan blue mixture was pipetted onto a plastic slide instead of the haemocytometer. This was also done in duplicate. The slide was then inserted into the slot on the front of the Countess automated cell counter (Countess) instrument and the count cells option was selected on the main screen. Cell density data (total, viable and dead), viability and cell size data was presented on screen and noted manually.

### 2.2.3 Optical density

A 1 ml sample of fresh medium was pipetted into a cuvette (Fisherbrand) and was used to blank the apparatus at a wavelength of 600 nm. Next, a 1 ml sample of the cell suspension was pipetted into a cuvette, placed in the UV spectrometer and the absorbance value recorded at the same wavelength. This was done in duplicate.

### 2.2.4 Measurement of capacitance

Off-line capacitance measurements from the Biomass Monitor were conducted as follows: Capacitance measurements at 0.2 and 10 MHz and 0.6 and 10 Mhz were carried out using the Biomass Monitor Model 210 developed by Aber Instruments Limited (Aber Instruments 2008). A 250 ml graduated cylinder containing a magnetic

stirring pellet was placed on top of a magnetic stirrer and heater (IKAMAG RCT). A 35 ml sample of supplemented medium was poured into the 250 ml glass graduated cylinder. The Biomass Monitor probe was attached to the head amplifier and the tip of the probe was adjusted so that it was immersed at least 10 mm into the medium. The Biomass Monitor probe used for all work was a four pin electrode (NBLP 470) and this was chosen to minimise the effects of polarisation (Davey and Kell 1998). The probe was secured by a retort stand and clamp which was marked to ensure that the same position was used for the duration of the experiment. The unit was connected to the mains and grounded via the back panel for extra safety, as this was stated explicitly in the user manual.

The Biomass Monitor was switched on and the dual frequency mode of 0.2 and 10 MHz was set. The magnetic stirrer was set to a speed of 120 RPM for all work unless otherwise stated. The temperature was set to 30 °C. The low pass filter was used to help reduce noise in measurements and was set at 5 $s^{-1}$. The apparatus was left for two hours to equilibrate until a steady baseline was achieved. The probe was then removed from the blank medium. The blank medium was transferred to a 50 ml centrifuge tube and a 40 ml cell suspension sample was gently poured from a separate centrifuge tube into the 250 ml graduated cylinder. The probe was immersed into this as described above and the reading allowed stabilise before recording. Data was collected manually once the readings stabilised.

Further to the setup and use of the Biomass Monitor as detailed above the following protocol was used for analysis of the high cell density suspension (2.3.3.2) and the real time culture (RT and RT 2, see 2.3.3.4) suspensions. When the Biomass Monitor was used at 2 frequency settings; 0.2 and 10 MHz and also 0.6 and 10 MHz, for the same cell suspension the following protocol was followed. The frequency was set at 0.2 and 10 MHz and probe immersed into the cell suspension at 30 °C, capacitance recorded then the probe removed, the frequency setting changed to 0.6 and 10 MHz, the probe immersed in blank medium and zeroed once the reading had stabilised (approximately 5 minutes). The probe was then removed from the blank medium and re-inserted into the cell suspension and the capacitance recorded once the reading had stabilised. The temperature was increased to 37 °C and the capacitance was recorded for both dual frequency settings as at 30 °C once the readings had stabilised. The next serial dilution followed and the analysis protocol

was followed starting again at 30 °C at the 2 dual frequency settings then heating to 37 °C until all serial dilutions were complete.

## 2.3 Experimental set up

### 2.3.1 Batch and Fed Batch cultures of CHO 320 cells

Both Batch (B) and Fed Batch (FB) cultures were cultivated for a period of 216 hours in medium, supplemented with 4 mM L-glutamine and 1 μM methotrexate (MTX) at 37 ºC, with 2 ml being drawn from both cultures per day for substrate and metabolite analysis. The results of the substrate and metabolite analysis can be found in Appendix E. Fed Batch cultures were maintained at 50 ml by the addition of 2 ml of supplemented medium beginning at 24 hours.

The Batch and Fed Batch cultures were compared in terms of cell growth kinetics and maximum cell density achievable (to progress onto use with the Biomass Monitor), with corresponding substrate consumption and metabolite production profiles being analysed (and presented in Appendix E.1-5) using commercial enzyme kits: glucose (Sigma Aldrich, GAGO20), glutamine kit, (Sigma Aldrich, GLN - 1), ammonia (Sigma Aldrich, AA0100) lactate assay kit (Biovision, K627 - 100), and the recombinant protein IFN-γ (Biacore analysis, T100). A CHO 320 cell culture which was started from a thawed ampoule was allowed to grow for 6 days and on day 6; cells were subcultured to a density of $0.3 \times 10^6$ cells/ml in $2 \times 250$ ml glass Erlenmeyer flasks. The 2 subcultures taken from the same original culture at the same time were used to commence a Batch and Fed Batch culture. The Batch culture had an initial volume of 50 ml and the Fed Batch culture had an initial volume of 52 ml.

Every 24 hours, starting from 0 hours, samples for cell counts by microscope and haemocytometer, substrate and metabolite analysis and protein quantification were taken.

### 2.3.2 Determination of possible interferences on the biomass probe in a bioreactor environment

Interferences including Biomass Monitor probe position in relation to vessel walls, base of vessel, pH and $pO_2$ probe, stirrer speed and presence of aeration were

investigated as these areas are reported in literature to cause interference with capacitance signal (Dabros et al. 2009; Davey and Kell 1998).

The Biomass Monitor probe was set up in the centre of a 1 L beaker so that the probe centre was 50 mm from the vessel wall. The tip of the probe was 50 mm from the base of the beaker in which there was a magnetic pellet. The beaker containing 1 L of EXCELL CHO DHFR$^-$ medium with supplements was situated on top of a hotplate and magnetic stirrer as per the schematic diagram shown in Figure 3. Apart from the test for the effect of agitation speed, the stirrer speed was set to 120 RPM for all measurements and all readings were taken at a temperature of 37 °C.

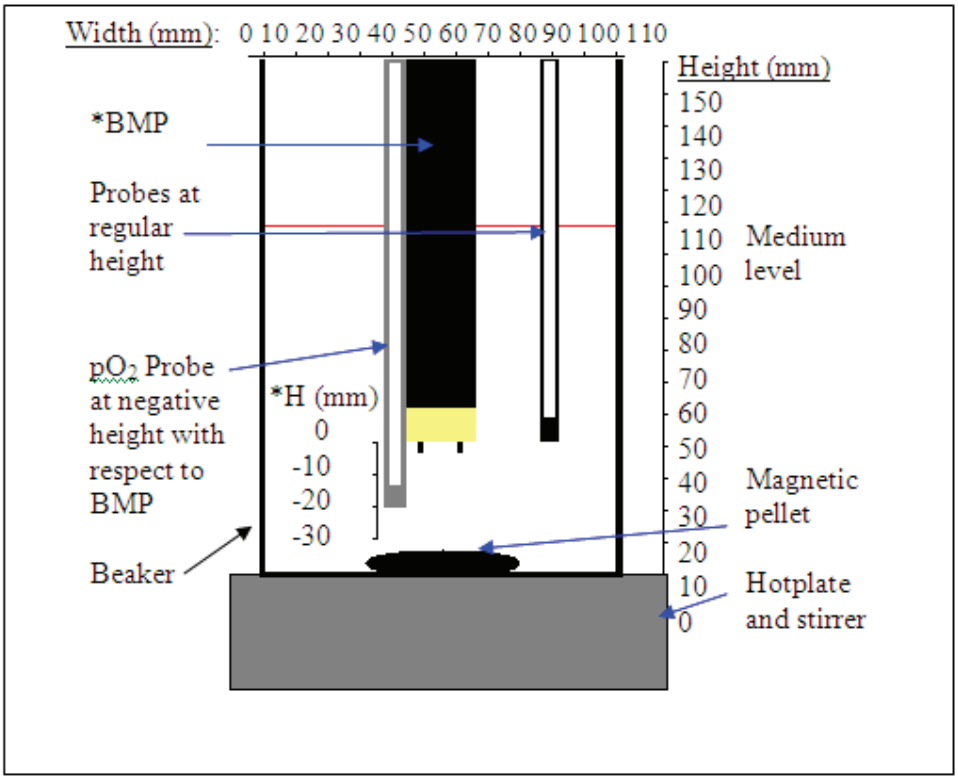


**Figure 3:** Schematic diagram of Biomass Monitor probe positional study.
(*BMP: Biomass Monitor probe, *H: Negative height of $pO_2$ probe relative to Biomass Monitor probe in mm).

The Biomass Monitor was turned on and equilibrated as described in Section 2.2.4, with dual frequency setting of 0.2 and 10 MHz for 2 hours. The vessel was covered with parafilm with the biomass probe protruding. Interferences were tested by moving the probe 10 mm at a time towards the suspected source of interference. For each movement, the capacitance signal was allowed five minutes to stabilise. Five

readings at 20 second intervals were taken. The average reading at each position was used for analysis.

It was decided not to bring the Biomass Monitor probe to a distance less than 20 mm from the base of the 1 L vessel as the electrodes may have been damaged if the stirrer pellet impacted in them.

To test the effect of agitation, the stirring rate was varied from 120 – 600 RPM in 120 RPM increments in a 1 L glass beaker with a magnetic pellet. For aeration, the presence of bubbles was investigated by sparging air through the 1 L beaker directly beneath the probe and to the side of the probe allowing a comparison between the two conditions.

### 2.3.3 Correlation determination for capacitance with viable cell density and viable cell volume and optical density with viable cell density

To determine both the lower and upper limits of viable cell concentration which the Biomass Monitor could detect, a high cell density suspension was cultured and serially diluted to a low cell density. The desired upper limit for this experiment was aimed to achieve above $40 \times 10^6$ cells/ml which is industrially relevant as cell densities encountered in industrial applications can reach $30 – 40 \times 10^6$ cells/ml, in perfusion and immobilised cultures (Zhang et al. 2008; Meuwly et al. 2007).

Cells were cultured as per Section 2.1.2 and inoculated into 500 ml Erlenmeyer flasks at a 120 ml cell suspension volume. Cells were harvested and concentrated on day 6 per 500 ml flask as follows: A 500 ml flask was removed from the incubator and the cells were counted as per Section 2.2.1. The 120 ml cell suspension was then concentrated by aliquotting $4 \times 30$ ml fractions into $4 \times 50$ ml centrifuge tubes and centrifuged at 200 RPM for 5 minutes. The supernatant was poured off. Each pellet was resuspended in 5 ml fresh medium. The $4 \times 5$ml resuspended cell suspensions were pooled in a 50 ml centrifuge tube creating a 20 ml high cell density fraction at which point cell density was determined as per Section 2.2.1, with a 1/10 dilution of the cell suspension sample in fresh medium to allow cell counting. (This was repeated for the other 500 ml Erlenmeyer flasks until a calculated cell density greater than $40 \times 10^6$ cells/ml was achieved for the next stage.)

The 20 ml high cell density fractions were centrifuged at 200 RPM for 5 minutes. Each of the pellets was resuspended in 5 ml of fresh medium and the

fractions pooled in a 50 ml centrifuge tube. The volume was adjusted to 40 ml with supplemented medium if necessary creating the high cell density suspension.

The cell suspension was serially diluted by removing 20 ml of cell suspension from the graduated cylinder and adding 20 ml fresh medium, the contents were gently mixed. This dilution procedure was repeated until the cell density was less than $0.3 \times 10^6$ cells/ml. At each dilution stage the cells cell density was determined as per Section 2.2.1., and samples were also analysed by Countess (Section 2.2.2), Biomass Monitor (2.2.4), and optical density (2.2.3).

The Biomass Monitor was used to measure capacitance of a high cell density suspension at 2 frequency settings; 0.2 and 10 MHz and also 0.6 and 10 MHz. The effect of measurement temperature was also investigated by recording capacitance readings at 30 °C and 37 °C for both dual frequency settings.

It was decided to repeat this experimental procedure, however with the inclusion of extra protocols as follows: The effect of a changing dual frequency was investigated as was the effect of a changing temperature on the capacitance readings.

#### 2.3.3.1 Prediction models for Biomass Monitor

Three types of calibration models were used in this study defined by the data used in their construction, high cell density suspension, high cell density suspension combined with real time culture data and real time data alone. The real time cultures (RT and RT2) used for this study were separate to the batch and fed batch cultures analysed earlier.

#### 2.3.3.2 High cell density suspension data prediction model

This model only involved cell density data from high cell density suspensions that were serially diluted and was referred to as HCD suspension in the results and discussion. High cell density suspensions were cultured as detailed in section 2.3.3.

#### 2.3.3.3 High cell density data and real time data

The high cell density and real time prediction model referred to as the HCD + RT model was constructed from the all of the individual HCD data points (2.3.3.2) and all of the RT data points (2.3.3.4), that are plotted on the graphs for the individual HCD and RT prediction models.

#### 2.3.3.4 Real time culture

The real time prediction model was solely from a real time (RT) culture. The real time cultures used for this study (i.e. RT and RT 2) were separate to the batch and fed batch cultures analysed earlier (3.1). Cells were cultured as per 2.1.2. On day 6 cells were subcultured into 10 × 250 ml Erlenmeyer flasks, each containing a 40 ml cell suspension volume. Each day a 250 ml Erlenmeyer flask was removed and cell densities determined by microscope and haemocytometer (2.2.1), Countess (2.2.2), optical density (2.2.3) and finally by the Biomass Monitor (2.2.4). Results were manually recorded.

#### 2.3.3.5 Analysis of data

In all three cases, the calibration curve was constructed by plotting the capacitance readings from the Biomass Monitor against the cell density or cell volume data as determined by the microscope and haemocytometer method as detailed in 2.2.1. As the Biomass Monitor was zeroed in fresh medium, the trendline was through the origin and the slopes were noted. The relationship between the capacitance value and viable cell density was a simple linear relationship with the cell density value equal to the capacitance value divided by the slope of the calibration curve and the same for the viable cell volume.

The slopes of the three calibration models formed from the HCD, HCD + RT and RT data were applied to predict the cell density of RT 2, conducted as detailed in 2.3.4.4. The data was compared to the measured RT 2 data range that was plotted as a Y=X line in the predicted versus measured graphs in the results and discussion section and the cell density data predicted from the HCD, HCD + RT and RT models can be seen displayed on the graphs and compared to the measured RT 2 data range.

This procedure was repeated for optical density (OD) data as it was decided to apply similar models for the prediction of viable cell density data to OD, as OD is a common method in the estimation of viable cell density.

#### 2.3.3.6 Validation of Biomass Monitor calibrations

To confirm that Biomass Monitor signal attained for the cell suspensions was indeed from the biomass content, after two dilutions, the probe was immersed in blank media to allow the capacitance readings to stabilise, ideally 0 pF/cm, but within the

acceptable range of +/- 0.2 pF/cm, (Aber Instruments). This validation was also conducted after the real time culture experiments. This check was to ensure that changes in the signal were due to the biomass content of a sample as the only difference between the blank media and test samples would be the biomass content of the samples.

### 2.4 Data analysis

#### 2.4.1 Calculation of specific growth rate

The specific growth rate (μ) for each culture was determined from of a plot of the natural log (ln) of viable cell density versus time. The exponential phase was determined by finding the time period where there was a linear relationship between ln (viable cell density) versus time. A number of trendlines were plotted between different points on this graph and the slope of the trendline with the highest $R^2$ value was taken to be the apparent specific growth rate. Maximum cell density was read from cell density versus time curves for Batch and Fed Batch cultures 1-3.

#### 2.4.2 Analysis of predictions

The predictions for viable cell density and viable cell volume by Biomass Monitor readings and cell density by optical density measurements were assessed using the root mean square error prediction (RMSEP).

**Equation 1:** $$\text{RMSEP}= \sqrt{\frac{\sum_{i=1}^{n}(\hat{y}_i - y_i)^2}{n}}$$

Where:

$y_i$ = Microscope and haemocytometer value.

$\hat{y}_i$ = Value predicted from slope of calibration curve.

n=number of samples the prediction was applied to.

# 3. Results and Discussion

### 3.1 CHO 320 cell growth data

To investigate the effect of medium addition on cell growth rate and maximum cell density, CHO 320 cells were cultured in Batch and Fed Batch conditions.

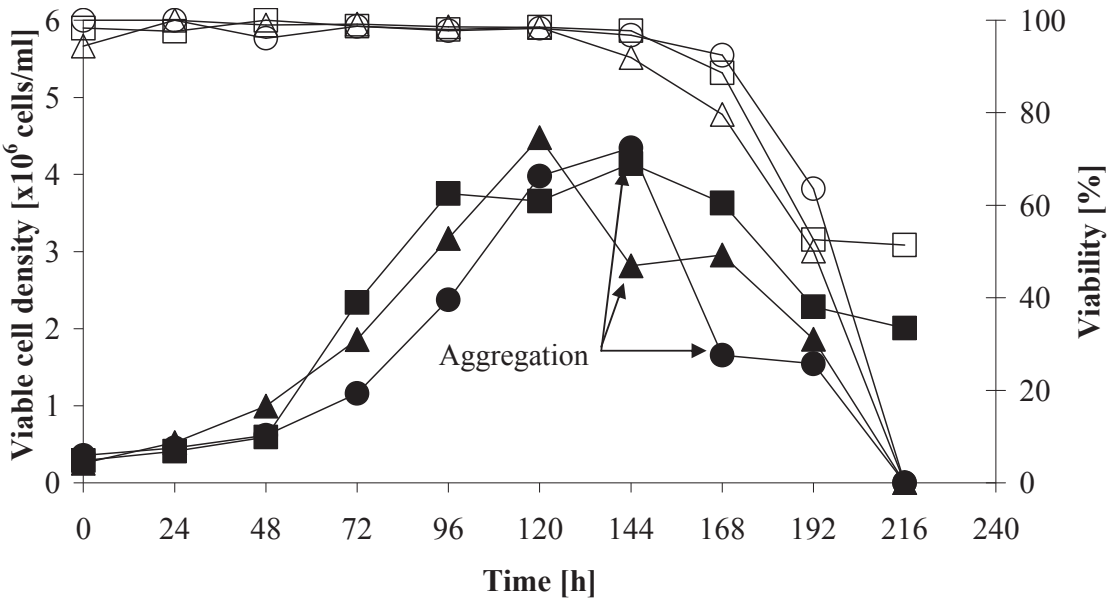


**Figure 4:** Viable cell density and viability versus time for Batch cultures 1-3. Symbols: Viable cell density for Batch culture 1 (■), Batch culture 2 (▲), Batch culture 3 (●), viability Batch 1 (□), Batch 2 (Δ) and Batch 3 (○).

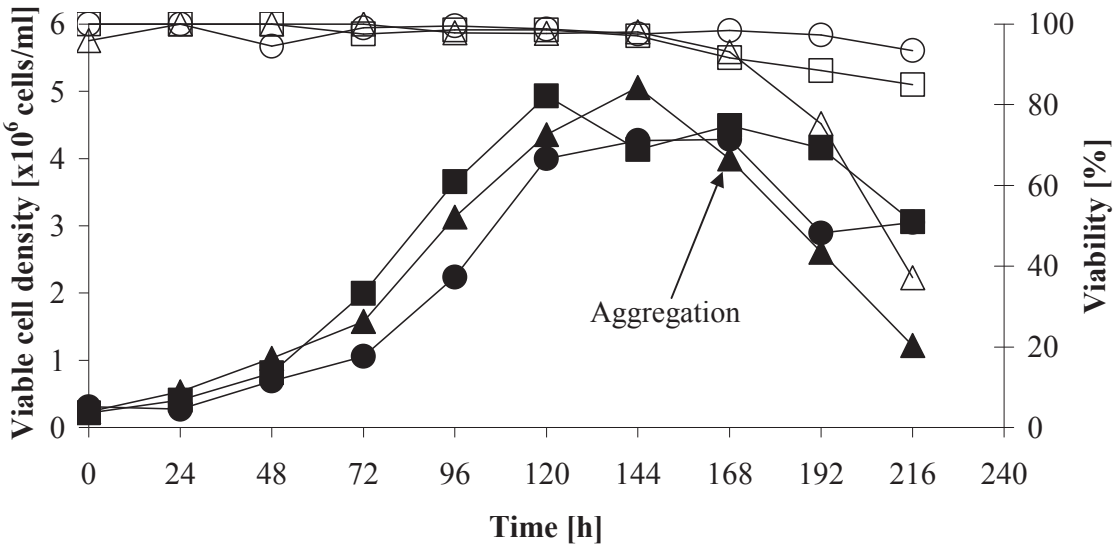


**Figure 5:** Viable cell density and viability versus time for Fed Batch cultures 1-3. Symbols: Viable cell density for Fed Batch culture 1 (■), Fed Batch culture 2 (▲), Fed Batch culture 3 (●), viability Fed Batch 1 (□), Fed Batch 2 (Δ) and Fed Batch 3 (○) versus time.

The growth phase of Batch cultures 1 - 3 (Figure 4) and Fed Batch cultures 1 - 3 (Figure 5), up to the time period of 120 hours was characterised by continuous cell density increase with high viability (V > 95 %) and was consistent with other reported studies (Michiels et al. 2011; Lim, et al. 2006). After 120 hours, the growth kinetics of the Batch and Fed Batch cultures diverged. The specific growth rates were summarised in Table 5.

With reference to the cell growth and death phases from Figure 4, viability decrease began with viability dropping below 90 %, indicating the onset of the death phase at 144 hours and reached 0 % by 216 hours in Batch cultures 2 and 3. Viability of Batch culture 1 did decrease but did not decrease below 90 % until the time period of 144 – 168 hours.

The results of the Fed Batch cultures in Figure 5 show feeding resulted in an increased viability by 24 hours in all three Fed Batch cultures in agreement with the observations of Huang Marquis and Gray (2004), with the lowest viability recorded

of 37.1 % at 216 hours. The first sign of a loss of viability in all Fed Batch cultures occurred between the time periods of 144 - 168 hours. The extent of the drop between 144 – 168 hours varies between the Batch and the Fed Batch cultures as can be seen from Table 3, with Batch cultures 2 and 3 viability decreasing to below 90 %.

**Table 3:** Summary of viability decrease for Batch and Fed Batch cultures with viability at end of culture displayed.

| Culture type and number | Viability decrease between 144-168 hours [%] | Viability at 216 hours [%] |
|---|---|---|
| Batch 1 | 97.7 – 88.6 | 51.4 |
| Batch 2 | 91.9 – 79.6 | 0 |
| Batch 3 | 96.7 – 92.5 | 0 |
| Fed Batch 1 | 97.1 – 91.6 | 85.0 |
| Fed Batch 2 | 98.1 – 93.1 | 37.1 |
| Fed Batch 3 | No drop | 93.0 |

It is known that cells adapted to suspension have a tendency to aggregate into large and uncontrolled cell clumps, which may lead to reduced product secretion, altered cell metabolism and cell death (Li et al. 2011). Aggregation is reported to be in part due to an inbuilt adaptive reaction of mammalian cells in response to stresses caused by physical or chemical means such as substrate limitation. This aggregation response is capable of adjusting the levels and/or activity of the genome protecting machinery through the synchronization of cell cycle arrest, DNA repair and apoptosis (Astley et al. 2007). Such an aggregation response was observed in both the Batch and Fed Batch cultures with the response in Batch cultures being apparent between the time periods of 144 - 168 hours (Figure 4) and the Fed Batch cultures exhibiting the response at 168 hours (Figure 5), indicating that feeding of 2 ml/day did not prevent aggregation, therefore to inoculate new cell cultures, cells should always be subcultured from an on-going culture by the time period of 120 hours (day 6). This is in order to avoid inoculating a new cell culture with aggregated cells.

The maximum cell densities and corresponding times are summarised in Table 4, with the average maximum cell densities being $4.32 \times 10^6$ cells/ml (B) and $4.75 \times 10^6$ cells/ml (FB), a 9 % difference between the Batch and Fed Batch cultures.

**Table 4:** Maximum cell densities and corresponding time displayed for Batch and Fed Batch culture 1-3.

| Culture type and number | Maximum cell density [$\times 10^6$ cells/ml] | Time (hours) |
|---|---|---|
| Batch 1 | 4.14 | 144 |
| Batch 2 | 4.48 | 120 |
| Batch 3 | 4.34 | 144 |
| Fed Batch 1 | 4.93 | 120 |
| Fed Batch 2 | 5.05 | 144 |
| Fed Batch 3 | 4.28 | 168 |

The only difference between the Batch and Fed Batch cultures was the 2 ml feed per day (or 4 % total culture volume) for the Fed Batch culture.

### 3.2 Identification of exponential phases

The specific growth rate (μ) for each culture as determined from the plots of the natural log (ln) of viable cell density versus time was given in Table 5.

**Table 5:** Specific growth rates of Batch and Fed Batch cultures.

| Culture type and number | Specific growth rate [$h^{-1}$] | $R^2$ | Time period (hours) |
|---|---|---|---|
| Batch 1 | 0.028 | 0.94 | 0 – 96 |
| Batch 2 | 0.026 | 0.99 | 0 – 96 |
| Batch 3 | 0.024 | 0.99 | 0 - 120 |
| Fed Batch 1 | 0.030 | 0.99 | 0 – 96 |
| Fed Batch 2 | 0.026 | 0.99 | 0 – 96 |
| Fed Batch 3 | 0.028 | 0.98 | 24 – 96 |

Specific growth rates were in agreement with other CHO cultures reported in literature by (Zhu et al. 2005; Jacobson and Morgan 1995; Hayter et al. 1991), however growth rate can be affected by subculture number and plasmid losses

(Kurano et al. 1990). The Fed Batch culture specific growth rates were not greatly increased by the feed of 2 ml/day.

### 3.3 The effect of environment on the capacitance signal

The results of the investigation into interferences to capacitance signal from the Biomass Monitor are presented in this section. The capacitance signal from the Biomass Monitor can be subject to interference from the vessel walls and metal structures in the reactor such as and $pO_2$ probes (Dabros et al. 2009; Davey and Kell, 1998).

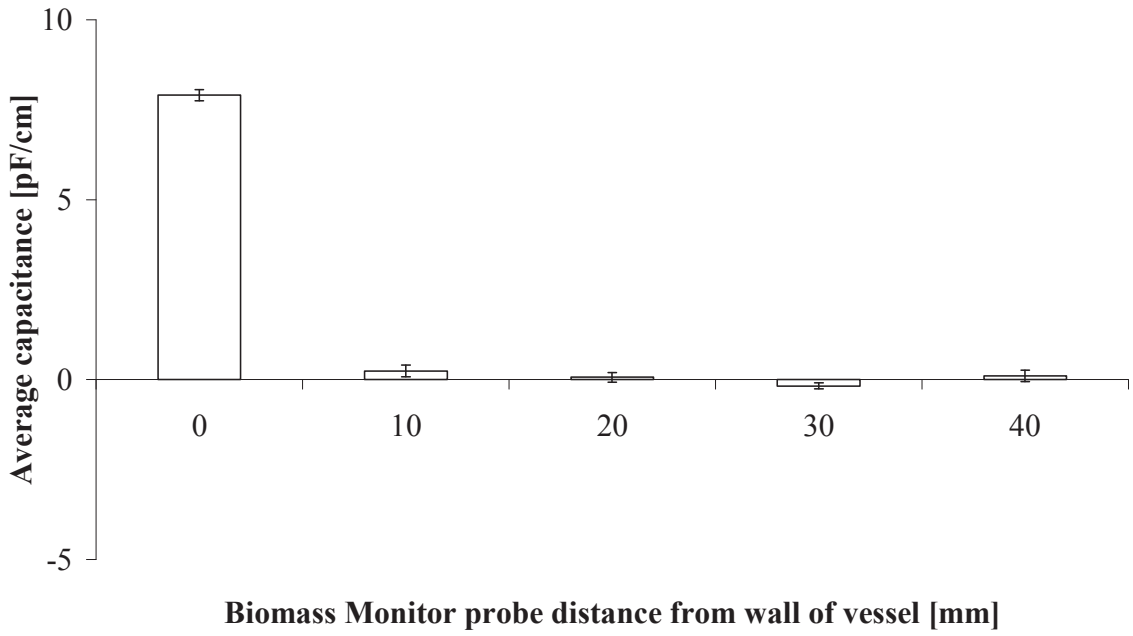


**Figure 6:** Average capacitance versus Biomass Monitor probe distance from wall of vessel.

As was seen from Figure 6, positioning the Biomass Monitor probe beside the glass wall of the vessel gave a positive capacitance value in an environment with no cells, while the capacitance values were negligible when the probe was at a distance of at least 10 mm from the vessel wall. This indicated that the walls of the vessel caused interference to the capacitance readings of the Biomass Monitor. In light of this the probe should not be situated in a reactor vessel within 10 mm of the side wall to minimise disturbances.

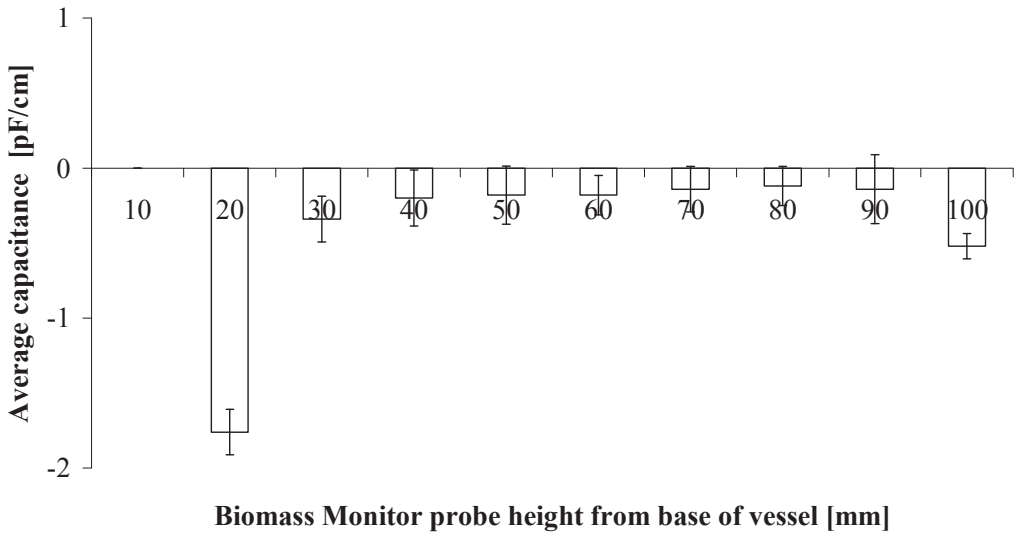


**Figure 7**: Average capacitance versus Biomass Monitor probe height from base of vessel.

As was seen in Figure 7, there are two points of interference, a height of 20 mm above the stirring pellet and 100 mm above which corresponded to the point where the electrodes were less than 20 mm from the liquid surface. This indicates that the biomass probe should be a minimum of 30 mm from the stirrer or turbine and the electrodes should be submerged under a minimum of 10 mm of medium.

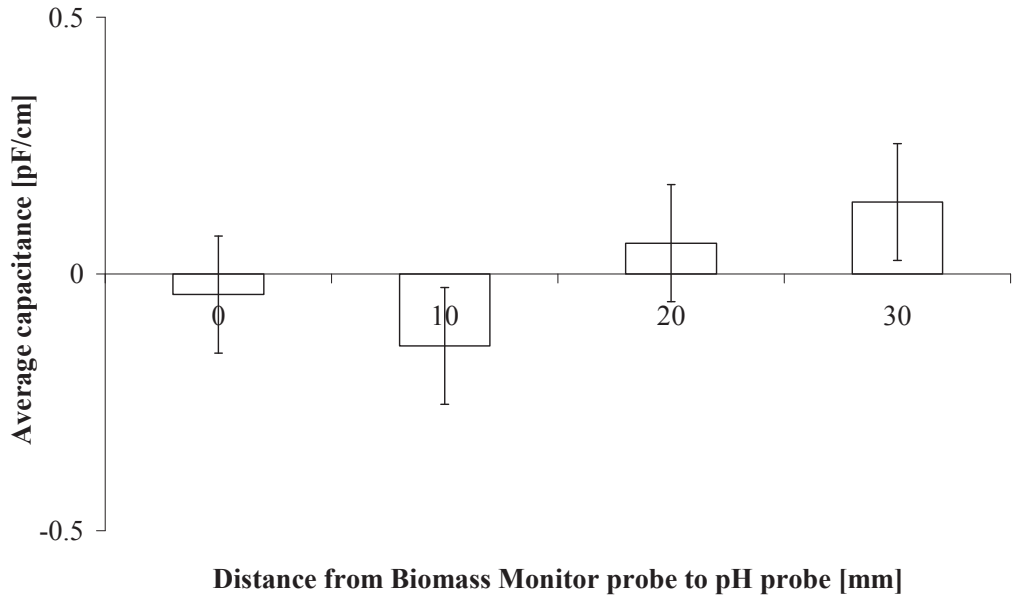


**Figure 8**: Average capacitance versus distance from Biomass Monitor probe to pH probe.

Figure 8 showed the average capacitance values when the Biomass Monitor probe was positioned at varying distances from the pH probe. As the pH probe was moved closer to the Biomass Monitor probe no noticeable interference to the capacitance signal could be attributed to the proximity of the pH probe. The pH probe was even moved directly below the Biomass Monitor probe and no quantifiable effect on the capacitance readings.

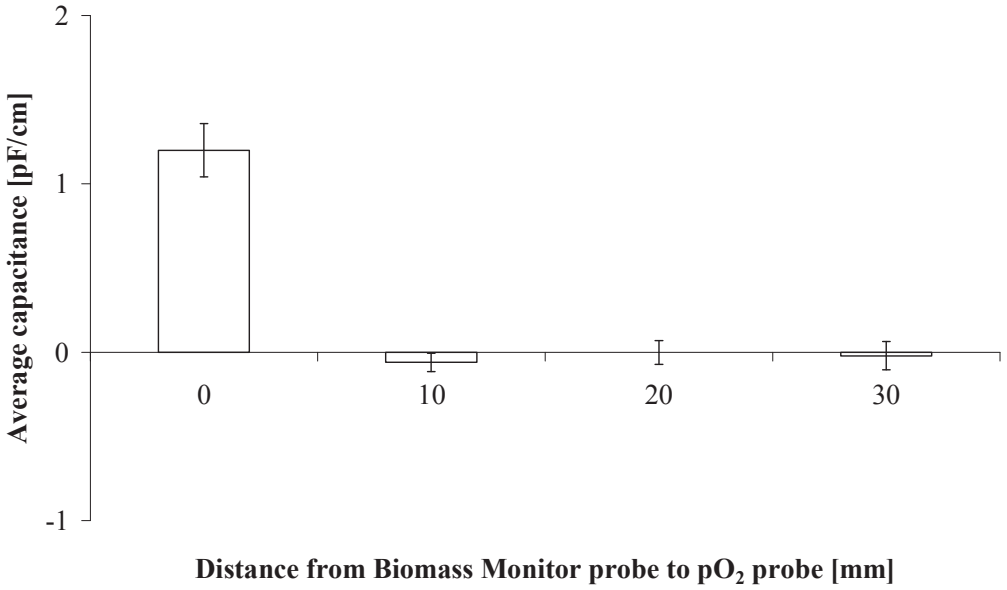


**Figure 9**: Average capacitance versus distance from Biomass Monitor probe to $pO_2$ probe.

In addition to the pH probe, another probe that is common in a bioreactor is the $pO_2$ probe which is of steel composition (Nienow 2006). In contrast to the pH probe the $pO_2$ probe was noted to affect the capacitance readings from the Biomass Monitor. This can be noted in both Figures 9 and 10.

As the $pO_2$ probe was moved closer to the biomass probe in a horizontal direction (Figure 3), interference to capacitance signal can be noted when the biomass probe and $pO_2$ probe are located directly alongside each other, with both the biomass probe and $pO_2$ probe 50 mm from the base of the vessel see Figure 3. This suggests that placement of the Biomass Monitor probe within 10 mm of the tip of the $pO_2$ probe may lead to interference and an incorrect capacitance signal in a culture environment. From the results of Figure 9 it can be recommended that the distance between the Biomass Monitor and $pO_2$ probes be no less than 10 mm in a culture environment.

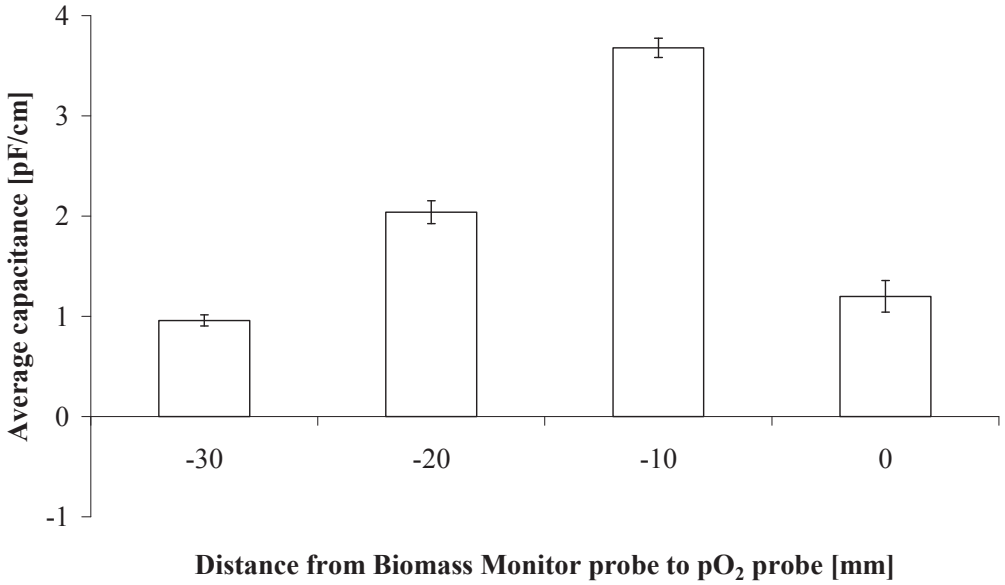


**Figure 10:** Average capacitance versus distance from Biomass Monitor probe to $pO_2$ probe.

Once the $pO_2$ and biomass probes were together and in direct contact, the $pO_2$ probe was moved upwards along the $pO_2$ probe shaft with low interference evident (data not shown), however, when the tip of the $pO_2$ probe was moved below the biomass probe (as denoted by the negative symbols in Figure 10) while the $pO_2$ probe was still being located directly beside the Biomass Monitor probe an interference was noted, particularly when the $pO_2$ probe was lowered and located at 10 mm below the electrodes of the Biomass Monitor probe, see Figure 3 for schematic diagram of experimental setup.

This indicates that if a longer $pO_2$ probe was used during a culture and the $pO_2$ probe tip was located within 10 mm, in direct contact, or up to 30 mm below the tip of the Biomass Monitor probe when the probes are aligned together (for example if the two probes were located in adjacent ports) interference may occur. A resulting recommendation is that one should not situate such probes in close proximity inside a bioreactor.

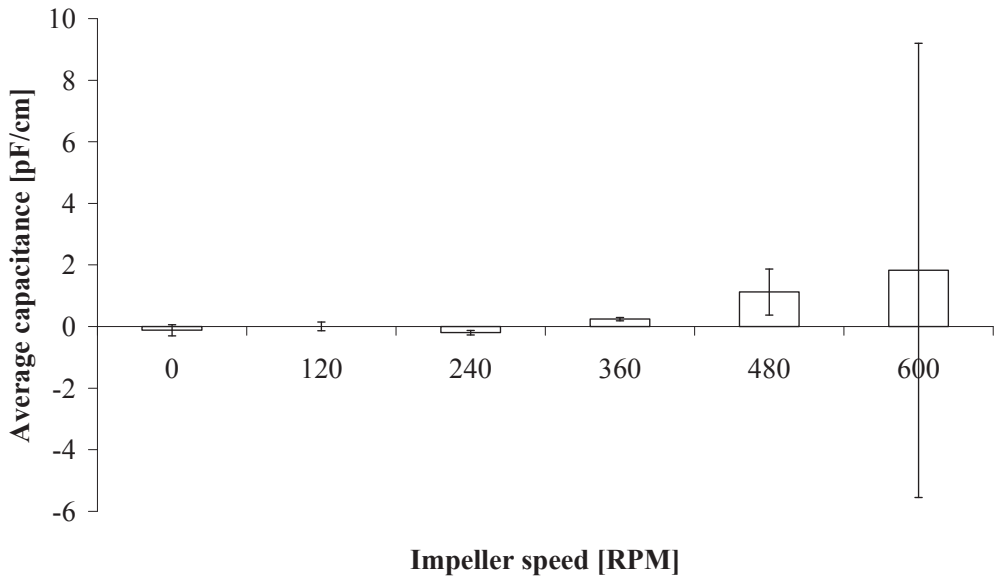


**Figure 11**: Average capacitance from Biomass Monitor probe versus a varying RPM speed.

As can be seen from Figure 11, impeller speed was varied in increments of 120 RPM and as the RPM passed 360, capacitance readings were found to change. The observation was that a vortex was created at the higher RPM speeds in which bubble entrainment occurred dynamically, i.e. bubbles both entered and left the medium through the upper interface and swirled among the electrodes; as RPM increased so did the intensity at which this took place, leading to the observation that the capacitance readings were not affected by the RPM itself but indirectly as bubbles were pulled from the surface and circulated around the biomass probe.

Table 6 shows the effect of aeration with the sparger in a position 30 mm below the biomass probe. The subsequent sparging led again to the interference of capacitance readings and an unsteady baseline. However when situated to the side of the biomass probe, interference decreased but was still present.

**Table 6**: Data for introducing aeration into the vessel in presence of biomass probe.

| Aeration/Position | Capacitance [pF/cm] Readings (every 20 seconds) | | | | | Average Capacitance [pF/cm] | Standard Deviation |
|---|---|---|---|---|---|---|---|
| | 0 | 20 | 40 | 60 | 80 | | |
| No Sparging | 0 | 0.1 | 0 | -0.1 | 0.1 | 0.02 | 0.083 |
| Sparger directly below Biomass Probe | -1.4 | -0.5 | -2.9 | -3.1 | 1.2 | -1.34 | 1.781 |
| Sparger at other side of vessel to biomass probe | 0.2 | -0.6 | -0.8 | -0.6 | -0.6 | -0.48 | 0.389 |

The results attained from the tests investigating the effect of environment on capacitance signal suggest that the following recommendations should be followed when placing the biomass probe into a reactor vessel. The biomass probe should be located no less than 10 mm from the side wall of the vessel; the side wall tested was the glass wall of a 1 L beaker and the same would apply to a bioreactor vessel wall. The stirrer should be more than 20 mm away from the biomass probe with the probe submerged with a minimum liquid height of 10 mm above the electrodes of the probe.

The pH probe had little effect on the capacitance signal but a 10 mm distance should be implemented. The distance of the $pO_2$ probe to the Biomass Monitor probe should be at least 10 mm when it is positioned either at the same level from the base of the vessel or if it is below the level of the Biomass Monitor electrodes, (Figure 9 and Figure 10). Finally the Biomass Monitor probe should be placed as far away as possible from the sparger to reduce the possibility that bubbles will interfere with the readings in a bioreactor, however this would need to be evaluated in a bioreactor before a culture was initiated.

## 3.4 Development of a capacitance calibration model to monitor biomass concentration in real time and comparison to other off-line techniques

### 3.4.1 Cell density determination

The ability of the Biomass Monitor to measure high cell densities in suspension was tested for the CHO 320 cell line. In addition the Biomass Monitor was compared to other methods including automatic cell counting with the Countess and optical density ($OD_{600}$) which is a common method for biomass determination in both yeast fermentations (Olsson and Nielsen 1997) and mammalian cell cultures (Akhnoukh, Kretzmer and Schügerl 1996).

An investigation of the effect of changing dual frequency of the Biomass Monitor and the influence of temperature on capacitance readings was also evaluated in this section.

### 3.4.2 Prediction model for viable cell density using the Biomass Monitor capacitance signal at dual frequency settings of 0.2 and 10 MHz and 0.6 and 10 MHz

In this section, the feasibility of using the Biomass Monitor as a tool to monitor cell density in real time was examined. Two dual frequency settings (0.2 and 10 MHz and 0.6 and 10 MHz) (Carvell and Dowd 2006) were investigated and compared in this work as it has been reported that while the 0.2 and 10 MHz setting offers accurate biomass estimations, however it is more susceptible to inaccuracies due to polarisation or over sensitivity to culture conditions (Davey and Kell 1998).

Mammalian cells are usually cultivated at 37 °C. Studying the effect of temperature variation on the capacitance signal is of major importance. It has been shown that lowering culture temperature to 30 °C allows for the enhancement of specific productivity of recombinant proteins (Ahn et al. 2008). Temperature change was noted to affect conductivity during the calibration of the Biomass Monitor. Capacitance readings were measured at 30 °C to investigate if capacitance is as effective to monitor and predict cell density at lower temperatures, refer to 3.4.3 (Influence of temperature on the Biomass Monitor predictions at both dual frequency settings for viable cell density).

Capacitance [pF/cm] values of a high cell density suspension was plotted against viable cell density [$\times 10^6$ cells/ml] as determined by microscope and haemocytometer counts to investigate if capacitance yielded a linear correlation to viable cell density for the CHO 320 cell line.

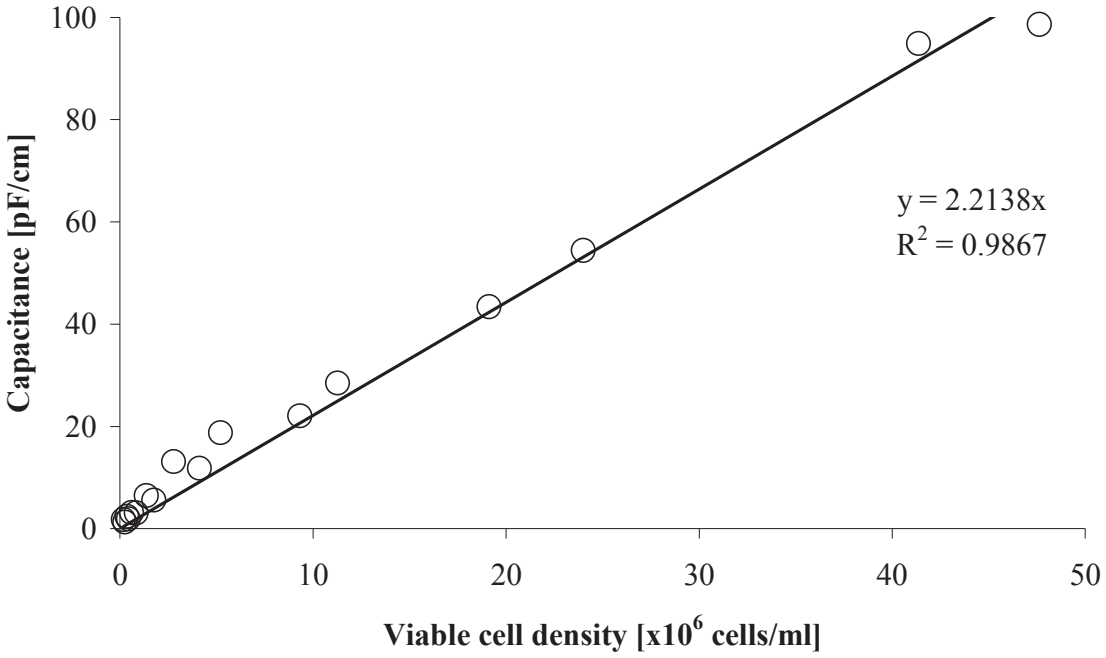


**Figure 12:** Capacitance versus viable cell density for complete HCD suspension at 0.2 and 10 MHz at 37 °C.

From Figure 12 it can be observed that the relationship between capacitance and viable cell density is of an overall linear trend ($R^2 = 0.98$), however cell density at the lower ranges appears to display a different relationship. This is similar to what was found by Cannizzaro et al. (2003). To investigate this, data was split into two cell density ranges with the higher cell density range displayed in Figure 13 and the lower cell density range in Figure 14 (labelled HCD). The differing slopes for the two cell densities ranges indicate that there is a different relationship between the capacitance and viable cell density for the two cell density ranges.

From the literature, a changing cell physiology can affect capacitance readings (Olsson and Nielsen 1997; Matanguihan, Konstantinov and Yoshida 1994). For the HCD suspension cultures, the cell density and physiology is representative of a single point at day 6 when the cell suspensions were harvested. It should be

noted that the relationship of capacitance to viable cell density may differ if the HCD suspension was to be diluted from a different part of the culture, for example if concentration of the cell suspensions took place on day 5 or before. It was however worth investigating if a calibration made from a high cell density suspension from a single point in a culture may be applied to data from any stage of a culture.

.

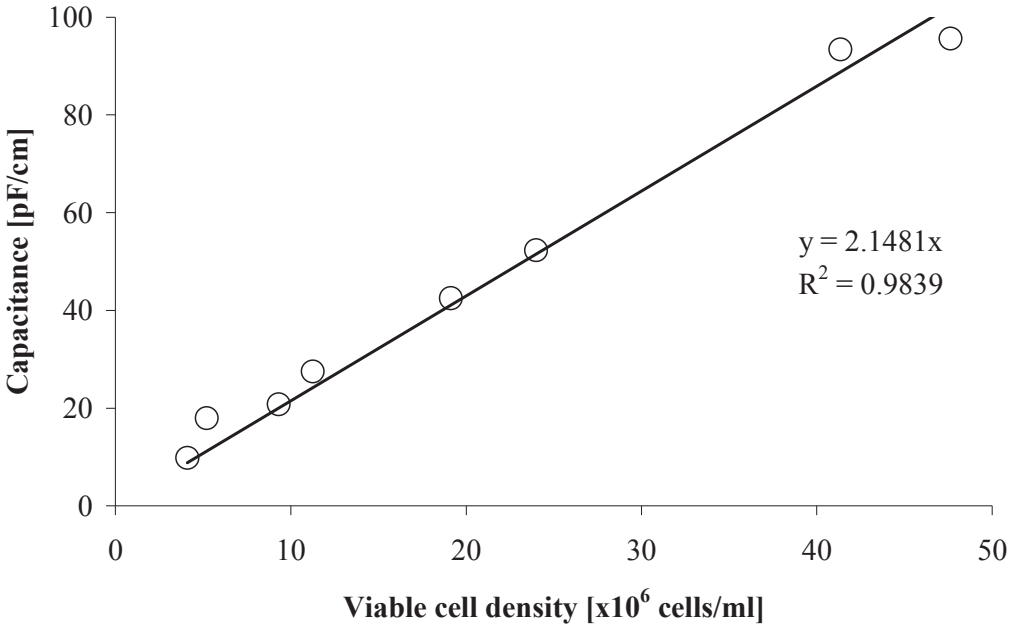


**Figure 13:** Capacitance versus viable cell density for HCD suspension in the higher viable cell density ranges at 0.2 and 10 MHz at 37°C.

The high cell density range has a different relationship between the lower cell density ranges indicating that if cell density increases to the ranges shown in Figure 13, a new prediction model would have to be used to predict viable cell density from the capacitance signal at this setting.

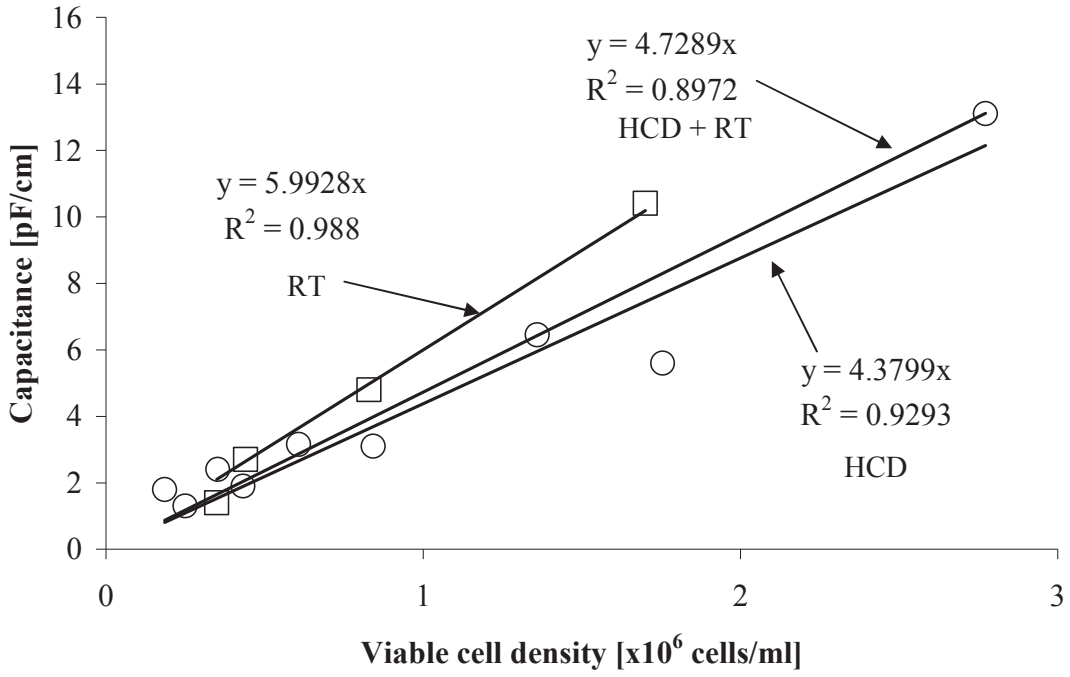


**Figure 14:** Calibration curves for capacitance versus viable cell density at 0.2 and 10 MHz at 37 °C. Symbols: HCD suspension (○) and RT data (□).

Figure 14 shows the calibration curves and equations for the various data sets investigated; the high cell density suspension (HCD), a combination of the high cell density suspension and the real time data (HCD + RT) and the real time data alone (RT). The slope of HCD suspension (y = 4.3799x) and RT data (y = 5.9928x) indicates a minor difference in relationship between the two models. The three slopes were applied to real time data to investigate the best model for prediction of viable cell density from the three different data sets see Figure 15.

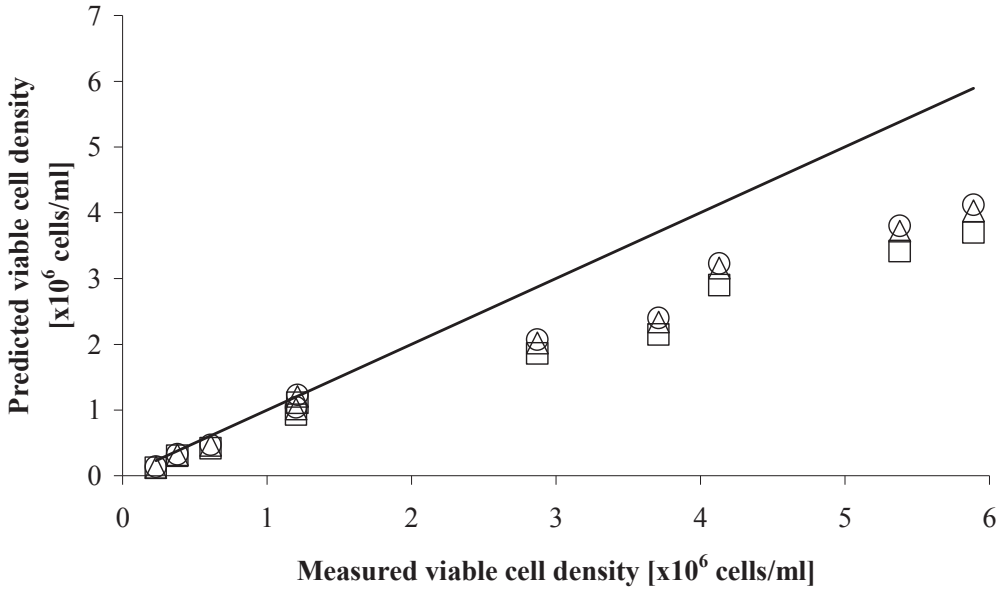


**Figure 15:** Predicted versus measured viable cell density from calibration curves of capacitance versus viable cell density at 0.2 and 10 MHz at 37 °C. Symbols: HCD suspension (○), HCD + RT data (Δ), RT data (□) and Y = X line (—). Refer to Figure 14 for prediction models.

The Y = X line represents the RT 2 cell density data measured using the reference method (microscope and haemocytometer).

All three models were applied to the real time data with the predictions being determined by extrapolation for the higher viable cell densities. From Figure 15, it was seen that there was very little difference between any of the predictions with the lowest RMSEP being 0.61 × $10^6$ cells/ml when the viable cell densities were predicted using the HCD suspension only calibration curve. The highest RMSEP was when only the real time culture data was used to construct the calibration curve (RMSEP = 1.29× $10^6$ cells/ml). The higher error value for this model may simply be due to lack of points used in the extrapolation of the calibration curve.

The underestimation of the models may be attributed to the low range of cell densities used in the construction of the three models, with cell densities not exceeding 3 x $10^6$ cells/ml (Figure 14), while the models are used to predict real time cell density ranges that exceed 3 × $10^6$ cells/ml.

The models accuracy may also have been affected by the RT 2 data in that the maximum cell density exceeded the RT data range; however the construction of the models did not incorporate this data range (Figure 43, Appendix D). RT and RT 2 cultures did show different growth characteristics beyond 96 hours indicating that reproducibility was not shared between the RT and RT 2 culture data, however they did share the same specific growth rate range of Batch cultures 1 – 3 in Table 5 (3.1) ($\mu_{spec}$ of RT = 0.27 $h^{-1}$ and RT 2 = 0.26 $h^{-1}$), with exponential phases ending at 96 hours, while the viability decreases after the maximum cell density is reached at 144 hours.

The calibration models may have been more robust, allowing a more accurate prediction of viable cell density if more RT cultures had been conducted and the data used for the construction of calibration curves.

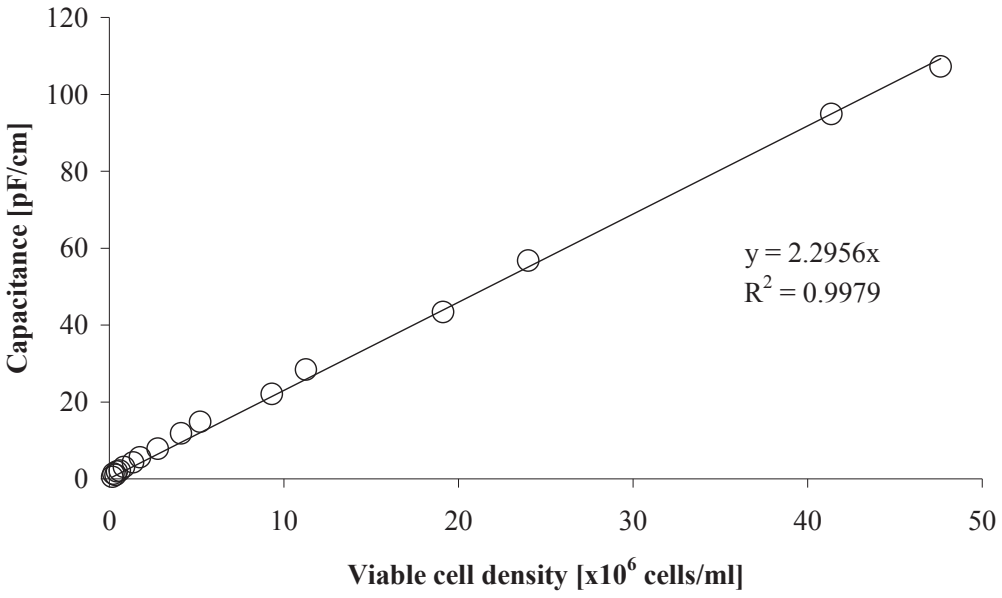


**Figure 16:** Capacitance versus viable cell density for CHO 320 HCD suspension at 0.6 and 10 MHz at 37 °C.

In contrast to when settings of 0.2 and 10 MHz were used, the relationship between capacitance and viable cell density at settings of 0.6 and 10 MHz (Figure 16) shows a more linear trend for the entire range of cell densities. This is in line with what was found in a similar study conducted by Ducommun et al. (2002). This indicates that

the calibration model would be suitable for a cell density range up to 48 × $10^6$ cells/ml, however with the real time cell density range only attaining cell densities in the range of 5 - 6 × $10^6$ cells/ml, the calibration curve range was decreased to be within the range of the real time culture data, see Figure 18.

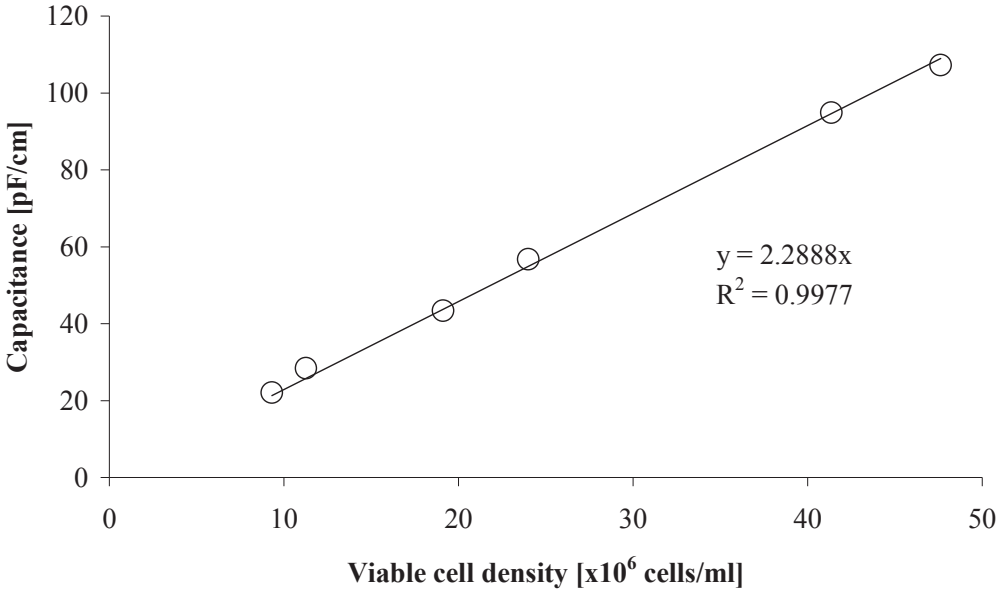


**Figure 17:** Capacitance versus viable cell density for CHO 320 HCD suspension in the higher cell density ranges at 0.6 and 10 MHz at 37 °C.

If cell density exceeded 10 × $10^6$ cells/ml then the model from Figure 17 could be applied to the real time culture data as opposed the model for the HCD line used in Figure 18.

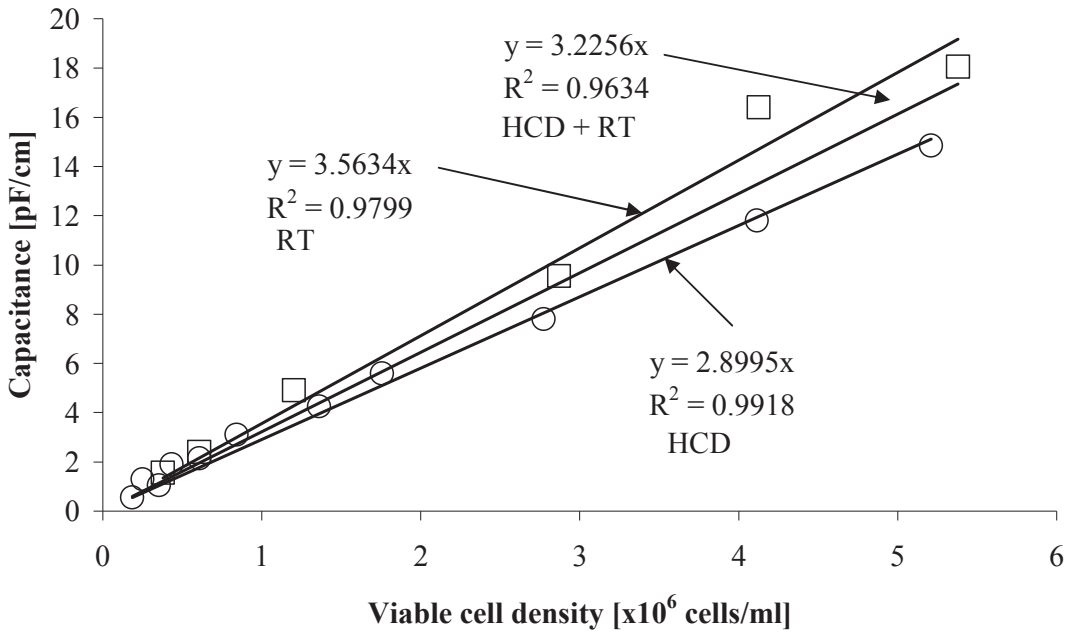


**Figure 18:** Calibration curves for capacitance versus viable cell density at 0.6 and 10 MHz at 37 °C. Symbols: HCD suspension (○) and RT data alone (□).

As before, the data points were split between a higher and lower viable cell density range to suit the cell density ranges. The divergence from a linear trend between the capacitance and the viable cell density values is less pronounced at these dual frequency settings and the slopes for the entire range, the lower range and the high range are a lot closer than those at the different capacitance setting. The calibration curves and corresponding slopes can be seen in Figures 16-18.

The linear trend between capacitance and viable cell densities for the data when the Biomass Monitor settings were at 0.6 and 10 MHz (refer to Figure 18) included higher viable cell densities than when the Biomass Monitor settings were at 0.2 and 10 MHz (refer to Figure 14), allowing the calibration model to include a higher cell density range. All 3 curves show a good linear correlation ($R^2 > 0.96$), with the lowest $R^2$ value in the HCD + RT data set.

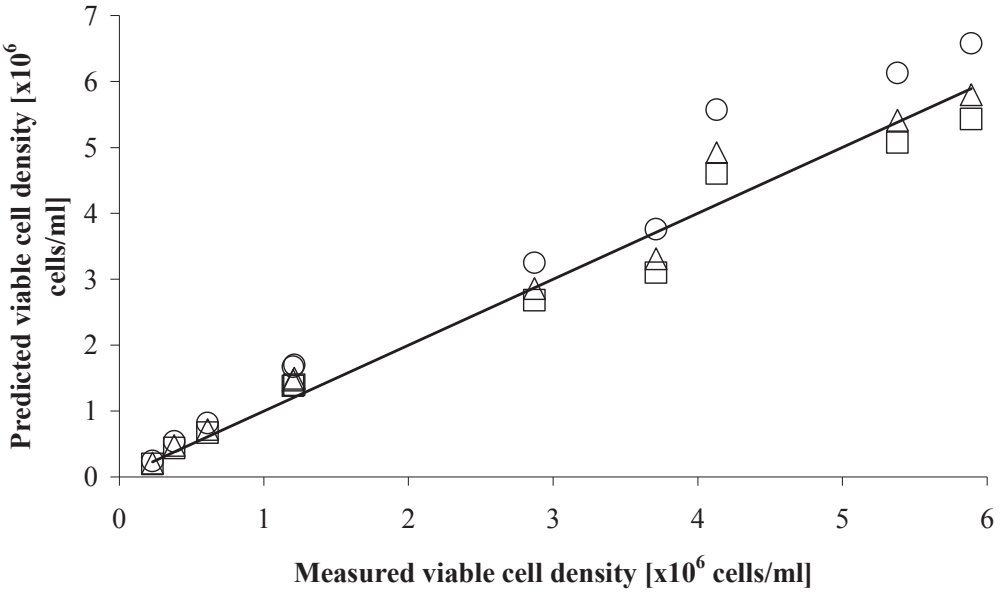


**Figure 19:** Predicted versus measured viable cell density from calibration curves of capacitance versus viable cell density at 0.6 and 10 MHz at 37 °C. Symbols: HCD suspension (○), HCD + RT data (Δ), RT data (□) and Y = X line (—). Refer to Figure 18 for prediction models.

The capacitance readings from the Biomass Monitor set at 0.6 and 10 MHz give better predictions for viable cell density increase and decrease over the course of a real time culture. All three models show predicted data close to the Y = X line (measured RT 2 data). The RMSEP values from calibration models including real time culture data are of the order $0.3 \times 10^6$ cells/ml. This magnitude of this error value is a half of the lowest error achieved when compared to those at the dual frequency settings of 0.2 and 10 MHz at 37 °C.

Extrapolation of data may not be the best approach as other factors may have to be taken into account, for example the affect of temperature or medium conductivity on capacitance readings. Medium conductivity was reported by Pucihar et al. (2001); Noble et al. (1999) to be a function of medium composition and temperature and a significant change (2 - 4 mS/cm) throughout a culture can change the relationship of capacitance to viable cell density, however such a large change was not noted in this study. For the Biomass Monitor settings at 0.2 and 10 MHz at 37 °C, the overall conductivity between the HCD suspension and the RT data used in this study varied by 1 mS/cm, with the recorded conductivity between 12.6 and

13.6 mS/cm. For dual frequency at 0.6 and 10 MHz the conductivity for the range of cell densities tested was in the range of 12.6 – 13.4 mS/cm and was not noted to vary considerably as temperature was fixed and there were no medium or NaOH additions throughout the work. The change of dual frequency from 0.2 and 10 MHz to 0.6 and 10 MHz did not affect the readings of medium conductivity. The influence of a changing temperature of the Biomass Monitor's dielectric spectra was investigated below.

### 3.4.3 Influence of temperature on the Biomass Monitor predictions at both dual frequency settings for viable cell density

In this section the influence of temperature reduction on the capacitance (dielectric spectra) was examined on both dual frequency settings of 0.2 and 10 MHz and 0.6 and 10 MHz. The same cell suspensions were tested, only the frequency settings changed.

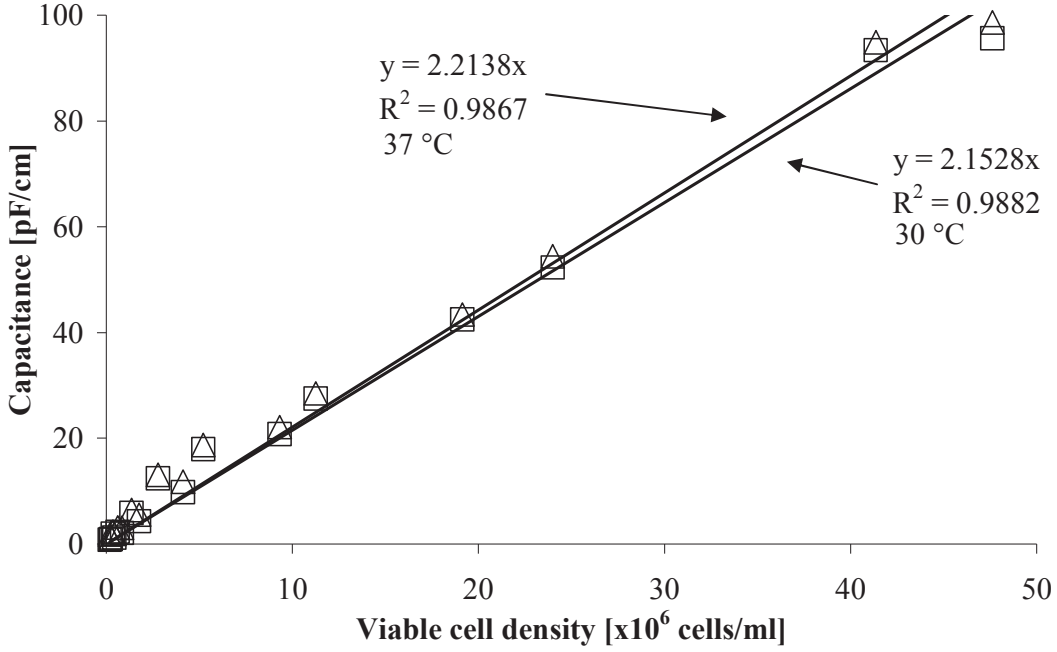


**Figure 20:** Capacitance versus viable cell density for complete HCD suspension at 0.2 and 10 MHz at 30 °C and 37 °C. Symbols: Capacitance at 30 °C (Δ) and 37 °C (□).

From Figure 20 it was noted that capacitance at 37 °C was marginally elevated than the readings conducted at 30 °C.

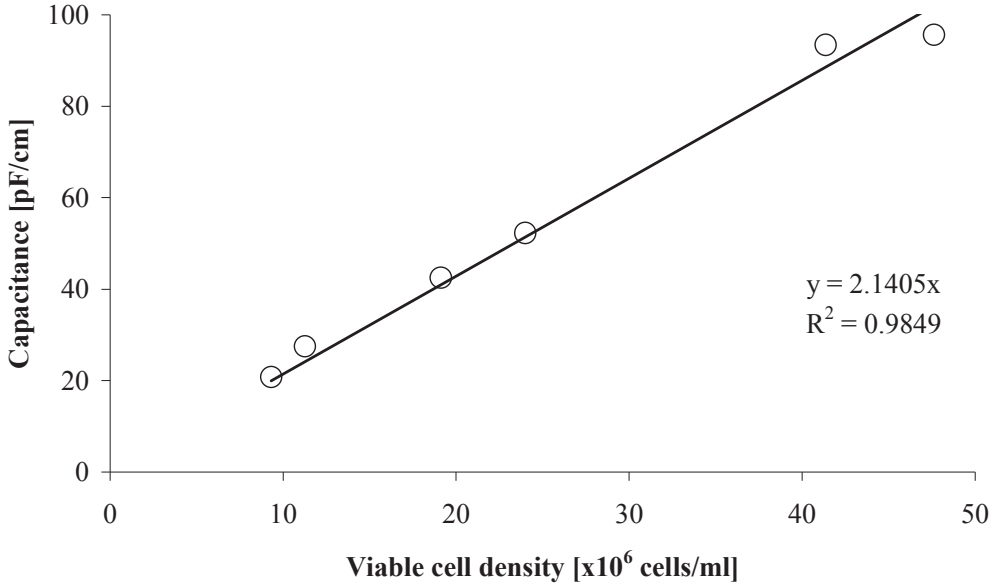


**Figure 21:** Capacitance versus viable cell density for HCD suspension in the higher cell density ranges at 0.2 and 10 MHz at 30 °C.

Capacitance versus viable cell density for HCD suspension in the higher cell density ranges at 0.2 and 10 MHz at 37 °C can be seen in Figure 13.

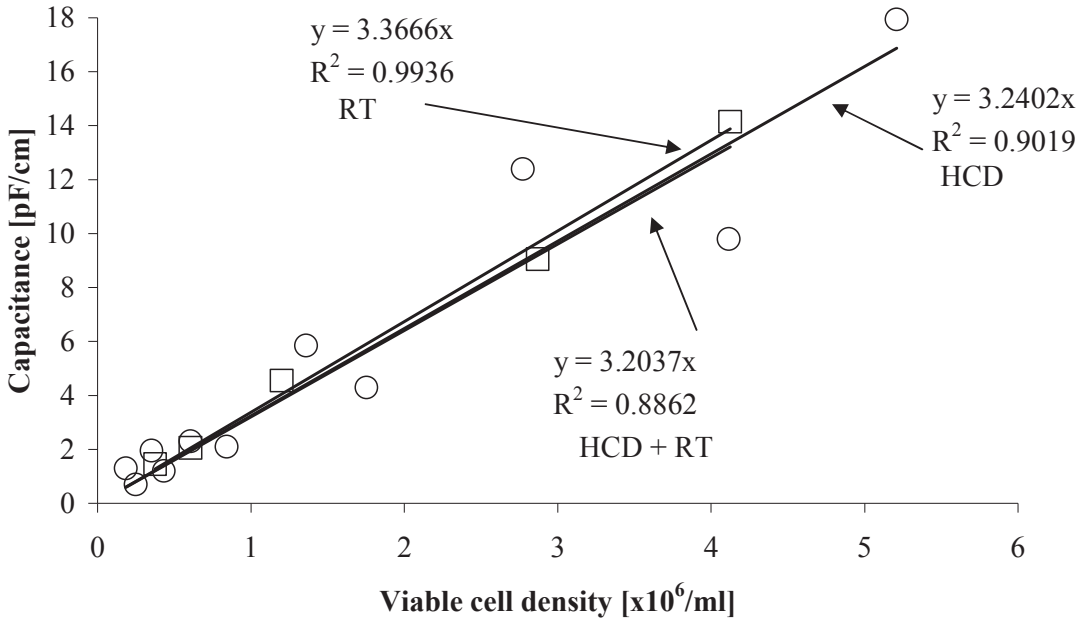


**Figure 22:** Calibration curves for capacitance versus viable cell density at 0.2 and 10 MHz at 30 °C. Symbols: HCD suspension (○) and RT data (□).

Figure 22 displays the three calibration curves that were used as a model to predict viable cell density from real time culture data. All three relationships were noted to be similar; however the $R^2$ values of the 3 calibration curves vary, with the HCD suspension data and HCD + RT data having lower $R^2$ values than the RT data which had the highest $R^2$ of 0.99. All three models had a low RMSEP in the range of 0.3 $\times 10^6$ cell/ml. The HCD calibration curve had a low $R^2$ value with a wide variation in the data used in the construction of the model. If the cell density range for the HCD was lowered the calibration model correlation factor would be decreased ($R^2$ would decrease to 0.8) due to the variation of the data, while the RMSEP would still be in the range of 0.3 $\times 10^6$ cell/ml so the cell density range up to 5.2 $\times$ $10^6$ cells/ml was incorporated into the model to allow a wider range of cell density data not exceeding the cell density range a real cell culture would be expected to reach. The HCD + RT calibration curve displays the lowest $R^2$ value due to the variation between the HCD suspension and RT data sets.

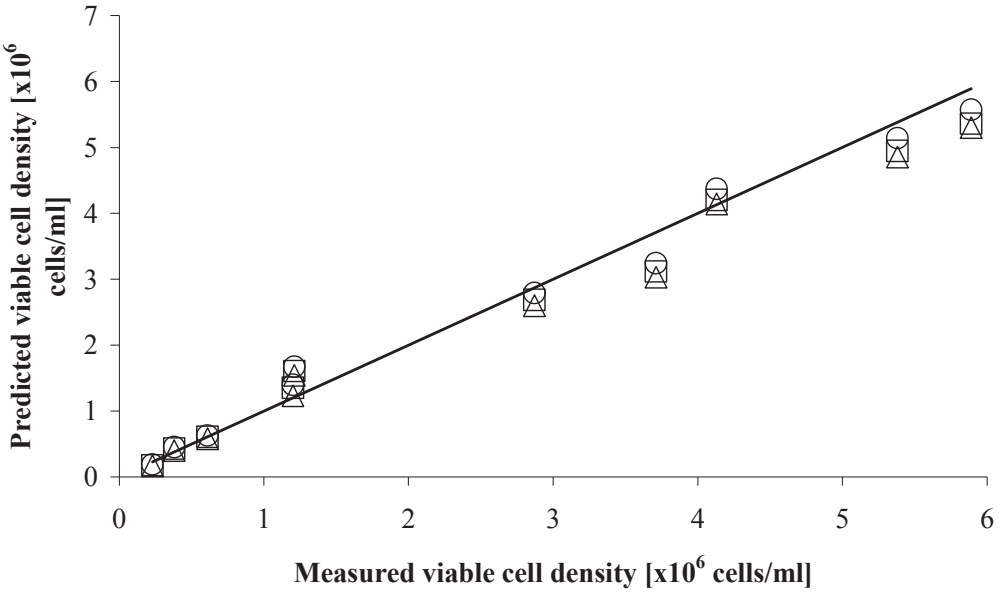


**Figure 23:** Predicted versus measured viable cell density from calibration curves of capacitance versus viable cell density at 0.2 and 10 MHz at 30 °C. Symbols: HCD suspension (○), HCD + RT data (Δ), RT data (□) and Y = X line (—). Refer to Figure 22 for prediction models.

As expected from Figure 23, all three predictions share similar accuracy in the prediction of viable cell density from the capacitance signal from the Biomass Monitor, with the RT data showing the best prediction to the RT 2 data (Y = X line) with an RMSEP of $0.26 \times 10^6$ cells/ml.

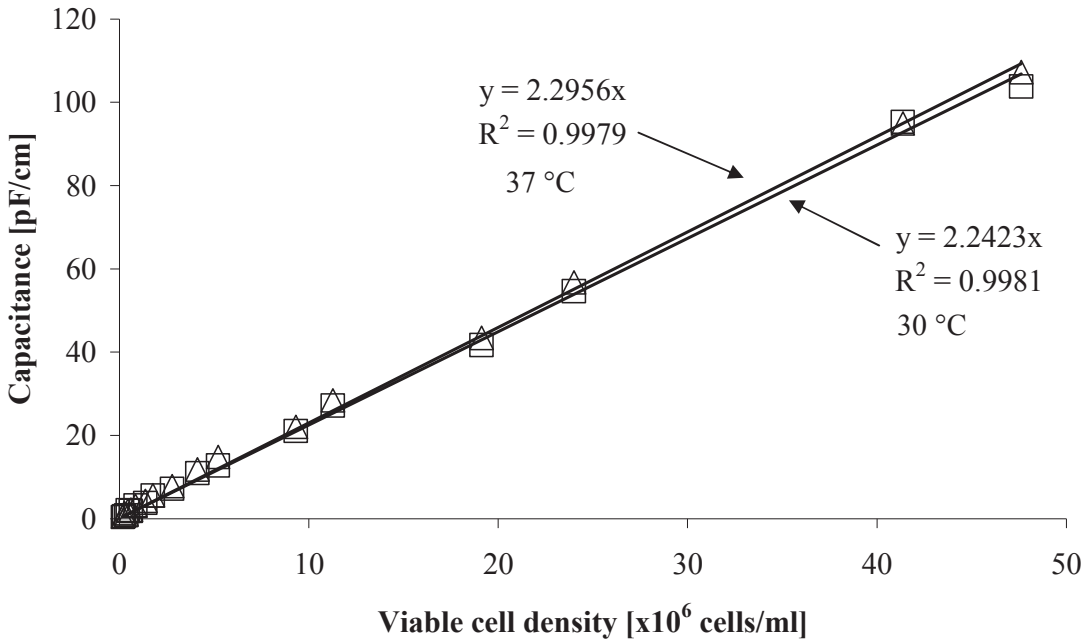


**Figure 24:** Capacitance versus viable cell density for HCD suspension at 0.6 and 10 MHz at 30 °C and 37 °C. Symbols: Capacitance at 30 °C (Δ) and at 37 °C (□).

Capacitance versus viable cell density for HCD suspension in the higher cell density ranges at 0.2 and 10 MHz at 37 °C can be seen in Figure 17. Similar to what was observed in Figure 20, capacitance values at 37 °C are higher than the values at 30 °C indicating that temperature has a small affect on capacitance readings from the Biomass Monitor.

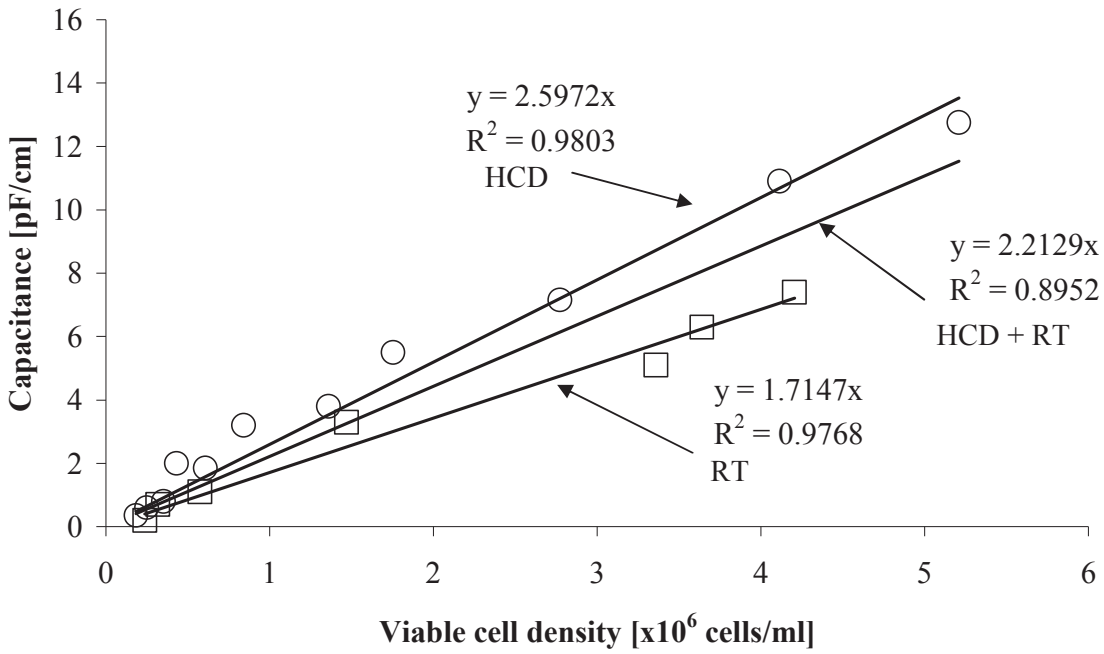


**Figure 25:** Calibration curves for capacitance versus viable cell density at 0.6 and 10 MHz at 30 °C. Symbols: HCD suspension data (○) and RT data alone (□).

From Figure 25 there was no significant divergence noted in the linear trend between the higher and lower cell density suspensions at 0.6 and 10 MHz at 30 °C. As before however, the data was split between a higher and lower viable cell density range at the point where a slight divergence from the linear trend could be detected. The point where this occurs for the HCD suspension data was at a higher value of viable cell density allowing the number of data points for the calibration curve to be increased when compared to the equivalent measurements at 37 °C.

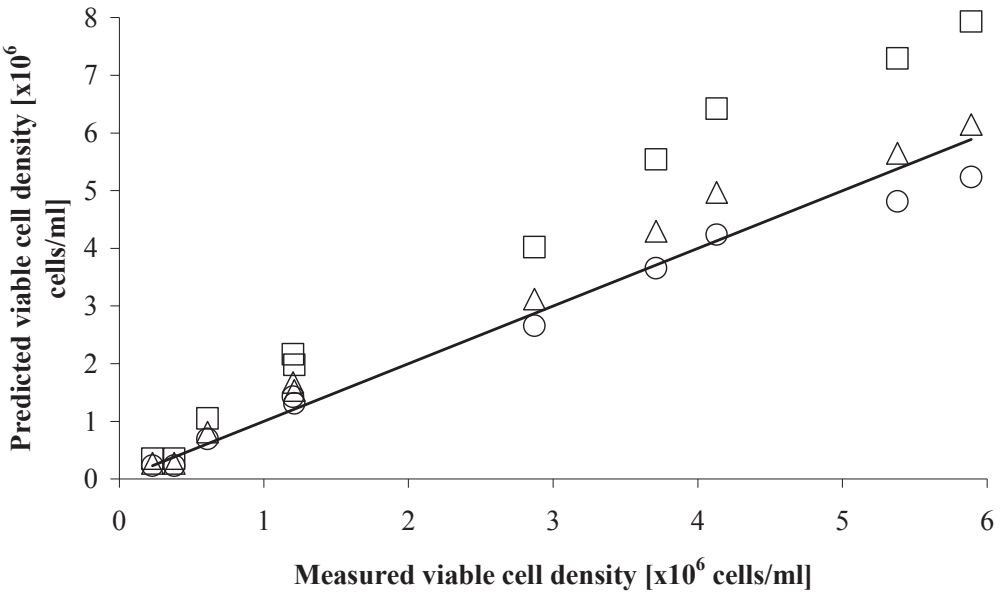


**Figure 26:** Predicted versus measured viable cell density from calibration curves of capacitance versus viable cell density at 0.6 and 10 MHz at 30 °C. Symbols: HCD suspension (○), HCD + RT data (Δ) RT data (□), and Y = X line (—). Refer to Figure 25 for prediction models.

From Figure 25 the RT data calibration curve has a lower slope and the resulting model over predicts the viable cell density for the data in RT 2 (Y = X line, Figure 26). The RMSEP for this model is significantly higher than for that of the other 2 models. When applied, the most accurate model is from the HCD suspension data with an error of $0.3 \times 10^6$ cells/ml. This was not the case for the equivalent measurements at 37 °C.

The conductivity at 30 °C is lower than that of the cultures analysed at 37°C. This supports the observation that frequency is dependant on temperature. The data at 37 °C displayed conductivity readings between 12.4 and 13.6 mS/cm, while the data at 30 °C was in the range of 10.7 – 11.4 mS/cm.

The prediction ability of a calibration model based on the capacitance signal from the Biomass Monitor appears to be influenced by a number of factors. The combination of the dual frequency setting and the measurement temperature appears to be significant as the best results at the setting 0.2 and 10 MHz were at 30 °C. The results for the predictions at 0.6 and 10 MHz are not as straightforward. At both temperatures, RMSEPs of approximately $0.3 \times 10^6$ cells/ml were achieved but

different calibration models gave higher error values. For measurements at 37 °C, the dual frequency setting 0.6 and 10 MHz did give better results than the 0.2 and 10 MHz setting but they were not as accurate at the predictions of the Biomass Monitor at 0.2 and 10 MHz and 30 °C. From Figure 23 the errors are all approximately one half of the equivalent error values at the higher temperature suggesting that selecting the best dual frequency setting will depend on the measurement temperature required.

The under estimation of the calibration models in predicting the viable cell density can be attributed to the range of cell densities incorporated into the calibration models with the cell density ranges at a relatively low range, while all models were used to predict culture data that exceeded $5 \times 10^6$ cells/ml at the end of the exponential phase. The RT and RT 2 culture data did not appear to show reproducibility. The models constructed from this data may have shown a decreased accuracy in the prediction of cell density from capacitance for this reason as they were constructed from one single set of data, this may have decreased the accuracy of the predicted data.

A more desirable prediction model would be one that allows a higher cell density range to be incorporated into the model construction. The number of data points available for the calibration curve also played a role as the RT calibration curve showed the highest RMSEP on two occasions. The fact that the HCD suspension data was based on cells from only day 6 of a culture does not appear to have been a factor in the ability of a calibration model to predict the viable cell density for the real time culture data which was measured over a number of culture days.

The Biomass Monitor has potential to be an effective tool for enumerating viable biomass down to a value of approximately $0.2 \times 10^6$ cells/ml for the CHO cell line (refer to Table 7 for cell density data) at both dual frequency settings and over both temperature ranges. A disadvantage of the Biomass Monitor documented in literature is that it suffers from low sensitivity; the limit of detection for mammalian cell culture is in the range of $0.2 - 0.5 \times 10^6$ cells/ml (Dabros et al. 2009; Aber Instruments 2008), however, as $0.3 \times 10^6$ cells/ml is the minimum cell density at which a cell culture of CHO 320 cells are inoculated, the biomass probe is able to detect such a density, it is suitable for use in CHO cell cultures with such low cell densities.

### 3.5 Prediction of viable cell volume from capacitance

The relationship between cell number and cell size was investigated with the CHO 320 cell line. Biovolume or viable cell volume, defined as "the entire volume enclosed by the plasma membrane of cells in a suspension", is a measurement that accounts for cell number and size, with capacitance being a function of viable cell volume and as well as cell density (Zeiser et al. 1999). For the purpose of this work biovolume was referred to as viable cell volume.

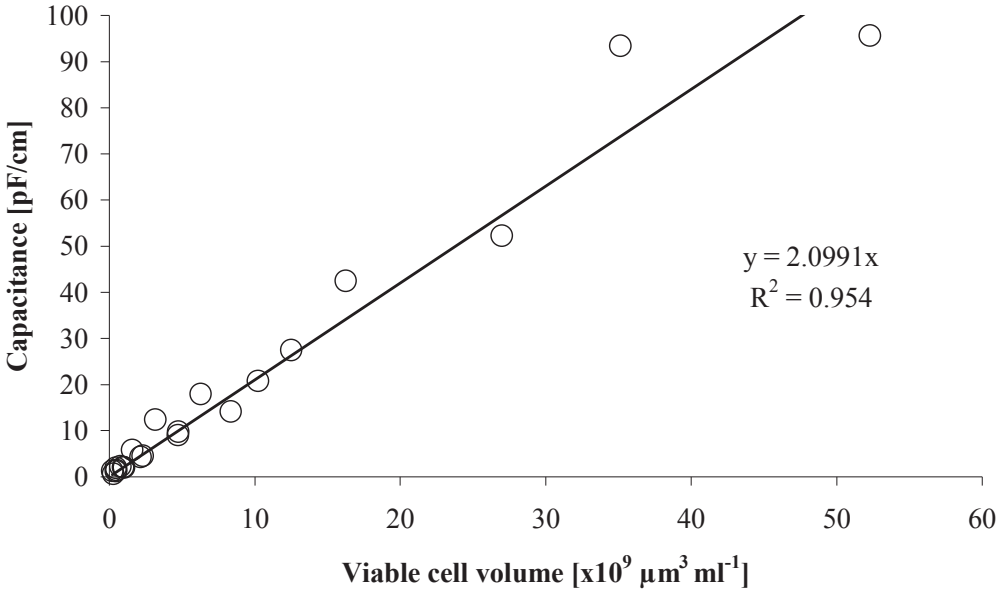


**Figure 27:** Capacitance versus viable cell volume for complete HCD suspension at 0.2 and 10 MHz at 37 °C.

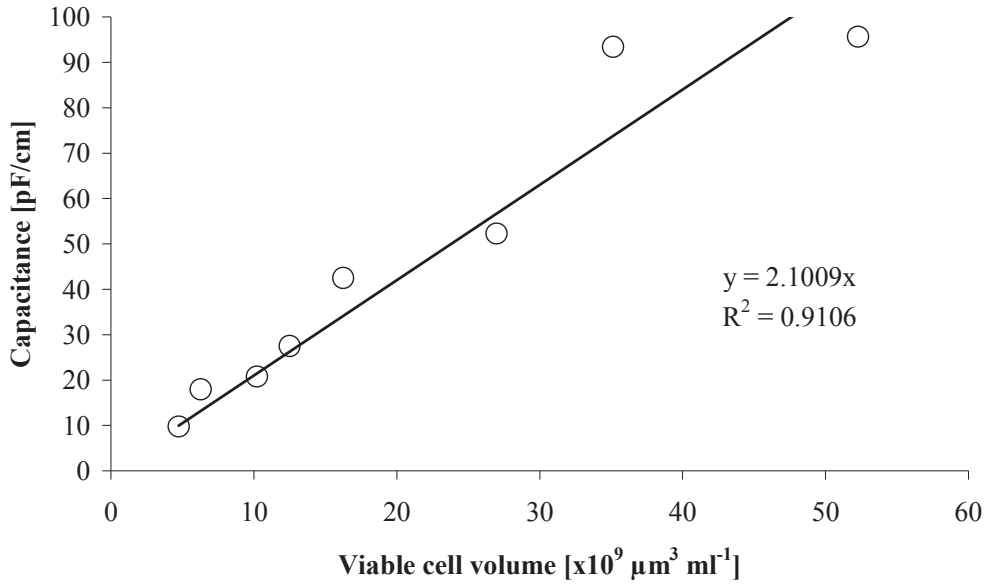


**Figure 28:** Capacitance versus viable cell volume for the higher ranges of viable cell volume 0.2 and 10 MHz at 37 °C.

From Figure 27, capacitance and viable cell volume share a linear relationship for the entire range of viable cell volumes investigated. It can be observed however that if only the lower viable cell volume ranges are included in the plot, the slope would be slightly higher. Figure 28 is a plot of capacitance against viable cell volume for the range of cell volumes greater than $6 \times 10^9$ $\mu m^3$ $ml^{-1}$ and the slope of this line is very similar to that of the slope for the entire range of viable cell volume indicating that the relationship shown in Figure 27 is greatly influenced by the capacitance values at high viable cell volumes. As the expected maximum cell volume from the shake flask culture being predicted would be less than $10 \times 10^9$ $\mu m^3$ $ml^{-1}$, it was decided to use only the range of viable cell volumes below this value that had a clear linear trend (Figure 29).

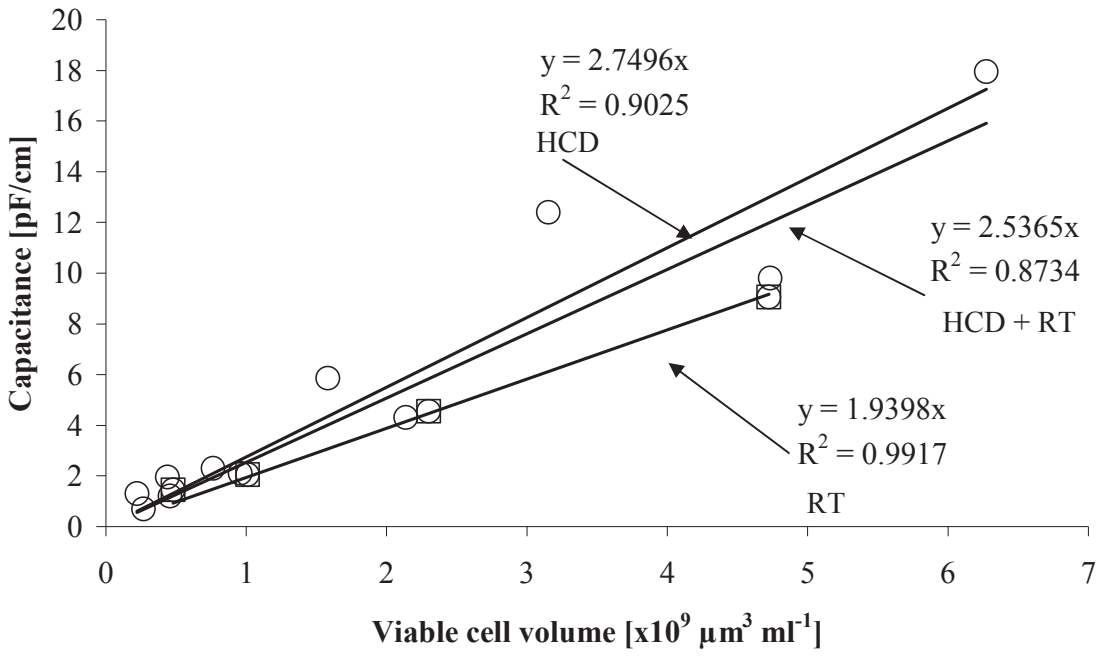


**Figure 29:** Calibration curves for capacitance versus viable cell volume at 0.2 and 10 MHz at 37 °C. Symbols: HCD (○) and RT (□).

The calibration curves constructed using the three data sets are shown in Figure 29. The linear relationship between capacitance and viable cell volume from the HCD and RT data sets are different as can be seen from the different slopes with the RT data showing the highest linear correlation ($R^2 = 0.99$).

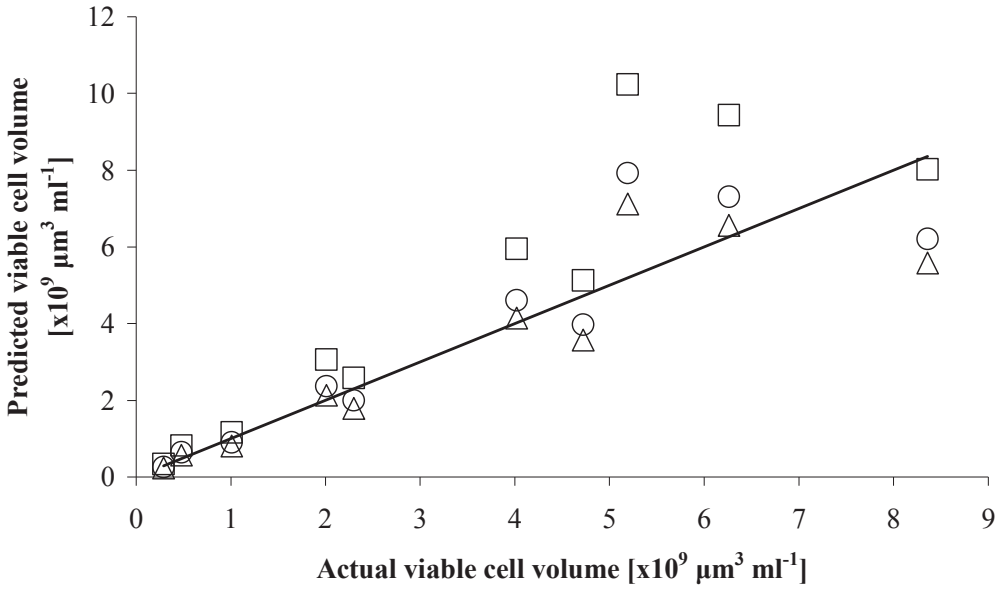


**Figure 30:** Predicted versus measured viable cell volume from calibration curves of capacitance versus viable cell volume at 0.2 and 10 MHz at 37 °C. Symbols: HCD suspension (○), HCD + RT data (Δ), RT data (□) and Y = X line (—). Refer to Figure 29 for calibration models.

From Figure 30, the closest predictions to the RT 2 data (Y = X line) are from the HCD suspension and the HCD + RT suspension. The RMSEP values achieved from the HCD suspension (1.2 $\times 10^9$ µm$^3$ ml$^{-1}$) and HCD + RT (1.15 $\times 10^9$ µm$^3$ ml$^{-1}$) calibration models (See Appendix D.1, Table 13), suggesting a HCD suspension that has been diluted and combined with RT data was best to perform a calibration curve for the prediction of viable cell volume from capacitance data. A plot of predicted viable cell volume versus actual viable cell volume gives a more complete picture and Figure 30 shows that all three model are capable of predicting cell volumes when the cell volume is low and it is only at the higher cell volumes that the RT or indeed any of the calibration models are unable to accurately predict the viable cell volume.

A similar analysis was performed for the capacitance data measured at 0.6 and 10 MHz at 37 °C and results of this can be seen in Figures 32 and 33. As before only the range of viable cell volumes likely to be encountered were used in the calibration curves from the HCD suspensions.

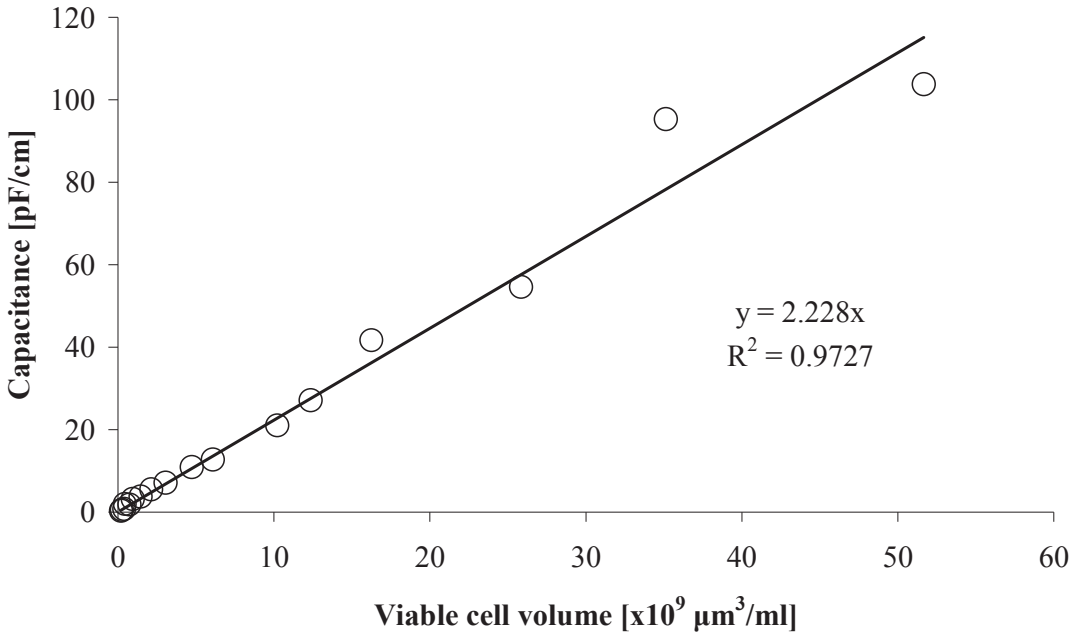


**Figure 31:** Capacitance versus viable cell volume for complete HCD suspension at 0.6 and 10 MHz at 37 °C.

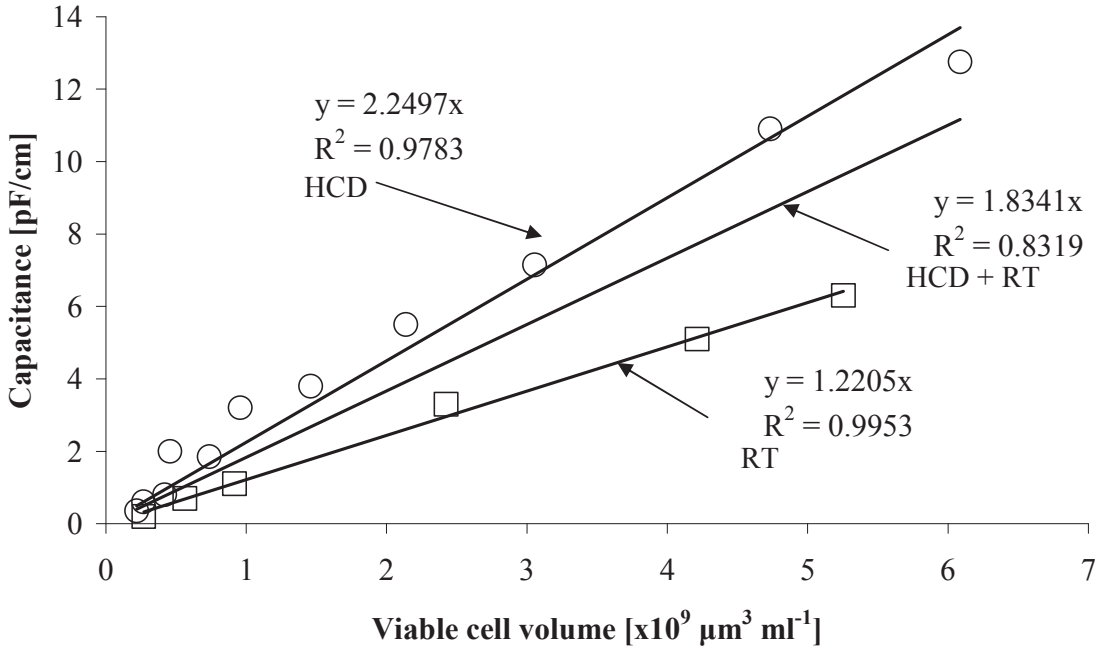


**Figure 32:** Calibration curves for capacitance versus viable cell volume at 0.6 and 10 MHz at 37 °C. Symbols: HCD suspension (○) and RT data (□).

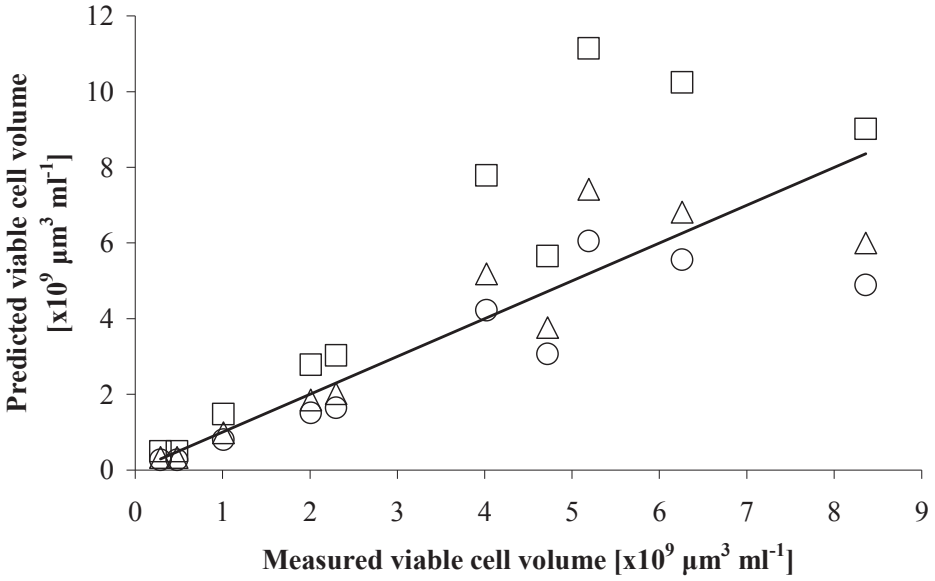


**Figure 33**: Predicted versus measured viable cell volume from calibration curves of capacitance versus viable cell volume at 0.6 and 10 MHz at 37 °C. Symbols: HCD suspension (○), HCD + RT data (Δ), RT data (□) and Y = X line (—). Refer to Figure 32 for prediction models.

Again, the model closest to the RT 2 data (Y=X line), with the lowest RMSEP of $1.15 \times 10^9$ µm$^3$ ml$^{-1}$, was the calibration model constructed with the combination of serially diluted HCD suspension fractions and real time data. The RT data prediction showing the highest error and an examination of the predicted values when the viable cell volume is high shows that the RT model is over predicting values and this is what gives the model its high RMSEP value.

### 3.5.1 Influence of temperature on the Biomass Monitor predictions for viable cell volume

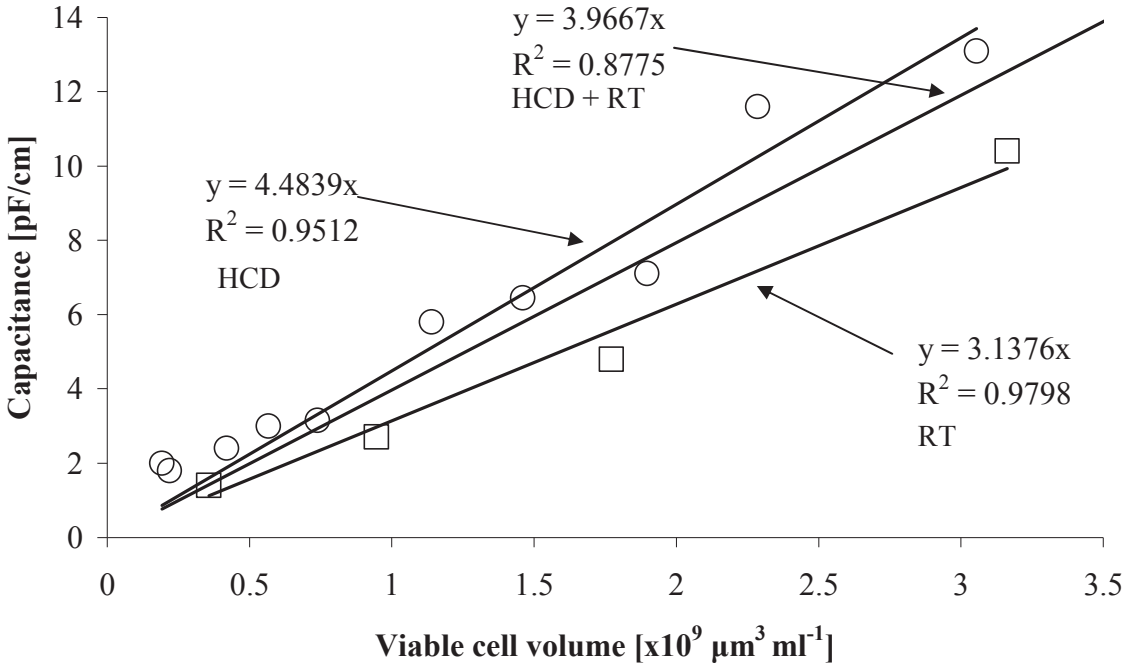


**Figure 34:** Calibration curves of capacitance versus viable cell volume at 0.2 and 10 MHz at 30 °C. Symbols: HCD suspension (○) and RT data (□).

As the best linear trend between capacitance and viable cell volume for the HCD suspension data was found for viable cell volumes less than $3.5 \times 10^9$ $\mu m^3$ $ml^{-1}$, only data points below this value were used to construct the calibration curve. The calibration curves from the HCD suspension data, the HCD suspension and the RT data combined and the RT data alone can be seen in Figure 34 and there are distinctly different slopes for the HCD suspension and RT data. The $R^2$ value for the curve representing the combination of HCD suspension and RT data is quite low at less than 0.88 so it is clear that there are 2 different calibration relationships from the different data sets (HCD suspension and RT data).

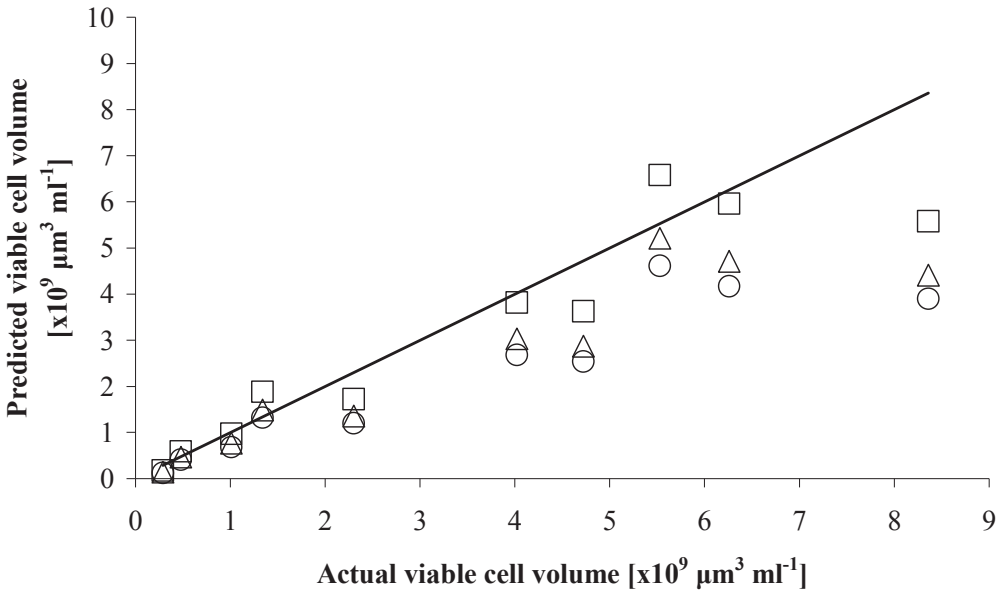


**Figure 35**: Predicted versus measured viable cell volume from calibration curves of capacitance versus viable cell volume at 0.2 and 10 MHz at 30 °C. Symbols: HCD suspension (○), HCD + RT data (Δ) RT data (□) and Y = X line (—). Refer to Figure 34 for prediction models.

Based on RMSEP values, the best prediction model was from the RT data alone with an error of $1.03 \times 10^9$ µm$^3$ ml$^{-1}$ but all calibration models including the RT data model tend to underestimate the value of viable cell volume. When the same capacitance data was used to model the viable cell densities, the error values were lower than the corresponding measurements at 37 °C but the same trend was not found for the viable cell volume predictions.

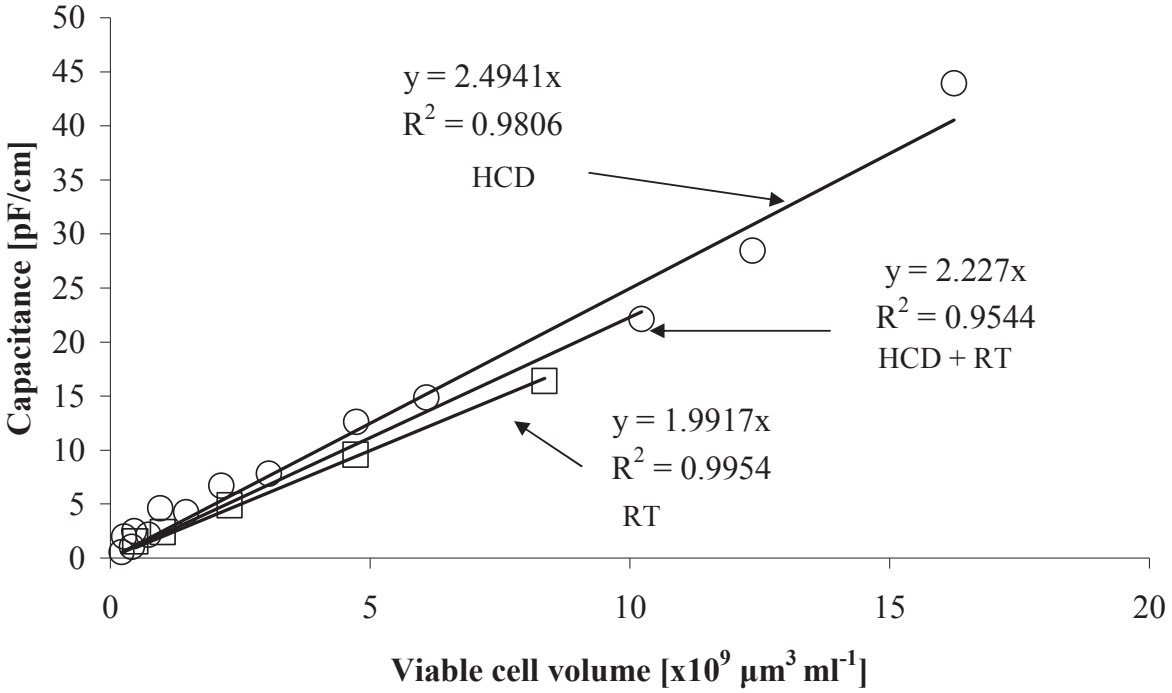


**Figure 36:** Calibration curves of capacitance versus viable cell volume at 0.6 and 10 MHz at 30 °C. Symbols: HCD suspensions (○) and RT alone (□).

Calibration curves for the three previously used data sets (HCD, HCD + RT and RT) are shown in Figure 36. The HCD suspension data no longer had a linear relationship for capacitance and viable cell volume at cell volumes greater than $15 \times 10^9$ $\mu m^3$ $ml^{-1}$ so only data points below this value of viable cell volume were used in the calibration curve. Again RT data and HCD suspension data have different relationships when capacitance was plotted against viable cell volume as is evident from an examination of the different slopes; HCD (y = 2.4941) and RT data (y = 1.9917). Once the data is combined, (HCD suspension + RT data (y = 2.227x)), the $R^2$ is lower which again highlights the difference between 2 distinct linear relationships.

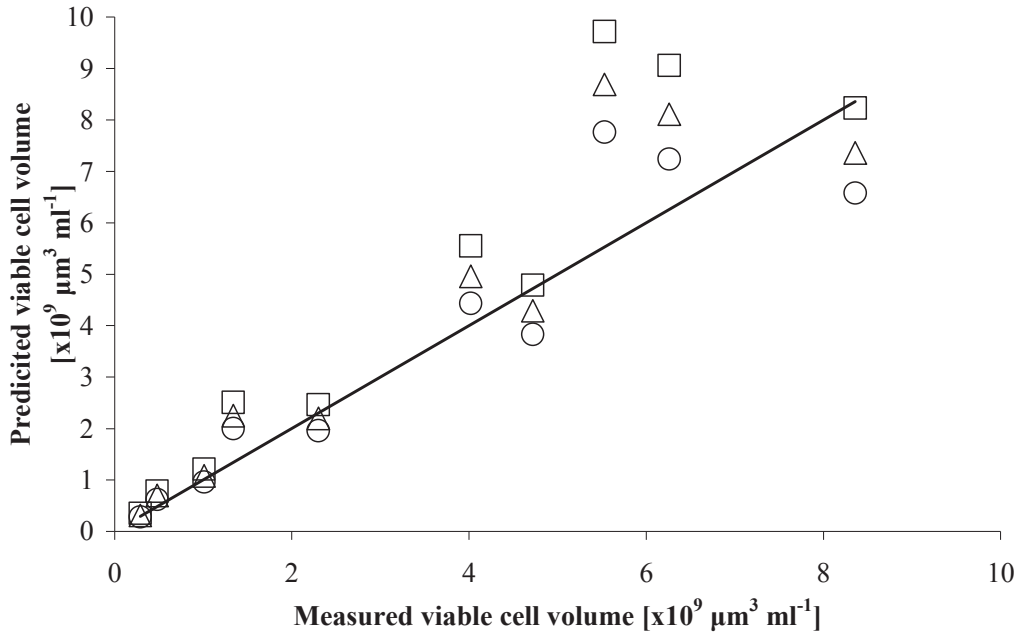


**Figure 37:** Predicted versus measured viable cell volume from calibration curves of capacitance versus viable cell volume at 0.6 and 10 MHz at 30 °C. Symbols: HCD suspension (○), HCD + RT data (Δ), RT data (□) and Y = X line (—). Refer to Figure 36 for prediction models.

The prediction model with the lowest RMSEP was that constructed from the HCD suspension data with an error of $1.03 \times 10^9$ $\mu m^3$ $ml^{-1}$. At both the measurement temperatures examined, the prediction model from RT capacitance data at the setting 0.6 and 10 MHz had the highest RMSEP values.

No clear trend between dual frequency setting and temperature was observed for the use of capacitance to predict the value of viable cell volume. No particular data set consistently produced better calibration models but the HCD suspension data generally have similar errors to the other models as with viable cell density predictions, the fact the cells in the HCD suspension all came from day 6 of a culture does not appear to have been a factor in the prediction ability of the calibration models they produced. The value for viable cell volume was based on average viable cell diameter as determined by the Countess and in all cases the diameters measured here were in the range expected for CHO cell lines (10 – 15 µm) (Searles, Todd and Kompala 1994).

### 3.6 Prediction of optical density versus viable cell density

Another common technique for biomass estimation is optical density (Marose et al. 1999). From the plot of optical density (measured from HCD suspensions) versus viable cell density in Figure 38, it can be seen that the response of the spectrometer is of an overall linear trend with a change in slope as the viable cell density exceeds the range of $5 \times 10^6$ cells/ml (V > 95 %).

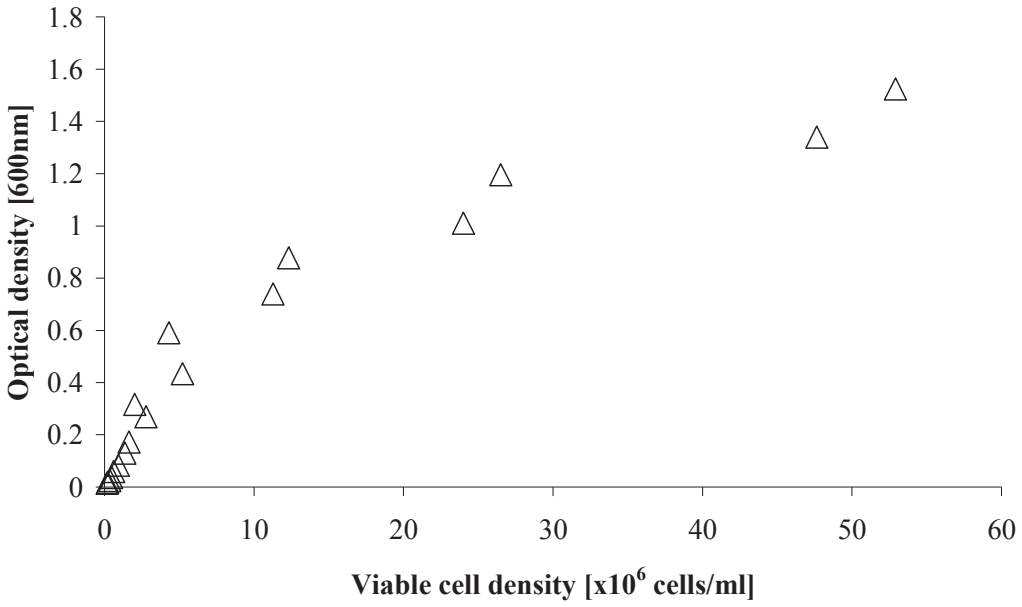


**Figure 38:** Optical density versus viable cell density for complete HCD suspension.

To assess the accuracy of optical density measurements to predict the viable cell density, a number of calibration curves were constructed using data from HCD suspensions, HCD suspension data and data from real time cultures and real time cultures on their own. This was a similar procedure to that applied to the capacitance data as measured by the Biomass Monitor. The calibration curves are shown in Figure 40. The slope for the RT data (y = 0.0825x) is quite different to that of the HCD suspension (y = 0.107x) and the combination of the HCD suspension and RT data sets (y = 0.1002).

Figure 38 shows a second linear relationship similar to what was observed for capacitance, this could be applied to high cell density cultures to estimate the

accuracy of optical density at a higher cell density range in future work, however viability would have to be high for this to be accurate.

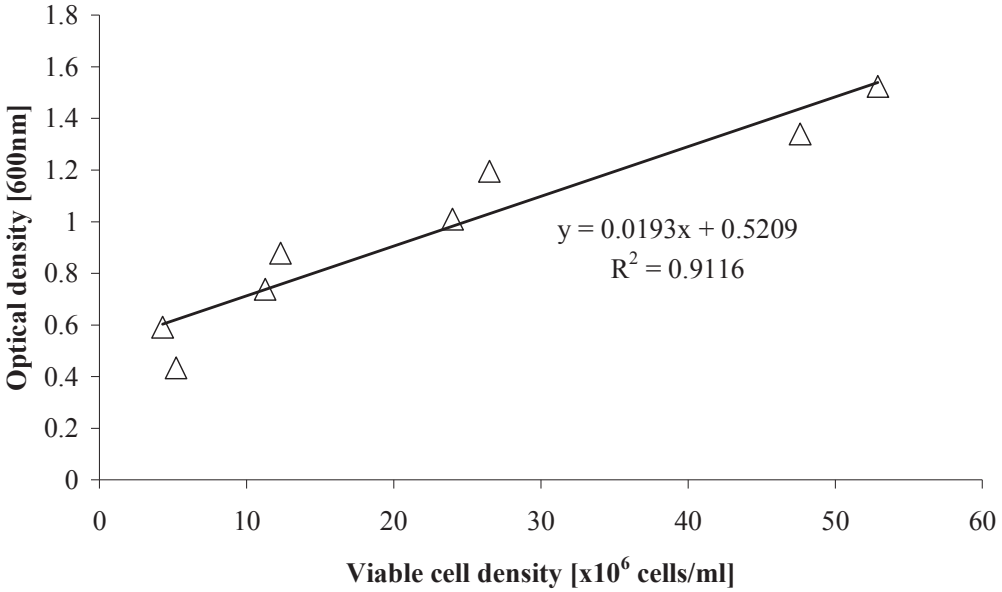


**Figure 39:** Optical density versus viable cell density for the higher cell density ranges.

Figure 39 shows the relationship between optical density and viable cell density at the higher cell density ranges (above $5 \times 10^6$ cells/ml). The relationship is linear while the slope varies to that of the lower range of optical density versus viable cell density (Figure 40). For future work such a calibration model would need to be tested on a higher range of cell densities from a real time culture similar to what was observed for capacitance readings at both dual frequency settings.

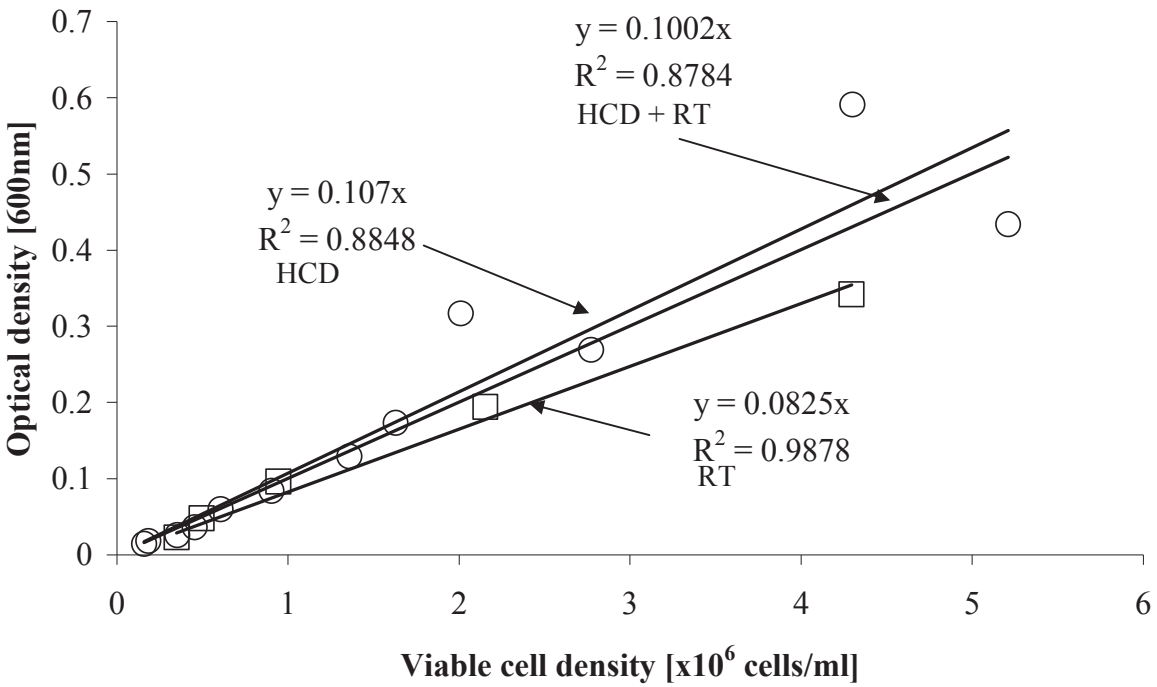


**Figure 40:** Optical density versus viable cell density for CHO 320 high cell density suspensions at 37 °C Symbols: HCD suspension (○) and RT data (□).

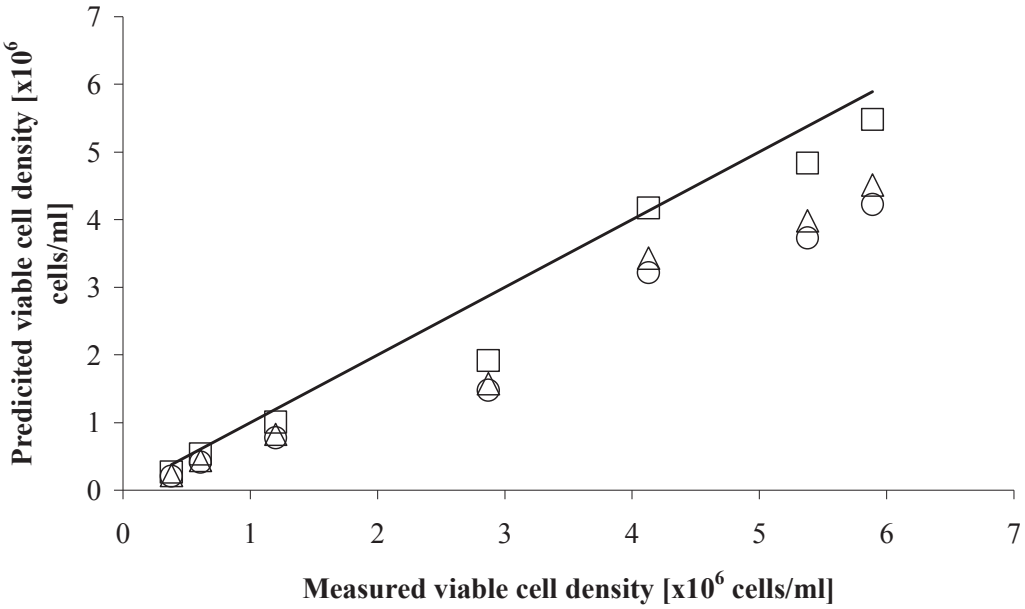


**Figure 41**: Predicted versus measured viable cell density from calibration curves of optical density versus viable cell density. Symbols: HCD suspension (○), HCD + RT data (Δ), RT data (□) and Y = X line (—). Refer to Figure 40 for prediction models.

Figure 41 shows the prediction values for viable cell density as measured by the optical density method. The RT data model is the most accurate to follow viable cell density (RMSEP = 0.48) to the end of the stationary phase corresponding to a time at 144 hours. All models were only applied to the data up to the end of the stationary phase as it is known OD shows poor reliability as viability decreases (Marose et al. 1999). When the models were applied to culture data in range of cell densities encountered for real time cultures and viability began to decrease, the RMSEP values increased significantly; HCD suspension (3.44) HCD suspension + RT data (3.64) and RT data (4.45).

The RMSEP for the RT calibration model (0.48) was significantly lower than those of the other two models, HCD suspension + RT data (1.01) and HCD suspension (1.20) suggesting that the serial dilution of the HCD suspension had an effect on the optical density measurement. The real time data was expected to give the best prediction as during the course of a culture the medium constitution would change with cell debris increasing and a colour change occurring as pH changed However, with the HCD suspension dilutions, the cell suspensions were being

diluted in fresh medium at each dilution yielding an inaccurate representation of cell suspension and medium condition.

### 3.7 Countess automated cell counter versus microscope and haemocytometer cell densities

**Table 7:** Comparison of cell densities measured by the Countess versus microscope and haemocytometer from the two HCD suspensions.

| Cell Density from: | |
|---|---|
| Microscope and haemocytometer [$\times 10^6$ cells/ml] | Countess [$\times 10^6$ cells/ml] |
| 47.63 | 46.50 |
| 41.36 | 39.70 |
| 24.00 | 22.00 |
| 19.13 | 17.50 |
| 11.26 | 11.00 |
| 9.31 | 8.50 |
| 5.21 | 4.90 |
| 4.12 | 3.60 |
| 2.77 | 2.60 |
| 1.76 | 1.15 |
| 1.36 | 1.15 |
| 0.84 | 0.80 |
| 0.61 | 0.57 |
| 0.43 | 0.39 |
| 0.35 | 0.32 |
| 0.25 | 0.20 |
| 0.19 | 0.18 |
| **RMSEP** | **0.84** |

The cell densities displayed in Table 7 were average cell densities taken from the HCD suspension counts. The error of both cell density determination methods was low with the maximum variation of up to 0.2 x $10^6$ cells/ml encountered for both

analysis techniques. If a much larger variation (0.5 x $10^6$ cells/ml or greater) between duplicate counts was encountered for a technique recounts were conducted.

The Countess automated sampling system was investigated as an alternative reference method to the microscope and haemocytometer method that was used throughout this work. The predicted viable cell density of the high cell density suspension data was compared to the value determined by the microscope and haemocytometer and the RMSEP was $0.84 \times 10^6$ cells/ml. When cell densities of less than $6 \times 10^6$ cells/ml were examined, the RMSEP value became $0.27 \times 10^6$ cells/ml. In all cases when the microscope haemocytometer and the Countess were used to analyse the same cell suspensions, the Countess gave a lower value for viable cell density than the microscope and haemocytometer method, however this could be investigated further in future work. This was only conducted for a comparison of the two techniques in this section and the Countess cell density data was not used elsewhere as the reference method was used for cell density data in all other parts of the Results and Discussion. The procedure for determining cell density using the Countess was less labour intensive than using the microscope and haemocytometer. Less specialist training was required for the use of the Countess as the software in the machine does the counting automatically.

For these reasons it has potential as a rapid method for measuring approximate viable cell density. The RMSEP of $0.27 \times 10^6$ cells/ml was still slightly higher than the lowest error achieved using the Biomass Monitor for prediction and that method has the advantage of being able to take automatic measurements in real time with in-situ sampling in a reactor.

# 4. Conclusions

In order to characterise the CHO 320 cell line a number of Batch and Fed Batch cultures were carried out. Growth rates of both Batch and Fed Batch cultures were similar for the first 120 hours, with the Fed Batch cultures exhibiting an overall elevated specific growth rate. The average specific growth rates of Batch cultures 1-3 was 0.026 $h^{-1}$ and it was 0.028 $h^{-1}$ for Fed Batch cultures 1-3. The average maximum viable cell density for Fed Batch cultures was 9 % higher than for Batch cultures. A more significant difference between the Batch and Fed Batch cultures was that in Fed Batch cultures, cell viability was prolonged by delaying cell death as the result of feeding. A feed of 2 ml/day was sufficient to prolong the 50 ml culture viability by 24 hours; however the culture was still susceptible to apoptosis.

The potential of the Biomass Monitor as a tool to predict viable cell density was investigated and demonstrated. The Biomass Monitor 210 was used to predict CHO 320 viable cell density and viable cell volume data from 3 calibration curves constructed from a high cell density culture that had been serially diluted to a cell density lower than the inoculation cell density required for the CHO 320 cell line, a combination of the high cell density data and data from a real time culture and finally data solely from a real time culture. The slopes of these 3 calibration curves were applied to real time cell density data under 2 conditions of dual frequency and temperature. Calibration models similar to that from the Biomass Monitor data were also constructed for the prediction of viable cell density from optical density readings.

The investigation into interferences to the biomass monitor probe showed that the position the probe should be at least 10 mm from the vessel walls. If it is in close proximity to the $pO_2$ probe, the head of the biomass monitor must be below the head of the $pO_2$ probe but optimally both shafts should be at least 10 mm apart. Stirrer speed at high rates causes an oscillation in the capacitance but should not cause a problem with mammalian cell culture as RPM will be low. Aeration from a sparger does cause some variation in capacitance readings from the Biomass Monitor. In any new bioreactor this should be tested to find a suitable position for the Biomass Monitor probe in relation to the sparger. The port furthest from the Biomass Monitor probe would be a good position for the sparger.

When the Biomass Monitor dual frequency settings of 0.2 and 10 MHz were used, it was found the relationship between capacitance and viable cell density was not linear for the entire cell density range examined. This was the case at both measurement temperatures although the non-linear relationship was more pronounced at 37 °C. When the settings were changed to 0.6 and 10 MHz, the capacitance and viable cell density showed a good linear trend for the whole cell density range when measured at both 30 and 37 °C. Despite this, the relationship between capacitance and viable cell density at low viable cell density values had a different slope to when the entire cell density range was examined.

It was found that when the measurement temperature was 37 °C degrees, the dual frequency setting of 0.6 and 10 MHz gave the most accurate predictions and the dual frequency setting of 0.2 and 10 MHz was better when the temperature was 30 °C. For all combinations of Biomass Monitor setting and temperature, 3 different types of calibration sets were used to predict the viable cell density of the test real time culture, but no one type of data set consistently gave better or worse results than the other. It can, however, be concluded that using a high cell density suspension for making calibrations is an option and it is not necessary to only make calibrations from real time culture data.

Although all models were shown to be reasonably accurate the least accurate being the model used for the prediction of viable cell density from capacitance readings at 0.2 and 10 MHz at 37 °C, the RT and RT 2 culture data used as part of the calibration models and in the predictions of viable cell density did not appear to show reproducibility. The models constructed from this data may have shown a decreased accuracy in the prediction of cell density from capacitance and so the validation of the model cannot be confirmed. However at both temperatures and dual frequency settings it was possible to measure the increase and decrease of the viable cell density values although accuracy varied with the different experimental set-ups. Measurement of cell densities as low as $0.18 \times 10^6$ cells/ml was found to be possible. The Biomass Monitor has potential as an on-line PAT tool to monitor viable cell density.

When the capacitance values from the Biomass Monitor were plotted against viable cell volume as calculated from the average cell diameter measured by the Countess and the viable cell density as measured by the microscope and haemocytometer, there were generally an overall linear relationship. The

relationship changed slightly at lower cell volumes so only the capacitance values at lower cell volumes were used to develop calibration models using similar sets as those used to predict viable cell density. While with capacitance and viable cell density data it was found that a particular dual frequency setting worked better at a particular temperature, this was not the case for viable cell volume predictions. Also no particular calibration model produced consistently better predictions. In general, predictions for viable cell volume were more accurate at lower values than the higher values.

Optical density and viable cell density calibration curves showed different relationships between the real time data and the serially diluted culture data in all of the conditions tested. The real time data of all cultures was accurate until 144 hours when a decrease in viable cell density was attributed to the loss of accuracy of the model and it was for this reason the data after this time period was not included in the RMSEP calculations. The RT calibration curve gave the most accurate prediction with the lowest RMSEP of 0.46 suggesting that calibration models should always be made from such data rather than HCD suspension data as during cell cultures, cell debris accumulation in the medium would contribute to the optical density of the sample. This would not be the case for the Biomass Monitor readings as they are not affected by suspended particles in the medium such as cell debris.

Viable cell density data from the Countess was compared to the viable cell densities measured by the microscope and haemocytometer and an RMSEP of 0.84 x $10^6$ cells/ml was calculated. It was found that Countess always gave a cell density value that was lower than that measured by the microscope and haemocytometer.

### 4.1 Recommendations and future work

The first recommendation would be to conduct more RT cultures assess the repeatability of the cultures used as part of the calibration models as there was an underestimation in some of the prediction models. This could be then used to construct a more robust calibration curve from numerous sets of RT data. The resulting models could subsequently be compared to the models in this work and may show an increased accuracy in the prediction of viable cell density from capacitance readings of the Biomass Monitor

Results from this study seem to indicate that the measurement temperature and the range of cell densities included in the calibration curve are both factors in determining the most suitable dual frequency for the Biomass Monitor. If this study was repeated, it is recommended that a wider range of dual frequencies are examined for only the range of cell densities to be encountered in a given application. This would need to be repeated for the same application if measurements were to be made at a different temperature. Another recommendation would be to determine the upper limits of detection for the Biomass Monitor for each dual frequency setting.

This Countess was used to determine the average cell diameter of a sample, and this value was used to determine the viable cell volume. As this device tends to give lower values for viable cell density, it may be that it cannot detect some cells which will have implications for the value of average cell diameter in a sample. This fact may explain some of the variability in the results for the use of capacitance to predict the value of viable cell volume. A recommendation for a future study would be to use a second method to determine the average cell diameter to confirm the value determined using the Countess. In future work the Biomass Monitor could be calibrated by HCD suspension serially diluted or a combination of both HCD suspension and RT data either from a shake flask or bioreactor. A bioreactor would allow a better prediction for two reasons, higher cell densities can be achieved and cells are most commonly grown in bioreactors in industrial applications.

The next step would be to use the Biomass Monitor for on-line measurement of capacitance in Batch and Fed Batch cultures to investigate how cell density and capacitance relationships may change in the bioreactor environment as cell density increases. The effect of changes in the medium due to growth, addition of antifoam or sodium hydroxide (NaOH) could also be investigated prior to implementing the

Biomass Monitor to control of growth rate in a Fed Batch culture environment. The use of the Biomass Monitor to indirectly measure growth rate from the cell density value could also be compared to other online biomass measurement systems such as calorimetry.

# 5. References

Aber Instruments. 2008. *Product catalogue*. Available from http://www.iul-instruments.de/pdf/059_biomass_monitor_230.pdf [Accessed 16/01/2012]

Ahn, W.S., Jeon, J., Jeong, Y., Lee, S.J. and Yoon, S.K. 2008. Effect of culture temperature on erythropoietin production and glycosylation in a perfusion culture of recombinant CHO cells. *Biotechnology and Bioengineering,* 101(6), pp. 1234-1244.

Akhnoukh, R., Kretzmer, G. and Schügerl, K. 1996. On-line monitoring and control of the cultivation of Spodoptera frugiperda Sf9 insect cells and β-galactosidase production by Autographa californica virus vector. *Enzyme and Microbial Technology*. 18(3), pp. 220-228.

Alford, J.S. 2006. Bioprocess control: Advances and challenges. *Computers & Chemical Engineering,* 30(10-12), pp. 1464-1475.

Altamirano, C., Paredes, C., Illanes, A., Cairó, J.J. and Gòdia, F. 2004. Strategies for fed-Batch cultivation of t-PA producing CHO cells: substitution of glucose and glutamine and rational design of culture medium. *Journal of Biotechnology*. 110 (2), pp.171-179.

Altamirano, C., Illanes, A., Becerra, S., Cairó, J.J. and Gòdia, F. 2006. Considerations on the lactate consumption by CHO cells in the presence of galactose. *Journal of Biotechnology,* 125(4), pp. 547-556.

Andersen, D.C. and Krummen, L. 2002. Recombinant protein expression for therapeutic applications. *Current Opinion in Biotechnology,* 13(2), pp.117-123.

Ansorge, S., Esteban, G. and Schmid, G. 2007. On-line monitoring of infected Sf-9 insect cell cultures by scanning permittivity measurements and comparison with off-line biovolume measurements. *Cytotechnology,* 55(2-3), pp.155-124.

Arden, N. and Betenbaugh, M.J. 2004. Life and death in mammalian cell culture: strategies for apoptosis inhibition. *Trends in Biotechnology,* 22(4), pp.174-180.

Astley, K., Naciri, M., Racher, A. and Al-Rubeai, M. 2007. The role of p21cip1 in adaptation of CHO cells to suspension and protein-free culture. *Journal of Biotechnology,* 130(3), pp.282-290.

Burgemeister, S., Nattkemper, T.W., Noll, T., Hoffrogge, R. and Flaschel, E. 2010. CellViCAM—Cell viability classification for animal cell cultures using dark field micrographs. *Journal of Biotechnology,* 149(4), pp. 310-316.

Burteau, C., Verhoeye, F.R., Mols, J.F., Ballez, J., Agathos, S.N. and Schneider, Y. 2003. Fortification of a protein-free cell culture medium with plant peptones improves cultivation and productivity of an Interferon-γ-producing CHO cell line. *In Vitro Cellular & Developmental Biology,* 39(7), pp.291-296.

Cannizzaro, C., Gügerli, R., Marison, I.W. and von Stockar, U. 2003. On-line Biomass Monitoring of CHO perfusion culture with scanning dielectric spectroscopy. *Biotechnology and Bioengineering,* 84(5), pp.597-610.

Capiaumont, J., Legrand, C., Carbonell, D., Dousset, B., Belleville, F. and Nabet, P. 1995. Methods for reducing the ammonia in hybridoma cell cultures. *Journal of Biotechnology,* 39(1), pp.49-58.

Carvell, J.P. and Dowd, J.E. 2006. On-line Measurements and Control of Viable Cell Density in Cell Culture Manufacturing Processes using Radio-frequency Impedance. *Cytotechnology.* 50(1-3), pp. 35-48.

Clincke, M., Guedon, E., Yen, F.T., Ogier, V., Roitel, O. and Goergen, J. 2011. Effect of surfactant pluronic F-68 on CHO cell growth, metabolism, production, and glycosylation of human recombinant IFN-γ in mild operating conditions. *Biotechnology Progress.* 27(1), pp. 181-190.

Dabros, M., Dennewald, D., Currie, D.J., Lee, M.H., Todd, R.W., Marison, I.W. and Stockar, U.v. 2009. Cole–Cole, linear and multivariate modelling of capacitance data for on-line monitoring of biomass. *Bioprocess and Biosystems Engineering.,* 32(2), pp. 161-173.

Davey, C.L. and Kell, D.B. 1998. The influence of electrode polarisation on dielectric spectra, with special reference to capacitive biomass measurements: I. Quantifying the effects on electrode polarisation of factors likely to occur during fermentations. *Bioelectrochemistry and Bioenergetics.* 46(1), pp.91-103.

Douris, V., Swevers, L., Labropoulou, V., Andronopoulou, E., Georgoussi, Z. and Iatrou, K. 2006. Stably Transformed Insect Cell Lines: Tools for Expression of Secreted and Membrane‐anchored Proteins and High‐throughput Screening Platforms for Drug and Insecticide Discovery *IN:* Bryony C. Bonning,Karl Maramorosch and Aaron J.Shatkin (ed.). *Advances in Virus Research.* Academic Press: pp.113-156.

Ducommun, P., Bolzonella, I., Rhiel, M., Pugeaud, P. and von Stockar, U., Marison I.W. 2001. On-Line determination of animal cell concentration. *Biotechnology and Bioengineering.* 5(72), pp.515-522.

Ducommun, P., Kadouri, A., von Stockar, U. and Marison, I.W. 2002. On-line determination of animal cell concentration in two industrial high-density culture processes by dielectric spectroscopy. *Biotechnology and Bioengineering.* 77(3), pp.316-323.

Farges, B., Chenu, S., Marc, A. and Goergen, J.-. 2008. Kinetics of IFN-γ producing CHO cells and other industrially relevant cell lines in rapeseed-supplemented Batch cultures. *Process Biochemistry.* 43(9), pp.945-953.

Fehrenbach, R., Comberbach, M. and Pêtre, J.O. 1992. On-line Biomass Monitoring by capacitance measurement. *Journal of Biotechnology.* 23(3), pp.303-314.

Gawlitzek, M., Valley, U., Nimtz, M., Wagner, R. and Conradt, H.S. 1995. Characterization of changes in the glycosylation pattern of recombinant proteins from BHK-21 cells due to different culture conditions. *Journal of Biotechnology.* 42 (2), pp.117-131.

Goh, L. and Yap, M.G.S. 2005. Determination of interferon-gamma in Chinese hamster ovary cell culture supernatant by coupled-column liquid chromatography. *Journal of Separation Science.* 28(16), pp.2104-2110.

Gouveia, R., Kandzia, S., Conradt, H.S. and Costa, J. 2010. Production and N-glycosylation of recombinant human cell adhesion molecule L1 from insect cells using the stable expression system. Effect of dimethyl sulfoxide. *Journal of Biotechnology.* 145(2), pp.130-138.

Guan, Y., Evans, P.M. and Kemp, R.B. 1998. Specific heat flow rate: An on-line monitor and potential control variable of specific metabolic rate in animal cell culture that combines microcalorimetry with dielectric spectroscopy. *Biotechnology and Bioengineering.* 58(5), pp.464-477.

Hansen, H.A. and Emborg, C. 1994. Influence of Ammonium on Growth, Metabolism, and Productivity of a Continuous Suspension Chinese Hamster Ovary Cell Culture. *Biotechnology Progress.* 10(1), pp.121-124.

Hayter, P.M., Curling, E.M.A., Baines, A.J., Jenkins, N., Salmon, I., Strange, P.G. and Bull, A.T. 1991. Chinese hamster ovary cell growth and interferon production kinetics in stirred Batch culture. *Applied Microbiology and Biotechnology.* 34(5), pp.559-564.

Huang, E.P., Marquis, C.P. and Gray, P.P. 2004. Process development for a recombinant Chinese hamster ovary (CHO) cell line utilizing a metal induced and amplified metallothionein expression system. *Biotechnology and Bioengineering.* 88 (4), pp.437-450.

Huang, Z., Li, G., Pei, W., Sosa, L.A. and Niu, L. 2005. Enhancing protein expression in single HEK 293 cells. *Journal of Neuroscience Methods.* 142 (1), pp.159-166.

Irani, N., Beccaria, A.J. and Wagner, R. 2002. Expression of recombinant cytoplasmic yeast pyruvate carboxylase for the improvement of the production of human erythropoietin by recombinant BHK-21 cells. *Journal of Biotechnology.* 93(3), pp.269-282.

Jacobson, B.S. and Morgan, T.L. 1995. Growth rates of hprt and tk mutant CHO cell lines. *Mutation Research/Genetic Toxicology.* 344(3-4), pp.141-145.

Jass, J., O'Neill, J.G. and Walker, J.T. 2001. Direct biofilm monitoring by a capacitance measurement probe in continuous culture chemostats. Ron J. Doyle (ed.) *Methods in Enzymology.* Academic Press: pp.63-70.

Joeris, K., Frerichs, J.G., Konstantinov, K. and Scheper, T. 2002. *In-situ* microscopy: Online process monitoring of mammalian cell cultures. *Cytotechnology,* 38(1-3), pp.129-134.

Justice, C., Brix, A., Freimark, D., Kraume, M., Pfromm, P., Eichenmueller, B. and Czermak, P. 2011. Process control in cell culture technology using dielectric spectroscopy. *Biotechnology Advances.* 29(4), pp.391-401.

Kallel, H., Jouini, A., Majoul, S. and Rourou, S. 2002. Evaluation of various serum and animal protein free media for the production of a veterinary rabies vaccine in BHK-21 cells. *Journal of Biotechnology.* 95(3), pp.195-204.

Kell, D., Markx, G.H., Davey, C.L. and Todd, R.W. 1990. Real-time monitoring of cellular biomass: methods and applications. *Trends in Analytical Chemistry.* 9(6), pp.190-194.

Kell, D. and Todd, R.W. 1998. Dielectric estimation of microbial biomass using the Aber Instruments Biomass Monitor. *Trends in Biotechnology.* 16 (4), pp.149-150.

Kiviharju, K., Salonen, K., Moilanen, U., Meskanen, E., Leisola, M. and Eerikäinen, T., 2007. On-line biomass measurements in bioreactor cultivations: comparison study of two on-line probes. *Journal of Industrial Microbiology & Biotechnology.* 34(8), pp.561-566.

Kurano, N., Leist, C., Messi, F., Gandor, C., Kurano, S. and Fiechter, A. 1990. Growth kinetics of Chinese hamster ovary cells in a compact loop bioreactor. Selection and characterization of an anchorage-independent subline and medium improvement. *Journal of Biotechnology.* 16(3-4), pp.245-258.

Kuwae, S., Ohda, T., Tamashima, H., Miki, H. and Kobayashi, K. 2005. Development of a fed-Batch culture process for enhanced production of recombinant human antithrombin by Chinese hamster ovary cells. *Journal of Bioscience and Bioengineering.* 100(5), pp.502-510.

Laken, H.A. and Leonard, M.W. 2001. Understanding and modulating apoptosis in industrial cell culture. *Current Opinion in Biotechnology,* 12(2), pp.175-179.

Lao, M. and Toth, D. 1997. Effects of Ammonium and Lactate on Growth and Metabolism of a Recombinant Chinese Hamster Ovary Cell Culture. *Biotechnology Progress.* 13(5), pp.688-691.

Lee, Y.Y., Wong, K.T.K., Nissom, P.M., Wong, D.C.F. and Yap, M.G.S. 2007. Transcriptional profiling of Batch and fed-Batch protein-free 293-HEK cultures. *Metabolic Engineering.* 9(1), pp.52-67.

Leelavatcharamas, V., Emery, A. and al-Rubeai, M. 1994. Growth and interferon-gamma production in Batch culture of CHO cells. *Cytotechnology.* 15(1-3), pp.65-71.

Li, L., Qin, J., Feng, Q., Tang, H., Liu, R., Xu, L. and Chen, Z. 2011. Heparin promotes suspension adaptation process of CHO-TS28 cells by eliminating cell aggregation. *Molecular Biotechnology.,* 47(1), pp.9-17.

Lim, S.F., Chuan, K.H., Liu, S., Loh, S.O.H., Chung, B.Y.F., Ong, C.C. and Song, Z. 2006. RNAi suppression of Bax and Bak enhances viability in fed-Batch cultures of CHO cells. *Metabolic Engineering,* 8(6), pp.509-522.

Link, T., Bäckström, M., Graham, R., Essers, R., Zörner, K., Gätgens, J., Burchell, J., Taylor-Papadimitriou, J., Hansson, G.C. and Noll, T. 2004. Bioprocess development for the production of a recombinant MUC1 fusion protein expressed by CHO-K1 cells in protein-free medium. *Journal of Biotechnology.* 110(1), pp.51-62.

Lopes, J.A., Costa, P.F., Alves, T.P. and Menezes, J.C. 2004. Chemometrics in bioprocess engineering: process analytical technology (PAT) applications. *Chemometrics and Intelligent Laboratory Systems.* 74(2), pp.269-275.

Markx, G.H. and Davey, C.L. 1999. The dielectric properties of biological cells at radiofrequencies: Applications in biotechnology. *Enzyme and Microbial Technology.* 25(3-5), pp.161-171.

Markx, G.H., ten Hoopen, H.J.G., Meijer, J.J. and Vinke, K.L. 1991. Dielectric spectroscopy as a novel and convenient tool for the study of the shear sensitivity of plant cells in suspension culture. *Journal of Biotechnology.* 19(2-3), pp.145-157.

Marose, S., Lindemann, C., Ulber, R. and Scheper, T. 1999. Optical sensor systems for bioprocess monitoring. *Trends in Biotechnology,* 17(1), pp.30-34.

Maskow, T., Röllich, A., Fetzer, I., Yao, J. and Harms, H. 2008. Observation of non-linear biomass–capacitance correlations: Reasons and implications for bioprocess control. *Biosensors and Bioelectronics.* 24(1), pp.123-128.

Matanguihan, R.M., Konstantinov, K.B. and Yoshida, T. 1994. Dielectric measurement to monitor the growth and the physiological states of biological cells. *Bioprocess and Biosystems Engineering.* 11(6), pp.213-222.

Matasci, M., Hacker, D.L., Baldi, L. and Wurm, F.M. 2008. Recombinant therapeutic protein production in cultivated mammalian cells: current status and future prospects. *Drug Discovery Today: Technologies.* 5(2-3), pp.37-42.

Maxwell, J.C. 1873. A treatise on electricity and magnetism. *Clarendon Press, Oxford.*

McDermot, R.H., Butler, M. 1993. Uptake of glutamate, not glutamine synthetase, regulates adaptation of mammalian cells to glutamine-free medium. *Journal of Cell Science.* 104(1), pp.51-58.

Meuwly, F., Ruffieux, P.-., Kadouri, A. and von Stockar, U. 2007. Packed-bed bioreactors for mammalian cell culture: Bioprocess and biomedical applications. *Biotechnology Advances.* 25(1), pp.45-56.

Michiels, J., Barbau, J., De Boel, S., Dessy, S., Agathos, S.N. and Schneider, Y. 2011. Characterisation of beneficial and detrimental effects of a soy peptone, as an additive for CHO cell cultivation. *Process Biochemistry.* 46(3), pp.671-681.

Neves, A.A., Pereira, D.A., Vieira, L.M. and Menezes, J.C. 2000. Real time monitoring biomass concentration in Streptomyces clavuligerus cultivations with industrial media using a capacitance probe. *Journal of Biotechnology.* 84(1), pp.45-52.

Nienow, A.W. 2006. Reactor engineering in large scale animal cell culture. *Cytotechnology.* 50(1-3), pp.9-33.

Noble, P.A., Dziuba, M., Harrison, D.J. and Albritton, W.L. 1999. Factors influencing capacitance-based monitoring of microbial growth. *Journal of Microbiological Methods.* 37(1), pp.51-64.

Noll, T. and Biselli, M. 1998. Dielectric spectroscopy in the cultivation of suspended and immobilized hybridoma cells. *Journal of Biotechnology.* 63(3), pp.187-198.

Olsson, L. and Nielsen, J. 1997. On-line and in situ monitoring of biomass in submerged cultivations. *Trends in Biotechnology.* 15(12), pp.517-522.

Opel, C.F., Li, J. and Amanullah, A. 2010. Quantitative modelling of viable cell density, cell size, intracellular conductivity, and membrane capacitance in Batch and fed-Batch CHO processes using dielectric spectroscopy. *Biotechnology Progress.* 26(4), pp. 1187-1199.

Park, J., Jung, S., Seo, H. and Kim, H. 2007. SB203580 enhances interleukin-1 receptor antagonist gene expression in IFN-γ-stimulated BV2 microglial cells through a composite nuclear factor-κB/PU.1 binding site. *Neuroscience Letters.* 416(2), pp.169-174.

Park, J.G., Choi, S.S. and Park, T.H. 2007. Enhancement of cell growth and viability of CHO cells in serum-free media by 30Kc6 gene expression. *Process Biochemistry.* 42(1), pp.8-15.

Pohl, H.A. 1978. Dielectrophoresis. *Cambridge University Press, Cambridge.*

Polevaya, Y., Ermolina, I., Schlesinger, M., Ginzburg, B. and Feldman, Y., 1999. Time domain dielectric spectroscopy study of human cells: II. Normal and malignant white blood cells. *Biochimica Et Biophysica Acta (BBA) - Biomembranes.* 1419(2), pp. 257-271.

Pucihar, G., Kotnik, T., Kandušer, M. and Miklavčič, D. 2001. The influence of medium conductivity on electropermeabilization and survival of cells in vitro. *Bioelectrochemistry.* 54(2), pp.107-115.

Schlaeger, E. and Schumpp, B. 1992. Propagation of a mouse myeloma cell line J558L producing human CD4 immunoglobulin G1. *Journal of Immunological Methods.* 146(1), pp.111-120.

Schneider, M., Marison, I.W. and von Stockar, U. 1996. The importance of ammonia in mammalian cell culture. *Journal of Biotechnology.* 46(3), pp.161-185.

Schwan, H.P. 1957. Electrical properties of tissue and cell suspensions. *Advances in Biological and Medical Physics.* 5 pp.147-209.

Searles, J.A., Todd, P. and Kompala, D.S. 1994. Viable Cell Recycle with an Inclined Settler in the perfusion Culture of Suspended Recombinant Chinese Hamster Ovary Cells. *Biotechnology Progress.* 10(2), pp.198-206.

Siano, S.A. and Mutharasan, R. 1991. NADH fluorescence and oxygen uptake responses of hybridoma cultures to substrate pulse and step changes. *Biotechnology and Bioengineering,* 37(2), pp.141-159.

Soley, A., Lecina, M., Gámez, X., Cairó, J.J., Riu, P., Rosell, X., Bragós, R. and Gòdia, F. 2005. On-line monitoring of yeast cell growth by impedance spectroscopy. *Journal of Biotechnology,* 118(4), pp.398-405.

Sommerfeld, S. and Strube, J. 2005. Challenges in biotechnology production—generic processes and process optimization for monoclonal antibodies. *Chemical Engineering and Processing.* 44(10), pp.1123-1137.

Sugiura, T. and Kakuzaki, M. 1998. Dynamics of recombinant protein production by mammalian cells in immobilized perfusion culture. *Enzyme and Microbial Technology.* 22(8), pp.699-704.

Sun, X. and Zhang, Y. 2004. Glutamine cannot support recombinant CHO cell growth and maintenance in the absence of glucose. *Process Biochemistry.* 39(6), pp.719-722.

Sunley, K. and Butler, M. 2010. Strategies for the enhancement of recombinant protein production from mammalian cells by growth arrest. *Biotechnology Advances.* 28(3), pp.385-394.

Takuma, S., Hirashima, C. and Piret, J.M. 2007. Dependence on glucose limitation of the $pCO_2$ influences on CHO cell growth, metabolism and IgG production. *Biotechnology and Bioengineering.* 97(6), pp.1479-1488.

Teixeira, A.P., Oliveira, R., Alves, P.M. and Carrondo, M.J.T. 2009. Advances in on-line monitoring and control of mammalian cell cultures: Supporting the PAT initiative. *Biotechnology Advances.* 27(6), pp.726-732.

Tsao, Y.-., Cardoso, A.G., Condon, R.G.G., Voloch, M., Lio, P., Lagos, J.C., Kearns, B.G. and Liu, Z., 2005. Monitoring Chinese hamster ovary cell culture by the analysis of glucose and lactate metabolism. *Journal of Biotechnology.* 118(3), pp.316-327.

Ulanovskaya, O., Cui, J., Kron, S. and Kozmin, S. 2011. A Pairwise Chemical Genetic Screen Identifies New Inhibitors of Glucose Transport. *Chemistry & Biology.* 18(2), pp.222-230.

U.S. Department of Health and Human Services: Food and Drug Administration., 2004. *Guidance for Industry PAT - A Framework for Innovative Pharmaceutical Development, Manufacturing, and Quality Assurance.*

Voisard, D., Esteban, G. and Baer, B. 2010. Capacitance Sensor as a Robust Tool for Cell Culture Monitoring in Process Development and Manufacturing. *Biomedical and Life Sciences ESACT Proceedings.* 4(6), pp. 811-817.

Vojinović, V., Cabral, J.M.S. and Fonseca, L.P. 2006. Real-time bioprocess monitoring: Part I: In situ sensors. *Sensors and Actuators B: Chemical.* 114(2), pp. 1083-1091.

Wang, Y., Chu, J., Zhuang, Y., Wang, Y., Xia, J. and Zhang, S. 2009. Industrial bioprocess control and optimization in the context of systems biotechnology. *Biotechnology Advances.* 27(6), pp.989-995.

White, S.F., Turner, A.P.F., Biltewski, U., Bradley, J. and Schmid, R.D. 1995. On-line monitoring of glucose, glutamate and glutamine during mammalian cell cultivations. *Biosensors and Bioelectronics,* 10(6-7), pp.543-551.

Wong, D.C.F., Wong, K.T.K., Nissom, P.M., Heng, C.K. and Yap, M.G.S. 2006. Targeting early apoptotic genes in Batch and fed-Batch CHO cell cultures. *Biotechnology and Bioengineering.* 95(3), pp.350-361.

Xing, Z., Bishop, N., Leister, K. and Li, Z.J. 2010. Modelling kinetics of a large-scale fed-Batch CHO cell culture by Markov chain Monte Carlo method. *Biotechnology Progress.* 26(1), pp. 208-219.

Xiong, Z., Guo, M., Guo, Y., Chu, J., Zhuang, Y. and Zhang, S. 2008. Real-time viable-cell mass monitoring in high-cell-density fed-Batch glutathione fermentation by Saccharomyces cerevisiae T65 in industrial complex medium. *Journal of Bioscience and Bioengineering.* 105(4), pp.409-413.

Yamaji, H., Manabe, T., Kitaura, A., Izumoto, E. and Fukuda, H. 2006. Efficient production of recombinant protein in immobilized insect cell culture using serum-free basal media after baculovirus infection. *Biochemical Engineering Journal.* 28(1), pp.67-72.

Yoon, S.K., Hong, J.K., Choo, S.H., Song, J.Y., Park, H.W. and Lee, G.M. 2006. Adaptation of Chinese hamster ovary cells to low culture temperature: Cell growth and recombinant protein production. *Journal of Biotechnology.* 122(4), pp.463-472.

Zeiser, A., Bédard, C., Voyer, R., Jardin, B., Tom, R. and Kamen, A.A. 1999. On-line monitoring of the progress of infection in Sf-9 insect cell cultures using relative permittivity measurements. *Biotechnology and Bioengineering.* 63(1), pp. 122-126.

Zhang, P., Lifen Tan, D., Heng, D., Wang, T., Mariati, Yang, Y. and Song, Z. 2010. A functional analysis of N-glycosylation-related genes on sialylation of recombinant erythropoietin in six commonly used mammalian cell lines. *Metabolic Engineering,* 12(6), pp.526-536.

Zhang, X., Stettler, M., Reif, O., Kocourek, A., DeJesus, M., Hacker, D.L. and Wurm, F.M. 2008. Shaken helical track bioreactors: Providing oxygen to high-density cultures of mammalian cells at volumes up to 1000 L by surface aeration with air. *New Biotechnology.* 25(1), pp.68-75.

Zhu, M.M., Goyal, A., Rank, D.L., Gupta, S.K., Boom, T.V. and Lee, S.S. 2005. Effects of Elevated pCO2 and Osmolality on Growth of CHO Cells and Production of Antibody-Fusion Protein B1: A Case Study. *Biotechnology Progress.* 21(1), pp. 70-77.

# 6. Appendices

## Appendix A. Cell culture Techniques

### Appendix A.1 Thawing

1. An ampoule was selected from the cell bank contained in liquid nitrogen. It was noted in the log book which ampoule was taken as well as name, date and location in tank.
2. The ampoule was thawed in a 37°C incubator.
3. Once thawed the ampoule was immediately sprayed with 70% IMS and transferred to the laminar flow cabinet.
4. Using a 5 ml pipette, the cells were transferred to a 50 ml centrifuge tube and 10 ml of un-supplemented EX-CELL CHO DHFR$^-$ medium at 37 °C was pipetted slowly down the side of the centrifuge tube.
5. The cell suspension was centrifuged at 200 RPM for 5 minutes and centrifuge tube was sprayed with 70 % IMS (Industrial Methylated Spirits) before being returned to the laminar flow cabinet to pour off the supernatant.
6. The supernatant was poured into a waste vessel.
7. With a 10 ml pipette, 10 ml of supplemented medium (4mM L-glutamine and 1 μM MTX) was added to the to cell pellet in the centrifuge tube.
8. The pellet was re-suspended by gently aspirating cell pellet into the medium.
9. The cells were counted by the microscope and haemocytometer (Section 2.2.1) and the cells were seeded in a 250 ml Erlenmeyer flask in appropriate volume to ensure cell density of $0.3 \times 10^6$ cells/ml, for example if the cell density in the 10 ml re-suspension was $0.6 \times 10^6$ cells/ml, 10 ml medium was added creating a 20 ml suspension at $0.3 \times 10^6$ cells/ml.
10. For scaling up, existing cell cultures were subcultured from the flask prepared above and seeded at $0.3 \times 10^6$ cells/ml in new flask or number of flasks.

## Appendix B. Cell density determination

### Appendix B.1 Cell counts by microscope and haemocytometer

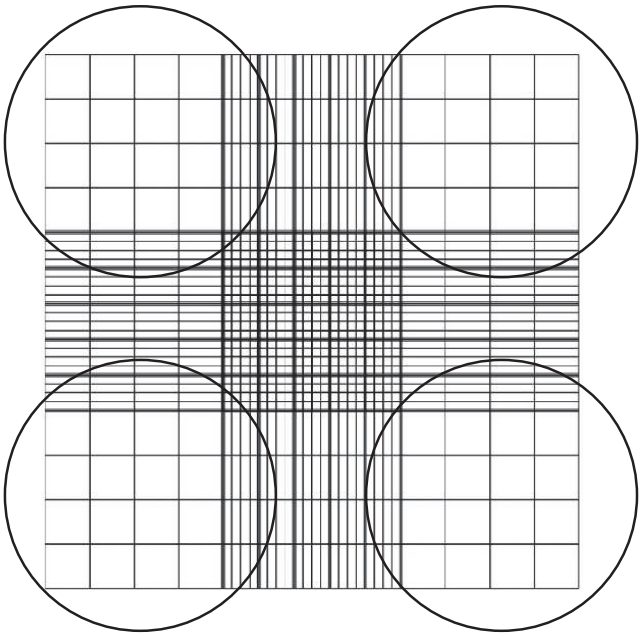

**Figure 42**: Haemocytometer view under microscope

1. Cell counting was based on the trypan blue exclusion method.
2. The cell culture vessel was swirled gently.
3. 20 µl cell suspension was removed from the vessel and pipetted into 1.5 ml micro centrifuge tube.
4. 20 µl of trypan blue was mixed with the cell suspension by aspiration of the combined contents in the micro-centrifuge tube and was incubated at room temperature for three minutes.
5. The haemocytometer and glass slide were removed from the storage box and wiped with 70% IMS and a dust free wipe.

6. Before addition of any cell/trypan blue moisture ensure the IMS is allowed evaporate off.
7. 10 µl of cell suspension/trypan blue mixture is pipetted onto haemocytometer.
8. Cells are counted in the external 4 grids (circled), refer to Figure 49.
9. Viable cells appeared clear and non-viable cells were stained blue.
10. Each of the 4 viable cell counts are added together, divided by 4 (to get average), multiplied by 2 (dilution factor) and by 10,000 (to scale up to cells/ml) to calculate number of viable and repeated for non-viable cells.
11. Viability is calculated by dividing viable cells by total number of viable and dead cells and multiplying by 100 to correct for percentage.

**Table 8**: Example of cell counts.

| Count | Viable cell number | Dead cell number |
|---|---|---|
| 1 | 16 | 1 |
| 2 | 21 | 2 |
| 3 | 20 | 1 |
| 4 | 21 | 0 |
| Average cell count per grid | 19.5 | 1 |
| Cell Density [$\times 10^6$ cells/ml] | 0.39 | 0.02 |
| Viability [%] | 95.12 | N/A |

**Appendix B.2 Cell counts by Countess automated cell counter**

1. Steps 2 – 5 were repeated from Appendix B.1.
2. Countess cell counter was switched on.
3. Countess plastic slide was removed from packaging.
4. 10 µl of cell suspension/trypan blue mixture was pipetted into a space in the plastic slide, this was repeated for the other section of the plastic slide allowing duplicate counts.
5. The zoom button was rotated to focus on the cells that can be seen on the main screen.

6. Once the cells were in focus, the count cells option was selected on the Countess main screen and the cells were counted automatically.
7. Total, viable and dead cell densities were displayed along with viability data, viable and dead cell diameter data and number of viable and dead cells.
8. Results were recorded manually.

**Appendix B.3 Cell density determination by Optical Density**

1. After the Biomass Monitor was used to analyse the cell suspension in a 40 ml volume, optical density was measured.
2. The UV-spectrometer was switched on and set to a wavelength of 600 nm.
3. 1 ml sample of supplemented medium was added to a cuvette, lid of UV-spectrometer closed and the blank option was selected.
4. A 1 ml sample of cell suspension was taken with a pipette and added to a cuvette following the zeroing of the UV-spectrometer.
5. The lid was closed over and the absorbance noted.

**Appendix B.4 Cell density determination by Capacitance**

1. The Biomass Monitor (BM), probe, 250 ml graduated cylinder, stirrer and hotplate, magnetic pellet and retort stand were brought to the work area.
2. The BM probe was connected to the Biomass Monitor and secured by retort stand.
3. The BM was switched on and it was ensured the earth line was connected.
4. Frequency was set to the desired range.
5. 40 ml of supplemented medium was added to the 250 ml graduated cylinder with a magnetic stirrer pellet placed at the bottom and the Biomass Monitor probe was placed into the medium.
6. The probe was in the medium 20 mm from the bottom of the graduated cylinder.
7. The retort stand was marked so that the same position could be used in subsequent analysis.
8. The Biomass Monitor was allowed equilibrate for 2 hours with the RPM set to 120 and the temperature set to 30 °C to achieve a steady baseline.
9. Every 30 minutes a clean cycle was conducted by selecting the option on the main screen.

10. This was followed by a zero cycle.
11. If any bubbles were noticed around the probe the probe was gently rocked to dislodge them.
12. After a steady baseline had been reached, a final clean and zero cycle was conducted.
13. The blank medium was poured into a centrifuge tube and 40 ml cell suspension was added to the graduated cylinder.
14. The probe was immersed in the solution.
15. After the reading had stabilised and the temperature was in the required range, the capacitance, conductivity and temperature were noted.

## Appendix C. Calculations:

### Appendix C.1 Calculation of viable cell volume

1. A cell can be assumed to be spherical in confirmation.
2. Volume of a sphere: $\left(\frac{4}{3}\right) * \pi * \left(r^3\right)$

Where:

$\pi$ = 3.14159.

r = Radius of a cell.

3. The average cell diameter from the Countess was used and divided by 2 to get the radius.
4. The radius was then substituted into the equation in point 2, above and volume of 1 cell was attained.
5. The volume of 1 cell was multiplied by the viable cell density to get the viable cell volume.

**Appendix D: RT and RT 2 Raw Data**

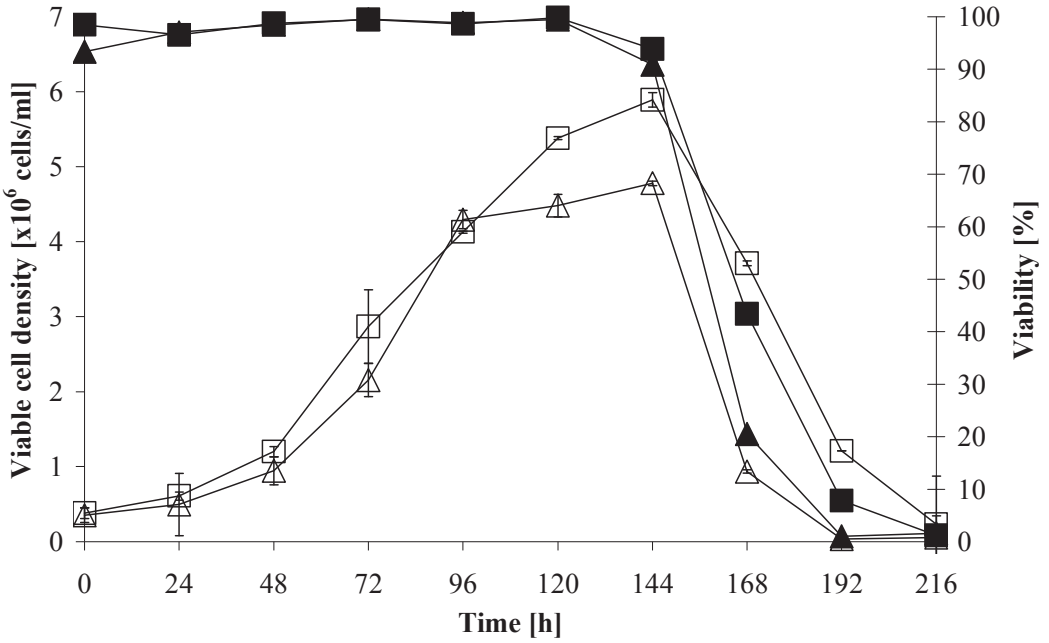


**Figure 43:** Raw cell density data for RT and RT 2 cultures. Symbols: Viable cell density RT (Δ), RT 2 (□), viability RT (▲) and viability RT 2 (■).

Cell growth data was the same until 96 hours of both cultures (corresponding to the end of the exponential growth phase) when the cultures diverged. The growth rate of the RT culture slowed in comparison to RT 2 culture between 96 and 144 hours. The death phase began at 144 hours, characterised by drop cell density and viability in both cultures (RT and RT 2).

**Appendix D.1 Raw data of cell density prediction models from capacitance readings**

**Table 9:** Cell density prediction from capacitance models at 0.2 and 10 MHz at 37 °C.

| Actual viable cell density (RT 2) [$\times 10^6$ cells/ml] | Predicted viable cell density from HCD [$\times 10^6$ cells/ml] | Predicted cell viable density from HCD + RT [$\times 10^6$ cells/ml] | Predicted viable cell density from RT [$\times 10^6$ cells/ml] |
|---|---|---|---|
| 0.38 | 0.42 | 0.39 | 0.30 |
| 0.61 | 0.69 | 0.64 | 0.50 |
| 1.20 | 1.23 | 1.14 | 0.90 |
| 2.87 | 2.60 | 2.41 | 1.90 |
| 4.13 | 3.99 | 3.70 | 2.92 |
| 5.38 | 4.27 | 3.95 | 3.12 |
| 5.89 | 4.71 | 4.36 | 3.44 |
| 3.71 | 2.74 | 2.53 | 2.00 |
| 1.21 | 1.34 | 1.24 | 0.98 |
| 0.23 | 0.12 | 0.11 | 0.09 |
| **RMSEP** | **0.61** | **0.78** | **1.29** |

Refer to Figure 15 for graphed data.

**Table 10:** Cell density prediction from capacitance models at 0.6 and 10 MHz at 37 °C.

| Actual viable cell density (RT 2) [$\times 10^6$ cells/ml] | Predicted viable cell density from HCD [$\times 10^6$ cells/ml] | Predicted viable cell density from HCD + RT [$\times 10^6$ cells/ml] | Predicted viable cell density from RT [$\times 10^6$ cells/ml] |
|---|---|---|---|
| 0.38 | 0.54 | 0.48 | 0.44 |
| 0.61 | 0.82 | 0.72 | 0.67 |
| 1.20 | 1.67 | 1.47 | 1.38 |
| 2.87 | 3.25 | 2.86 | 2.68 |
| 4.13 | 5.57 | 4.92 | 4.60 |
| 5.38 | 6.13 | 5.41 | 5.07 |
| 5.89 | 6.58 | 5.80 | 5.43 |
| 3.71 | 3.76 | 3.31 | 3.10 |
| 1.21 | 1.70 | 1.50 | 1.40 |
| 0.23 | 0.24 | 0.21 | 0.20 |
| **RMSEP** | **0.62** | **0.31** | **0.32** |

Refer to Figure 19 for graphed data.

**Table 11:** Cell density prediction from capacitance models at 0.2 and 10 MHz at 30 °C.

| Actual viable cell density (RT 2) [$\times 10^6$ cells/ml] | Predicted viable cell density from HCD [$\times 10^6$ cells/ml] | Predicted viable cell density from HCD +RT [$\times 10^6$ cells/ml] | Predicted viable cell density from RT [$\times 10^6$ cells/ml] |
|---|---|---|---|
| 0.38 | 0.45 | 0.40 | 0.43 |
| 0.61 | 0.63 | 0.58 | 0.61 |
| 1.20 | 1.40 | 1.23 | 1.35 |
| 2.87 | 2.79 | 2.60 | 2.69 |
| 4.13 | 4.37 | 4.14 | 4.20 |
| 5.38 | 5.14 | 4.85 | 4.95 |
| 5.89 | 5.57 | 5.30 | 5.36 |
| 3.71 | 3.24 | 3.03 | 3.12 |
| 1.21 | 1.67 | 1.54 | 1.60 |
| 0.23 | 0.19 | 0.17 | 0.18 |
| **RMSEP** | **0.26** | **0.36** | **0.32** |

Refer to Figure 23 for graphed data.

**Table 12:** Cell density prediction from capacitance models at 0.6 and 10 MHz at 30°C.

| Actual Viable cell density (RT 2) [$\times 10^6$ cells/ml] | Predicted viable cell density from HCD [$\times 10^6$ cells/ml] | Predicted viable cell density from HCD + RT [$\times 10^6$ cells/ml] | Predicted viable cell density from RT [$\times 10^6$ cells/ml] |
|---|---|---|---|
| 0.38 | 0.23 | 0.27 | 0.35 |
| 0.61 | 0.69 | 0.81 | 1.05 |
| 1.20 | 1.42 | 1.67 | 2.16 |
| 2.87 | 2.66 | 3.12 | 4.02 |
| 4.13 | 4.24 | 4.97 | 6.42 |
| 5.38 | 4.81 | 5.65 | 7.29 |
| 5.89 | 5.24 | 6.15 | 7.93 |
| 3.71 | 3.66 | 4.29 | 5.54 |
| 1.21 | 1.31 | 1.54 | 1.98 |
| 0.23 | 0.23 | 0.27 | 0.35 |
| **RMSEP** | **0.30** | **0.40** | **1.39** |

Refer to Figure 26 for graphed data.

**Table 13:** Capacitance and viable cell volume model applied to real time data at 0.2 and 10 MHz at 37 °C.

| Actual viable cell volume (RT 2) [$\times 10^9$ $\mu m^3$ $ml^{-1}$] | Predicted viable cell volume from HCD [$\times 10^9$ $\mu m^3$ $ml^{-1}$] | Predicted viable cell volume from HCD + RT [$\times 10^9$ $\mu m^3$ $ml^{-1}$] | Predicted viable cell volume from RT [$\times 10^9$ $\mu m^3$ $ml^{-1}$] |
|---|---|---|---|
| 0.48 | 0.64 | 0.57 | 0.82 |
| 1.01 | 0.90 | 0.81 | 1.16 |
| 2.30 | 2.00 | 1.79 | 2.58 |
| 4.72 | 3.97 | 3.57 | 5.13 |
| 8.36 | 6.21 | 5.58 | 8.02 |
| 6.26 | 7.31 | 6.56 | 9.43 |
| 5.19 | 7.92 | 7.12 | 10.23 |
| 4.02 | 4.61 | 4.14 | 5.95 |
| 2.01 | 2.37 | 2.13 | 3.06 |
| 0.29 | 0.26 | 0.24 | 0.34 |
| **RMSEP** | **1.20** | **1.15** | **2.02** |

Refer to Figure 30 for graphed data.

**Table 14:** Capacitance and viable cell volume model applied to real time data at 0.6 and 10 MHz at 37 °C.

| Actual viable cell volume (RT 2) [$\times 10^9$ $\mu m^3$ $ml^{-1}$] | Predicted viable cell volume from HCD [$\times 10^9$ $\mu m^3$ $ml^{-1}$] | Predicted viable cell volume from HCD + RT [$\times 10^9$ $\mu m^3$ $ml^{-1}$] | Predicted viable cell volume from RT [$\times 10^9$ $\mu m^3$ $ml^{-1}$] |
|---|---|---|---|
| 0.48 | 0.27 | 0.33 | 0.49 |
| 1.01 | 0.80 | 0.98 | 1.47 |
| 2.30 | 1.64 | 2.02 | 3.03 |
| 4.72 | 3.07 | 3.76 | 5.65 |
| 8.36 | 4.89 | 6.00 | 9.01 |
| 6.26 | 5.56 | 6.82 | 10.24 |
| 5.19 | 6.05 | 7.42 | 11.14 |
| 4.02 | 4.22 | 5.18 | 7.78 |
| 2.01 | 1.51 | 1.85 | 2.79 |
| 0.29 | 0.27 | 0.33 | 0.49 |
| **RMSEP** | **1.3** | **1.15** | **2.61** |

Refer to Figure 33 for graphed data.

**Table 15:** Capacitance and viable cell volume model applied to real time data at 0.2 and 10 MHz at 30 °C.

| Actual viable cell volume (RT 2) [$\times 10^9$ μm$^3$ ml$^{-1}$] | Predicted viable cell volume from HCD [$\times 10^9$ μm$^3$ ml$^{-1}$] | Predicted viable cell volume from HCD + RT [$\times 10^6$ cells/ml] | Predicted viable cell volume from RT [$\times 10^6$ cells/ml] |
|---|---|---|---|
| 0.48 | 0.41 | 0.47 | 0.59 |
| 1.01 | 0.68 | 0.77 | 0.97 |
| 2.30 | 1.20 | 1.36 | 1.72 |
| 4.72 | 2.54 | 2.87 | 3.63 |
| 8.36 | 3.90 | 4.41 | 5.58 |
| 6.26 | 4.17 | 4.71 | 5.96 |
| 5.53 | 4.61 | 5.21 | 6.58 |
| 4.02 | 2.68 | 3.03 | 3.82 |
| 1.34 | 1.32 | 1.49 | 1.88 |
| 0.29 | 0.12 | 0.14 | 0.18 |
| **RMSEP** | **1.81** | **1.53** | **1.03** |

Refer to Figure 35 for graphed data.

**Table 16:** Capacitance and viable cell volume model applied to real time data at 0.6 and 10 MHz at 30 °C.

| Actual viable cell volume (RT 2) [$\times 10^9$ $\mu m^3$ $ml^{-1}$] | Predicted viable cell volume from HCD [$\times 10^9$ $\mu m^3$ $ml^{-1}$] | Predicted viable cell volume from HCD + RT [$\times 10^6$ cells/ml] | Predicted viable cell volume from RT [$\times 10^6$ cells/ml] |
|---|---|---|---|
| 0.48 | 0.62 | 0.70 | 0.78 |
| 1.01 | 0.96 | 1.08 | 1.21 |
| 2.30 | 1.96 | 2.20 | 2.46 |
| 4.72 | 3.83 | 4.29 | 4.79 |
| 8.36 | 6.58 | 7.36 | 8.23 |
| 6.26 | 7.24 | 8.11 | 9.06 |
| 5.53 | 7.76 | 8.69 | 9.72 |
| 4.02 | 4.43 | 4.96 | 5.55 |
| 1.34 | 2.00 | 2.25 | 2.51 |
| 0.29 | 0.28 | 0.31 | 0.35 |
| **RMSEP** | **1.03** | **1.30** | **1.71** |

Refer to Figure 37 for graphed data.

**Table 17:** Optical density model applied to real time data.

| Actual viable cell density (RT 2) [$\times 10^6$ cells/ml] | Predicted viable cell density from HCD [$\times 10^6$ cells/ml] | Predicted viable cell density from HCD + RT [$\times 10^6$ cells/ml] | Predicted viable cell density from RT [$\times 10^6$ cells/ml] |
|---|---|---|---|
| 0.38 | 0.21 | 0.22 | 0.27 |
| 0.61 | 0.41 | 0.44 | 0.53 |
| 1.20 | 0.78 | 0.83 | 1.01 |
| 2.87 | 1.48 | 1.58 | 1.92 |
| 4.13 | 3.21 | 3.43 | 4.17 |
| 5.38 | 3.73 | 3.98 | 4.84 |
| 5.89 | 4.22 | 4.51 | 5.48 |
| **RMSEP** | **1.2** | **1.01** | **0.48** |

Refer to Figure 40 for graphed data.

## Appendix E. Analysis of substrates, metabolites and product

### Appendix E.1 Glucose

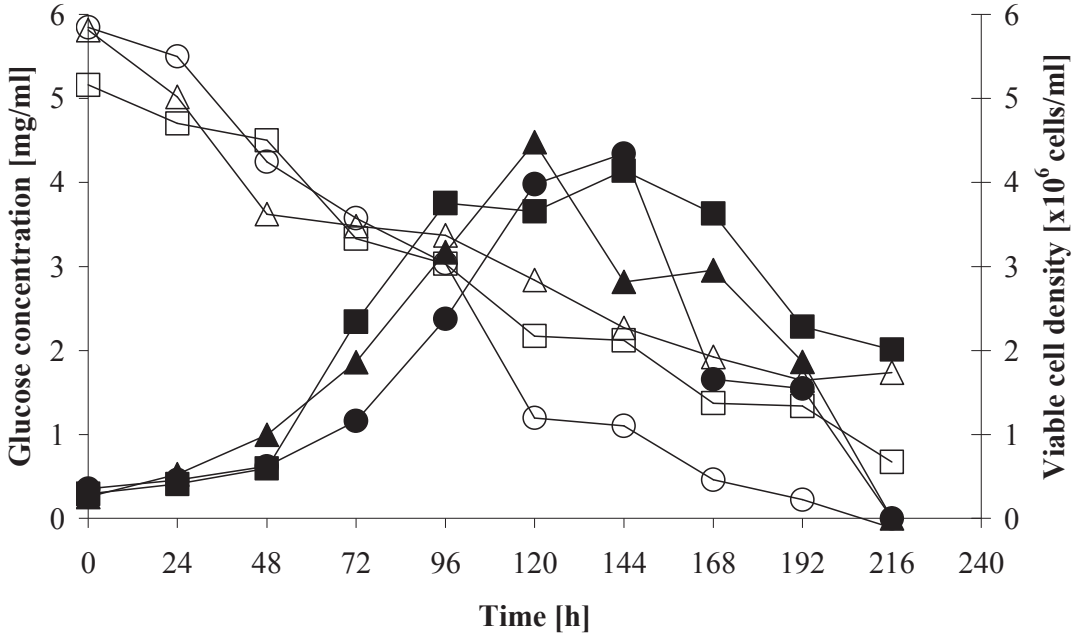


**Figure 44:** Glucose concentration and viable cell density versus time for Batch cultures 1-3. Symbols: Viable cell density for Batch 1 (■), Batch 2 (▲), Batch 3 (●) cultures, glucose concentration for Batch 1 (□), Batch 2 (Δ) and Batch 3 (○) cultures versus time.

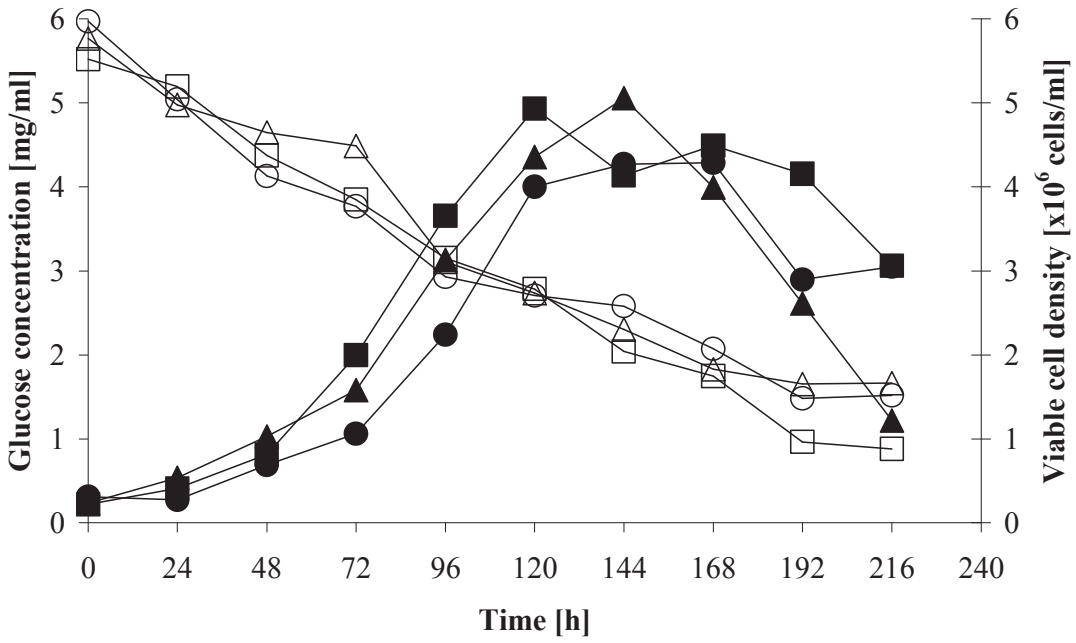


**Figure 45:** Glucose concentration and viable cell density versus time for Fed Batch cultures 1-3. Symbols: Viable cell density for Fed Batch 1 (■), Fed Batch 2 (▲), Fed Batch 3 (●) cultures, glucose concentration for Fed Batch 1 (□), Fed Batch 2 (Δ) and Fed Batch 3 (○) cultures versus time.

**Table 18:** Summary of glucose concentrations at end of exponential phase.

| Culture type | Glucose concentration at end of exponential phase [mg/ml] | Glucose concentration at end of culture [mg/ml] |
|---|---|---|
| Batch 1 | 16.8 | 3.7 |
| Batch 2 | 18.7 | 9.6 |
| Batch 3 | 6.6 | 0 |
| Fed Batch 1 | 17.5 | 4.9 |
| Fed Batch 2 | 17.3 | 9.2 |
| Fed Batch 3 | 16.3 | 8.4 |

Table 18 shows glucose is not the reason the exponential phase ended the table indicates the majority of cultures had over 50 % of the original glucose concentration present at the end of the exponential phase. Lactate accumulation can be attributed to

a decrease in cell growth as Takuma, Hirashima and Piret (2007) reported that lactate, a waste product of glucose metabolism can affect growth of cells and protein productivity levels.

**Appendix E.2 Lactate**

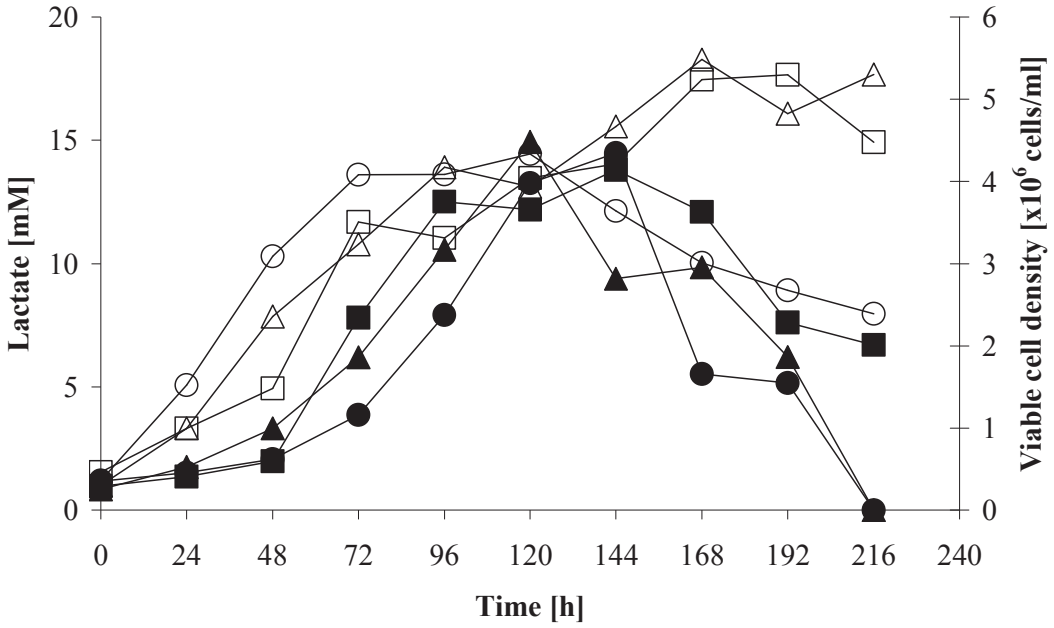


**Figure 46:** Lactate concentration and viable cell density versus time for Batch cultures 1-3. Symbols: Viable cell density for Batch 1 (■), Batch 2 (▲), Batch 3 (●) cultures, lactate concentration for Batch 1 (□), Batch 2 (Δ) and Batch 3 (○) cultures versus time.

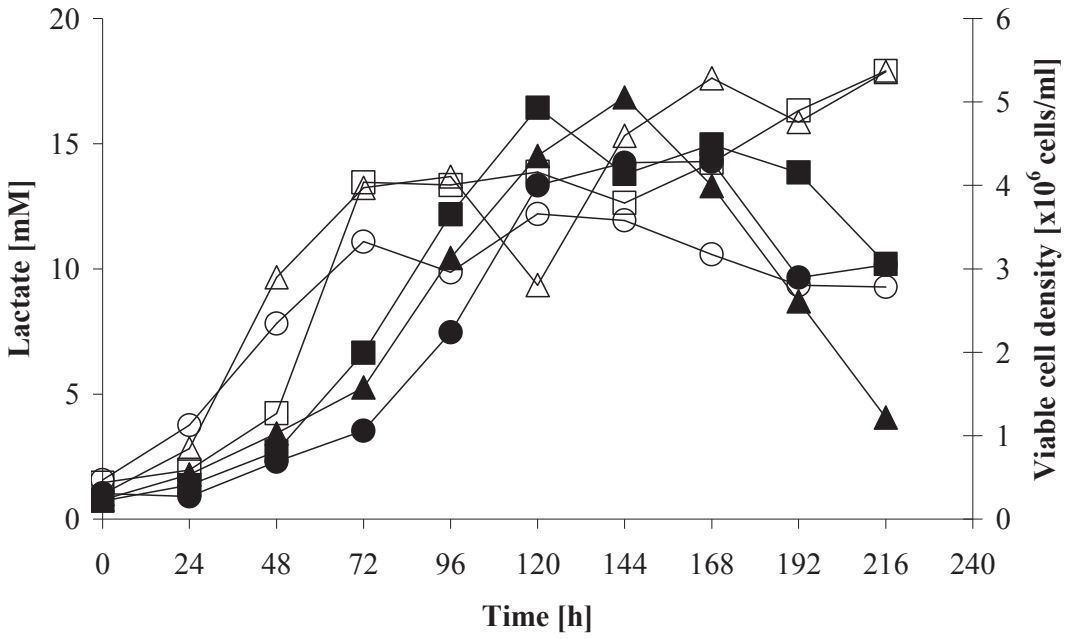


**Figure 47:** Lactate concentration and viable cell density versus time for Fed Batch cultures 1-3. Symbols: Viable cell density for cultures Fed Batch 1 (■), Fed Batch 2 (▲), Fed Batch 3 (●), lactate concentration for cultures Fed Batch 1 (□), Fed Batch 2 (Δ) and Fed Batch 3 (○) versus time.

**Table 19:** Summary of lactate concentrations.

| Culture type | Lactate concentration at end of exponential phase [mM] | Max lactate concentration [mM] |
|---|---|---|
| Batch 1 | 11.0 | 17.6 |
| Batch 2 | 13.9 | 18.3 |
| Batch 3 | 13.6 | 14.5 |
| Fed Batch 1 | 13.3 | 17.9 |
| Fed Batch 2 | 13.7 | 17.9 |
| Fed Batch 3 | 9.0 | 12.2 |

Lactate concentrations encountered in mammalian cell cultures with CHO cell lines generally have a maximum concentration in the range of 15 millimoles/L (millimolar, [mM]) or 1.35 mg/mL (Farges et al. 2008; Hansen and Emborg 1994).

**Appendix E.3 Glutamine**

The other major energy source for mammalian cells in culture is the amino acid glutamine. It has a role as both an energy provider and also as an important source of carbon and nitrogen atoms especially for purine and pyramidine synthesis (White et al. 1995).

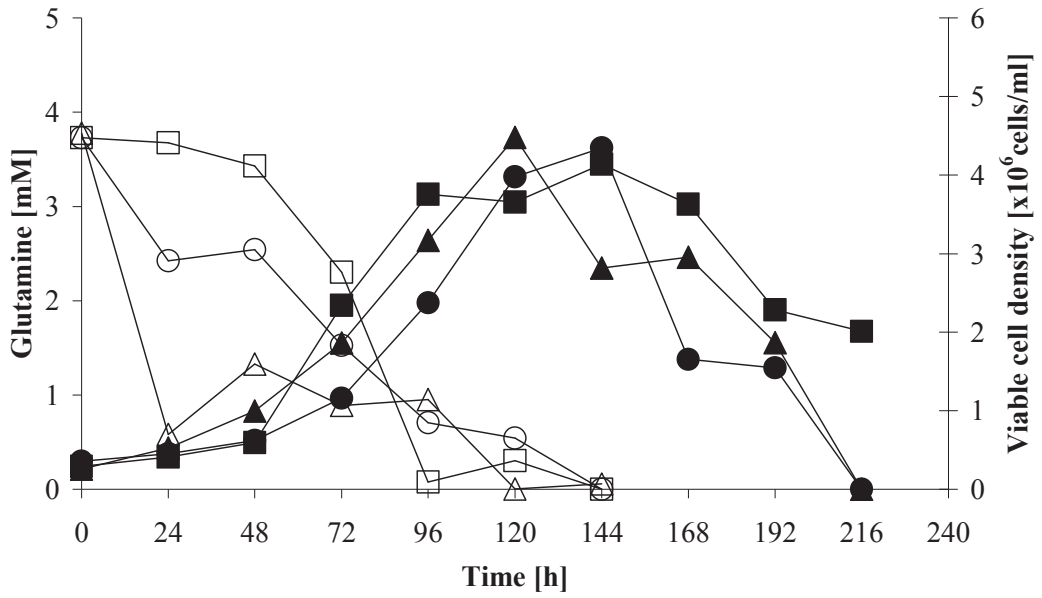


**Figure 48:** Glutamine concentration and viable cell density versus time for Batch cultures 1-3. Symbols: Viable cell density for Batch 1 (■), Batch 2 (▲), Batch 3 (●) cultures, glutamine concentration for Batch 1 (□), Batch 2 (Δ) and Batch 3 (○) cultures versus time.

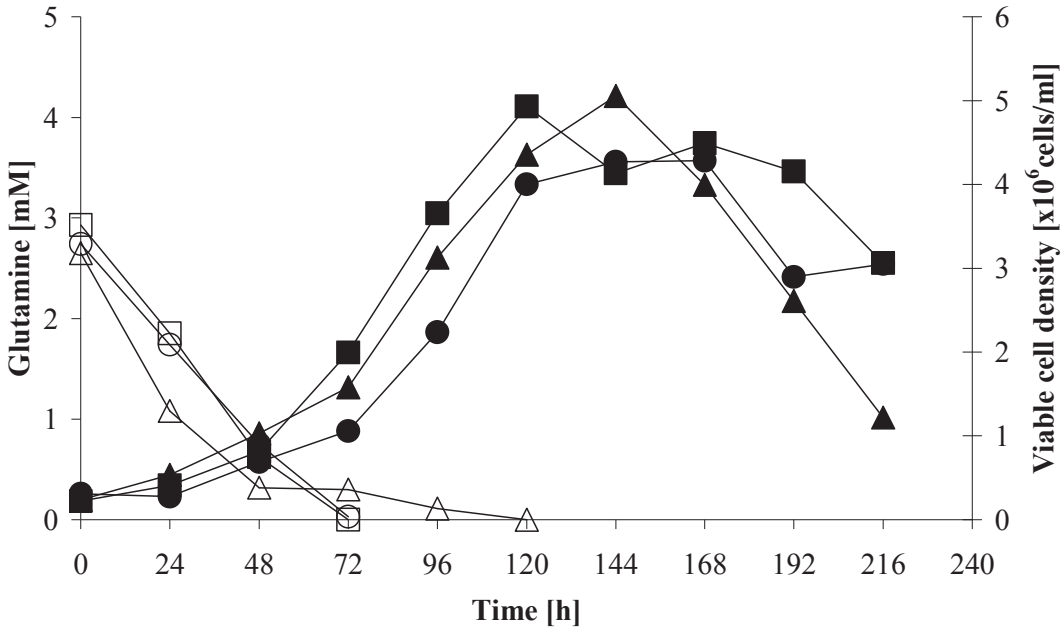


**Figure 49:** Glutamine concentration and viable cell density versus time for Fed Batch cultures 1-3. Viable cell density for cultures Fed Batch 1 (■), Fed Batch 2 (▲), Fed Batch 3 (●) cultures, glutamine concentration for Fed Batch 1 (□), Fed Batch 2 (Δ) and Fed Batch 3 (○) cultures versus time.

Glutamine depleted quicker in Fed Batch cultures when compared to Batch cultures, however no effect on specific growth rate was noted.

**Appendix E.4 Ammonia**

The main source in the accumulation of ammonia in mammalian cell cultures is the amino acid metabolism in particular, glutamine. Ammonia inhibition seems to play a more important role than lactate accumulation with levels as low as 2-3 mM causing a significant reduction in cell growth (Schneider, Marison and von Stockar 1996).

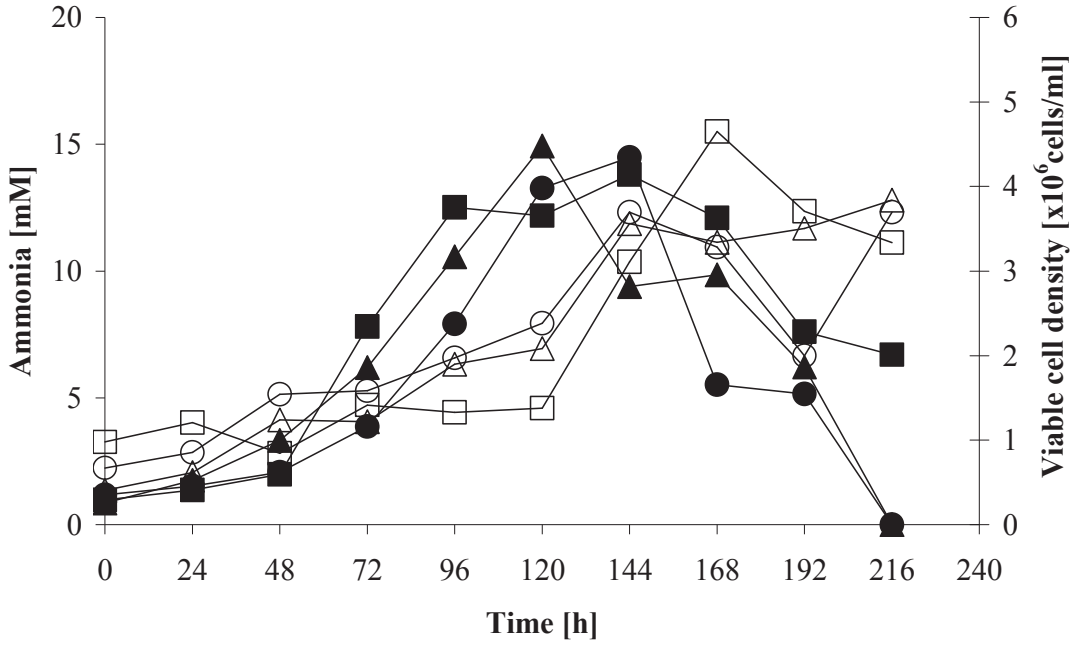


**Figure 50:** Ammonia concentration and viable cell density versus time for Batch cultures 1-3. Symbols: Viable cell density for cultures Batch 1 (■), Batch 2 (▲), Batch 3 (●) cultures, ammonia concentration for cultures Batch 1 (□), Batch 2 (Δ) and Batch 3 (○) cultures versus time.

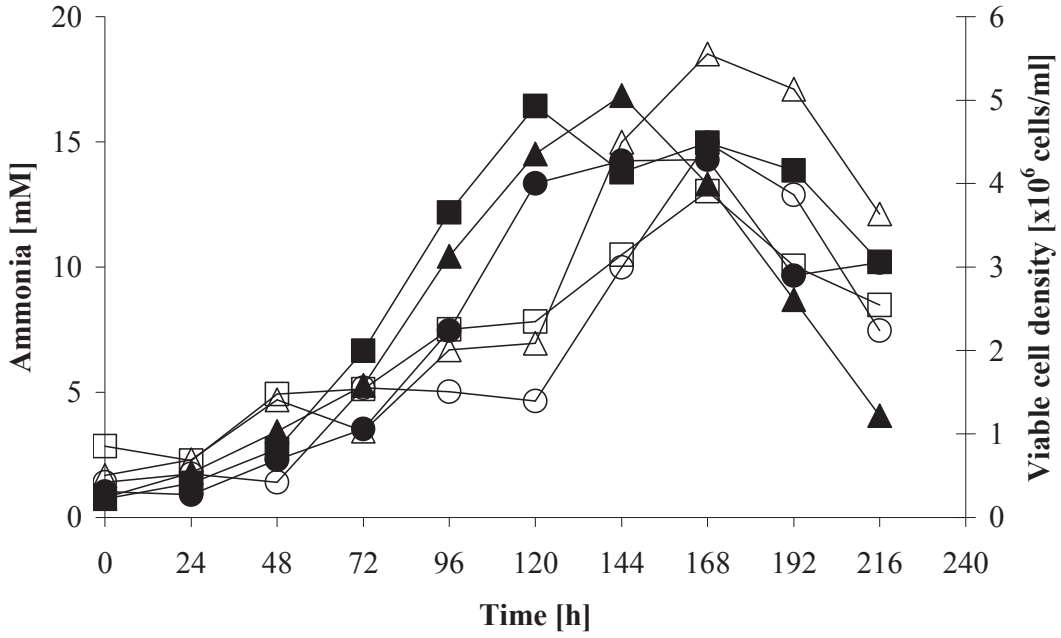


**Figure 51:** Ammonia concentration and viable cell density versus time for Fed Batch cultures 1-3. Viable cell density for Fed Batch 1 (■), Fed Batch 2 (▲), Fed Batch 3 (●) cultures, ammonia concentration for Fed Batch 1 (□), Fed Batch 2 (Δ) and Fed Batch 3 (○) cultures versus time.

**Table 20:** Batch and Fed Batch ammonia concentration at 120 hours and maximum concentration.

| Culture type | Ammonia concentration at 120 hours [mM] | Maximum ammonia concentration [mM] |
|---|---|---|
| Batch 1 | 4.6 | 15.5 |
| Batch 2 | 6.9 | 12.8 |
| Batch 3 | 7.9 | 12.3 |
| Fed Batch 1 | 7.8 | 13.0 |
| Fed Batch 2 | 6.9 | 18.5 |
| Fed Batch 3 | 4.6 | 14.9 |

The resulting build-up of ammonia from glutamine metabolism and degradation can be toxic to the cell culture system (McDermot and Butler 1993). Another source of ammonia such as alanine was expected as there was only 4 mM L-glutamine in the

medium preparation, while maximum concentrations of ammonia were above 8 mM (Capiaumont et al. 1995).

Glucose and glutamine consumption along with lactate production profiles share a similarity with what is reported in literature for IFN-γ producing CHO cell line (Farges et al. 2008; Lao and Toth 1997).

**Table 21**: Product and metabolite yields for CHO 320 cells.

| Parameter | Unit | Batch CHO 320 cells | Fed Batch CHO 320 Cells |
|---|---|---|---|
| Biomass/glucose | $10^6$ cells/mg | 0.77 (+/- 0.17) | 1.01 (+/-0.26) |
| Lactate/Glucose | mmol/mmol | 0.46 (+/- 0.07) | 0.53 (+/- 0.15) |
| Ammonia/Glutamine | mmol/mmol | 2.01 (+/- 0.10) | 3.17 (+/- 0.57) |
| Biomass/Glutamine | $10^6$ cells/µmol | 0.85 (+/- 0.08) | 1.55 (+/-0.17) |
| IFN/Biomass | µg/$10^6$ cells | 0.40 (+/- 0.03) | 0.27 (+/- 0.01) |

Typical values of $Y_{lactate/glucose}$ (mmol/mmol) are lower than ranges encountered for other CHO cell lines while the Y ammonia/Gln was much higher than the theoretical maximum of 2 mmol/mmol supporting the fact of a second source of ammonia in the cell culture (Xing et al. 2010; Lao and Toth 1997).

**Appendix E.5 Interferon gamma**

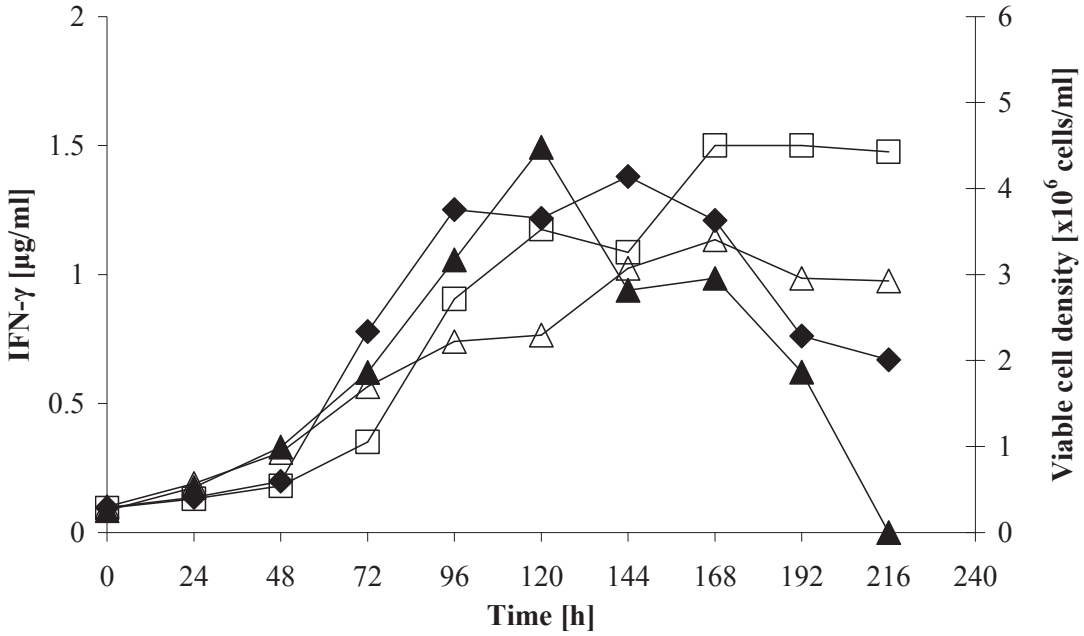


**Figure 52:** Interferon gamma (IFN-γ) concentration and viable cell density versus time for Batch cultures 1-3. Symbols: Viable cell density for cultures Batch 1 (■), Batch 2 (▲) and IFN- γ concentration for cultures Batch 1 (□), Batch 2 (Δ) versus time.

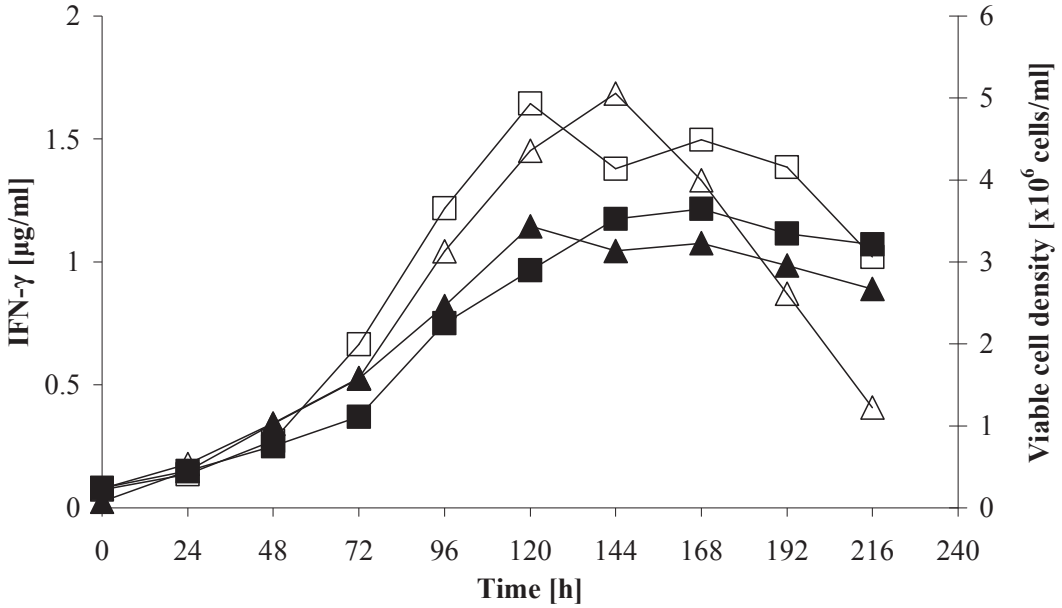


**Figure 53:** Interferon gamma (IFN-γ) concentration and viable cell density versus time for Fed Batch cultures 1-3. Symbols: Viable cell density for cultures Fed Batch 1 (■), Fed Batch 2 (▲) and IFN-γ concentration for cultures Fed Batch 1 (□), Fed Batch 2 (Δ) versus time.

The advantages of Fed Batch culture over batch, perfusion and continuous cultures, is that it enables a higher protein production (Kuwae et al. 2005) and limit the toxic affect of metabolites on protein production levels (Lee et al. 2007).

**Table 22:** Maximum concentrations of IFN- γ for Batch and Fed Batch cultures.

| Culture type | Maximum [IFN-γ] concentration | Time [h] |
|---|---|---|
| Batch 1 | 1.50 | 168 |
| Batch 2 | 1.13 | 168 |
| Fed Batch 1 | 1.21 | 168 |
| Fed Batch 2 | 1.15 | 120 |

IFN-gamma production was growth associated, in agreement with findings of (Farges et al. 2008; Leelavatcharamas, Emery and al-Rubeai 1994).

IFN-Gamma concentration was lower than the expected concentrations of 1.5 - 3 μg/ml reported to be achieved by Clincke et al. (2011) and 2-2.5 μg/ml obtained by Goh and Yap (2005) while other CHO variants reportedly can produce two and ten times the amount produced in this study (Wong et al. 2006).

**Table 23:** Specific rates of IFN- γ production.

| Parameter | Unit | Batch CHO 320 cells | Fed Batch CHO 320 Cells |
|---|---|---|---|
| $q_{IFN-\gamma}$ spec | $\mu g/10^6$ cell $h^{-1}$ | 0.0024 (+/- 0.001) | 0.0019 (+/- 0.0004) |
| $q_{IFN-\gamma}$ spec | $\mu g/10^6$ cell $d^{-1}$ | 0.05 (+/- 0.004) | 0.04 (+/- 0.010) |
| $q_{IFN-\gamma}$ spec | μg/ml $h^{-1}$ | 0.007 (+/- 002) | 0.007 (+/-0.006) |
| $q_{IFN-\gamma}$ spec | μg/ml $d^{-1}$ | 0.18 (+/- 0.04) | (0.18 +/- 0.20) |